Actin, Auxin, and Plant Patterning

-

The role of actin-binding proteins and super-resolution microscopy in tobacco cells

(*Nicotiana tabacum* L. cv. Bright Yellow 2)

Zur Erlangung des akademischen Grades eines

DOKTORS DER NATURWISSENSCHAFTEN

(Dr. rer. nat.)

Fakultät für Chemie und Biowissenschaften
Karlsruher Institut für Technologie (KIT) - Universitätsbereich
genehmigte

DISSERTATION

von

Steffen Durst

aus Karlsruhe

Dekan: Prof. Dr. M. Bastmeyer
Referent: Prof. Dr. P. Nick
Korreferent: Prof. Dr. G.U. Nienhaus
Tag der mündlichen Prüfung: 19.04.2012

Danksagung

Die vorliegende Dissertation wurde am Botanischen Institut des Karlsruher Instituts für Technologie (KIT), Lehrstuhl 1 – Molekulare Zellbiologie, im Zeitraum von April 2009 bis April 2012 angefertigt.

Mein besonderer Dank gilt Herrn Prof. Dr. Peter Nick für die hervorragende Betreuung der Doktorarbeit und das in mich gesetzte Vertrauen.

Herrn Prof. Dr. Gerd Ulrich Nienhaus danke ich für die Übernahme des Korreferats.

Ein ganz besonderer Dank gebührt Dr. Jan Maisch. Er hat mich über die ganze Zeit der Doktorarbeit unterstützt, stand jederzeit mit Rat und Tat zur Verfügung, hat mich stets angetrieben und motiviert sowie unzählige Manuskripte gelesen und Verbesserungsvorschläge eingebracht.

Per Niklas Hedde danke ich für die tolle Unterstützung und Zusammenarbeit im Bereich der Photoaktivierungslokalisationsmikroskopie. Für die Initiierung der Kooperation und die Einführung in die photoaktivierbaren Fluoreszenzproteine danke ich zudem Dr. Susan Böhme.

Alexandra Leonard und Linda Brochhausen leisteten durch ihre Bachelor Arbeiten für diese Dissertation einen wertvollen Betrag. Dafür danke ich beiden sehr. Ebenso möchte ich den von mir betreuten Praktikanten danken, die durch ihre Fragen und Eindrücke ein stetiger Antrieb für mich waren.

Für die exzellente technische Unterstützung im Labor und speziell im Bereich der Zellkultur möchte ich mich ganz herzlich bei den Auszubildenden Olivia und Anna sowie den Technischen Mitarbeitern Sybille, Sabine und Ernst bedanken.

Dem kompletten Botanischen Institut 1 möchte ich für die tolle Arbeitsatmosphäre und Zusammenarbeit während der letzten Jahre danken.

Für den Spass und die vielen langen Unterhaltungen, die mich wissenschaftlich wie auch menschlich weitergebracht haben, danke ich zudem ganz besonders den aktuellen sowie ehemaligen Dachgeschossbewohnern Kai, Annabelle, Sebastian, Jan, Natalie, Rita, Bea, Holger, Stephan, Benjamin, Aleksandra und Isabel.

Für die bedingungslose Unterstützung meiner Familie, die mein Studium und diese Dissertation erst möglich gemacht haben, bin ich unendlich dankbar.

Zusammenfassung

Der interzellulare polare Transport des Phytohomons Auxin stellt den elementaren Baustein der pflanzlichen Polarität und Musterbildung dar. Die Forschung der letzten Jahre hat gezeigt, dass die Organisation der Aktinfilamente eine entscheidende Rolle für den polaren Auxinfluss spielt und dass dieser durch Auxin selbst reguliert werden kann. Zusätzlich ist schon länger bekannt, dass die einzelnen Aktinisotypen stark konserviert sind, was den Schluss nahelegt, dass die unterschiedlichen Funktionen auf die Vielzahl unterschiedlichster Aktinbindeproteine und deren Komplexen zurückzuführen ist.

Im ersten Teil der Dissertation wird die mögliche Beteiligung von Aktinbindeproteinen als Mediator des Auxinsignals auf die Reorganisation des Aktinzytoskeletts untersucht. Als Modellsystem für die Analyse der Beteiligung von Aktinbindeproteinen am Auxinfluss und der daraus resultierenden Polarität wurde die Tabakzelllinie BY-2 (*Nicotiana tabacum* L. cv. Bright Yellow 2) herangezogen. Sie zeichnet sich durch ein Zellteilungsmuster aus, das auf einer schwachen Kopplung zwischen den Teilungsvorgängen benachbarter Zellen beruht und sensitiv auf Veränderungen des Auxinflusses reagiert. Die Überexpression des *Nicotiana tabacum* Actin-depolymerizing factor 2 (NtADF2) im homologen System verursachte eine Modifikation der Aktinkonformation und führte zum Zusammenbruch des charakteristischen Teilungsmusters. Durch Zugabe von Phosphatidylinositol 4,5-bisphosphat (PIP_2), einem natürlichen Inaktivierungslipid von ADF, konnte dieses teilweise und durch die Zugabe von Phalloidin, das durch seine stabilisierende Wirkung funktionell um ADF-Funktionen kompetitiert, sogar komplett wiederhergestellt werden. Die Komplementationsergebnisse, unterstützt durch Daten einer induzierbaren NtADF2 RNAi knockout BY-2 Zelllinie, führten zu einem Modell, in dem NtADF2 durch Modifikation der Aktinstabilität eine wichtige Funktion zwischen Auxinsignal und Aktinreorganisation inne hat.

Im zweiten Teil wurde der fluoreszenzmikroskopischen Unterscheidbarkeit verschiedener Actinbindeprotein-dekorierter Aktinpopulationen nachgegangen. Es gelang, das ubiquitär an Aktinfilamente bindende Hefepeptid Lifeact an ein fluoreszentes Protein zu fusionieren, das aufgrund seiner Tetramerbildung und im Gegensatz zu einer monomeren Sonde, nur Aktinfilamente binden konnte, bei denen die Bindestelle sterisch frei lag. Auf diese Weise konnte eine funktionelle Aktinpopulation um den Zellkern visualisiert werden, die an der Kernbewegung beteiligt war. Zusätzlich war es möglich mit dem verwendeten photoaktivierbaren und photostabilen Fluoreszenzprotein psRFP, Photoaktivierungs-lokalisationsmikroskopie (PALM) zu betreiben und so filamentöses Aktin mit einer Auflösung im niedrigen nm-Bereich samt anschließender drei-dimensionaler Rekonstruktion in lebenden Pflanzenzellen darzustellen.

Table of Contents

List of Abbreviations

2,4-D	2,4-dichlorophenoxy acetic acid
4-Cl-IAA	4-chloroindole-3-acetic acid
ABP	Actin-binding proteins
ADF	Actin-depolymerizing factor
AF	Actin filaments
BY-2	*Nicotiana tabacum* L. cv Bright Yellow 2
Dex	Dexamethasone
DP	Division pattern
FABD2	Fimbrin actin-binding domain 2
GFP	Green fluorescent protein
IAA	Indole-3-acetic acid
LatB	Latrunculin B
mTalin	mouse-Talin
NAA	1-naphthalene acetic acid
PAA	2-phenyl acetic acid
PALM	Photoactivation localization microscopy
pa-FP	Photoactivatable fluorescent protein
PIP_2	Phosphatidylinositol 4,5-bisphosphate
psRFP	Photoswitchable red fluorescent protein
RFP	Red fluorescent protein
SE	Standard error
TAMBY-2	Transient *Agrobacterium*-mediated transformation of BY-2
YFP	Yellow fluorescent protein

1. Introduction

Our entire world is shaped by patterns, which are more or less easy to detect. These patterns are often manmade, like road coatings, the cultivation of gardens, parkways, or whole acre landscapes in agriculture. Having a closer look to the individual elements constituting entire plants reveals, that also here a distinct pattern formation is active. These patterns apparently are able to maintain a basic order and can combine unique parts to complex patterns without any superior institution like the human brain. The formation of roots, branching of shoots, or efflorescences occur in no case randomly, but follow stringent patterns that are often highly conserved, such that they can be used for determination of different plant species.

Figure 1.1: Patterns from gigantic to small. (Left) Layout of the city Karlsruhe, copper engraving by Heinrich Schwarz 1721; http://www.karlsruhe.de/ as of February 2012. (Middle) Various patterns of *Buxus sempervirens* at the Botanical Garden of Madeira. (Right) Efflorescence of *Helianthus annuus*, single flowers are distributed to Fibonacci numbers, picture taken by Christoph Eidenberger.

What does a “pattern” mean anyway? In general, it can be defined as a non-random spatial or temporal distribution of various parts forming an ensemble (Bünning, 1965). Such arrangements exist for the external shape of a plant, its composition of organs and tissues, and the assembly of organelles and protein complexes constituting the individual cells. At every level of complexity, a coordination of the single elements is necessary. How is this achieved? There have to be signals, whose distributions have direct influence on the differentiation of specific parts as well as on forming the whole entity. During the last century different phytohormones have been identified as pivotal players and could be correlated to the previously described phenomena such as the formation of efflorescences or apical branching (Beveridge *et al.*, 2003). However, despite intense research, many aspects of the relation between phytohormones and pattern formation have remained unsettled.

In this dissertation, the emphasis was put on sub-cellular patterning – the re-organization of filamentous actin as reaction on the phytohormone auxin and the consequences of this re-organization in tobacco cells. The signaling from auxin to actin during pattern formation had

remained unraveled up to now. Therefore, the motivation of this work was to illuminate this process by identification of potential auxin-signal mediators.

1.1 Auxin, small and cryptic but essential and pervasive

As probably the most important of all plant hormones, auxins play a central role in almost all plant developmental processes. It is hard to imagine that such a small molecule forms the basis of so many different signaling pathways. But since it is the case, it is not a big surprise that auxins have been in focus of science since the first description of a “growth signal” by the Darwins (Darwin and Darwin, 1881), and the independent discovery by H. Cholodny (1928) in Russia and F.W. Went (Went and Thimann, 1937) in the Netherlands. During more than a century of science many questions could be answered, but this raised numerous new questions.

1.1.1 The molecule

All natural auxins are built up of at least one aromatic ring and a carboxylic acid group (Taiz and Zeiger, 2006). They are found in plants as free acid and in conjugated forms. The most important auxin is indole-3-acetic acid (IAA) which is responsible for the majority of so far known auxin effects in plants. Therefore, in the following, the term “auxin” is defined as IAA if not stated otherwise. In addition to IAA, three other natural auxins have been identified up to now (for a recent review, see Simon and Petrášek, 2011), which differ from IAA in composition and stability (4-chloroindole-3-acetic acid; 4-Cl-IAA) or metabolic derivatization (indole-3-butyric acid; IBA). For the third auxin (2-phenyl acetic acid; PAA; Wightman and Lighty, 1982) no specific function could be identified in plants. Figure 1.2 shows an overview of the four natural auxins and their structural differences.

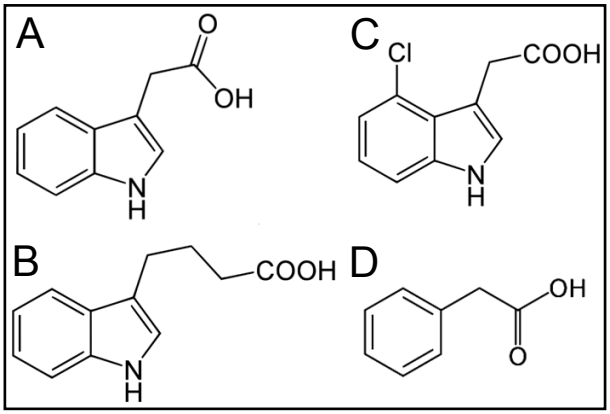

Figure 1.2: Naturally occurring auxins. (A) Indole-3-acetic acid. (B) Indole-3-butyric acid. (C) 4-chloroindole-3-acetic acid. (D) 2-phenyl acetic acid. (Simon and Petrášek, 2011)

In addition to these four natural auxin several synthetic auxins such as 2,4-dichlorophenoxy acetic acid (2,4-D) or 1-naphthalene acetic acid (NAA) have been developed which are more stable and therefore more suitable for scientific or agricultural applications.

1.1.2 General functions of auxin in plant development

Auxin plays a key role in the transmission of environmental and endogenous signals. Originally defined as enhancer of cell elongation growth (Normanly *et al*., 2010), auxin regulates, in addition, apical dominance, leaf senescence, fruit setting, growth and ripening, and plays an essential role in tropistic responses to light and gravity (for review, see Davis, 2010). As a central function auxin defines directional cues fundamental to patterning (for review, see Berleth and Sachs, 2001).

These patterning events depend mainly on a directional flow of auxin. This cell-to-cell process has been described by a modified chemiosmotic model (for review, see Lomax *et al*., 1995), implying influx through locally confined carriers and an (ubiquitously active) ion-trap mechanism, and locally confined efflux through different carriers.

1.1.3 Auxin-dependent patterning and how it is achieved

Auxin-dependent patterning is based on cell polarity. Cell polarity and polar auxin flow are linked by dynamic localization of auxin efflux carriers through directional intracellular traffic in a self-amplifying feedback loop. Directional flux through carriers and non-directional influx by the ion trap generates a lateral inhibition, resulting in an ordered pattern (for review, see Friml, 2010; Nick, 2010), elegantly shown for the venation in developing leaves (for review, see Sachs, 2000), and the definition of new primordia in the growing meristem (Reinhard *et al*., 2000).

Figure 1.3 shows a cellular model of IAA influx. Besides the passive diffusion, the two influx carriers Auxin resistant 1 and Like Auxin resistant (AUX1; Bennett *et al*., 1996; Yang *et al*., 2006; LAX; Swarup *et al*., 2008) are involved in this process, both belonging to the family of plasma membrane amino acid permeases. Their important role in polarized auxin transport was nicely shown by Laňková *et al*. (2010) using 1-naphthoxy acetic acid (1-NOA), 2-naphthoxy acetic acid (2-NOA), and 3-chloro-4-hydroxyphenyl acetic acid (CHPAA) to block theses auxin influx carriers, leading to a loss of polar cell file growth in tobacco BY-2 cultures. After entering the cell, IAA is deprotonated because the pH changes from acidic to neutral. The fore-mentioned ion trap is now activated and the only way to leave the cell is via efflux carriers, which get their energy from H^+-ATPases using the free H^+ from dissociated IAA. These efflux carriers have been identified as PIN-formed proteins (PIN) and they show a very specific localization. Their intracellular distribution is asymmetric causing a directional

flow of auxin. In addition to this asymmetric pattern, PIN underlay a continuous cycling between cell membrane and the endoplasmatic reticulum (ER), which is controlled by auxin as regulator and actin as track.

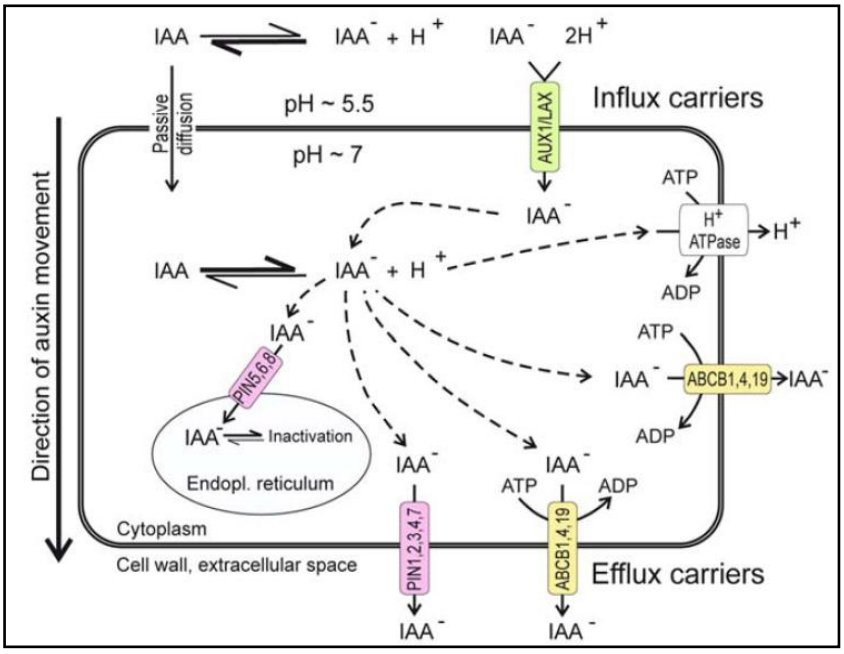

Figure 1.3: Model of intracellular auxin transport. Undissociated IAA molecules enter cells by passive diffusion, whereas the less lipophilic, and therefore less permeable, dissociated auxin anions (IAA^-) are imported via auxin influx $2H^+$ co-transporters of the AUX1/LAX family. In the more alkaline intracellular environment, IAA dissociates and requires active transport through the PIN or ABCB efflux transporter proteins to exit the cell. Asymmetric subcellular localization of PIN proteins determines directionality of auxin flow. A part of the cytosolic IAA is transported by PIN5 and presumably also PIN6 and PIN8 into the lumen of the endoplasmic reticulum. This compartmentalization serves to regulate auxin metabolism. Whereas PIN transporter activity is supposed to use an H^+ gradient that is maintained by the action of the plasma membrane H^+-ATPase, ABCB transporters harbor ATPase activity. (Friml, 2010)

The fact that the efflux carriers have to be perpetually transported from ER to the plasma membrane and back again and that auxin mediates a re-organization from bundled to fine actin filaments places actin into the focus of this mechanism.

1.2 The actin-auxin oscillator

During the growth responses of Graminean coleoptiles to light (perceived by phytochrome) and auxin, actin undergoes dynamic changes in bundling (Waller and Nick, 1997). This bundling became manifest on the biochemical level as increased actin sedimentability and correlated with differences in auxin sensitivity (Waller *et al.*, 2002) leading to an oscillator model where auxin-signaling triggered the re-organization of F-actin bundles into finer filaments. In turn, this enables more efficient transport of auxin-signaling components towards the cell pole (for review, see Nick, 2010). The auxin-triggered re-organization could

later be confirmed *in vivo* (Holweg *et al*., 2004; Maisch and Nick, 2007), and was shown to stimulate polar auxin transport (Nick *et al*., 2009).

In addition to cell expansion, also the synchrony of cell division depends on the actin-auxin-oscillator. Cell divisions in tobacco cell suspensions follow a clear pattern with elevated frequencies of files composed of an even number of cells (Campanoni *et al*., 2003; Maisch and Nick, 2007) caused by weak coupling between the divisions of neighboring cells. This coupling is dependent on polar auxin flow. When actin was constitutively bundled by overexpression of YFP-mTalin, the synchrony of cell division was impaired. However, by exogenous auxins, a normal array of actin filaments (AF) could be restored and this treatment rescued division synchrony (Maisch and Nick, 2007) demonstrating that a normal (debundled) configuration of actin was necessary and sufficient for a polar auxin flow. Later, using transgenic rice plants overexpressing YFP-mTalin, the stimulatory effect of actin debundling on auxin flow could be demonstrated directly using radioactively labeled indole-3-acetic acid (Nick *et al*., 2009).

The model of the actin-auxin oscillator postulates that the auxin-signal must be conveyed to actin causing its re-organization. Neither the mechanism nor the players for this signaling have been identified. Since AF can be modified by a plethora of actin-binding proteins (ABP; for review, see Staiger, 2010), it is likely that also the auxin-signal could be mediated by one or a complex of several ABP.

1.3 Actin, highly conserved but flexible in function

As a part of the plant cytoskeleton, actin has to fulfill a bunch of highly different tasks. For example, actin plays an important role as part of the intracellular transport machinery of various cargoes. These cargoes are widespread and contain organelles like mitochondria (Birtalan *et al*., 2012). Most of these transport events are widely accepted to be accomplished by a class of mechanochemical enzymes called myosins. Myosins are able to bind actin filaments, and move along AF carrying their bound cargo under constant hydrolysis of ATP and conformational changes (Shimmen and Yokota, 2004; Shimmen, 2007). In addition to these transport functions, AF structure the vacuolar and transvacuolar cytoplasmic strands of plant cells (Staiger *et al.*, 1994; Verbelen and Tao, 1998; Sheahan *et al.*, 2007). Additionally to the transport function the actin cytoskeleton is also responsible to anchor organelles at defined intracellular positions (nuclear movement and anchorage, for review, see Campbell and Reece 2003; Frey *et al.*, 2010; Klotz and Nick, 2012). As a result of these different tasks, actin filaments strongly control the whole cellular architecture. To achieve this multitude of functional tasks, the conformation of the actin cytoskeleton has to be adjusted from a network of fine cross-linked to heavily bundled filamentous structures or

vice versa, depending on the particular situation. For instance, to maintain the nucleus at its appropriate position during the cell cycle, non-dynamic actin filaments are needed, whereas filaments in the cortical region of a cell have to be highly dynamic to give the cell the opportunity to react immediately on altered requirements in respect to vesicle transport or external stimuli like pathogens (Qiao *et al.*, 2010).

Plant actins share 83 to 88 % amino acid sequence identity compared to actins of green algae, most protists, fungi, and animals. Within the families, the amino acid sequence identity is even higher at about 95 % (Meagher *et al.*, 1999a, 1999b). This means that actin is extremely conserved. Thus, there is not enough variability of different isoforms to accommodate the diverse functionality without binding partners. The basic structure of filamentous actin is composed of monomeric asymmetric actin subunits with a molecular weight of 42 kDa. Each monomer contains four subdomains, nucleotide- and divalent cation-binding sites (Kabsch *et al.*, 1990). Assembly of monomeric actin into filamentous actin (F-actin) as well as maintenance of F-actin and its disassembly is regulated by a huge number of actin-binding proteins (Hussey *et al.*, 2002; Staiger and Blanchoin, 2006).

The distinct decoration of actin filaments with different sets of actin binding proteins leads to multiple functional subpopulations and allows to complete the different tasks, mentioned above.

1.4 Actin-binding proteins and their pivotal role in actin filament organization

Actin as part of the cytoskeleton and a backbone of cellular transport is subject to multiple structural modifications caused by direct or complex-based binding of actin-binding proteins (ABP). Up to now, more than 70 classes of ABP have been identified in eukaryotic cells (Kreis and Vale, 1999; Pollard *et al.*, 2000). Because of this abundance functional characterization and categorization is essential in addition to their identification.

1.4.1 Categorization of functional families of actin-binding proteins

It is more or less possible to distinguish between two main groups of ABP, monomer-binding proteins or polymer-binding proteins. In both groups, as pointed out below, several subgroups can be differentiated although they often overlap in function.

As monomer-binding proteins profilins, adenylate cyclase-associated proteins (CAP) or actin-depolymerization factors (ADF) are well known. Their functions are widespread: They prevent spontaneous nucleation, shuttle new actin subunits onto filaments, enhance

nucleotide exchange or act as sequestering proteins (for a recent review, see Staiger *et al*., 2010). In most cases, different ABP classes have to cooperate to fulfill their actual function. Profilins for example, are able to bind stretches of proline residues as they appear in both proline-rich formin-homology domains (FH1 and FH2) of formins (for review, see Deeks *et al*., 2002; Blanchoin and Staiger, 2008) leading to a proper localization of this major nucleation factor. In addition to this nucleation function from monomers, formins can also bundle AF and nucleate new filaments from the side of existing bundles (Michelot *et al.*, 2005, 2006). Because of this side-binding, formins can also be sorted into the second main group of the polymer-binding proteins. These proteins contribute to the formation of higher-order structures by stabilizing, bundling and crosslinking AF, respectively (Staiger *et al.*, 2010). Prominent members of this group are LIM-domain containing proteins (LIM; Thomas *et al.*, 2006), fimbrins (FIM), both *bona fide* bundling and crosslinking proteins (Kovar *et al.*, 2000) or villins (VLN) which belong to the superfamily of gelsolins. The gelsolins cannot only bundle, but can also sequester filaments (for review, see Thomas *et al.*, 2009).

To get better insight into the role of ABP with regard to auxin-mediated actin re-organization, selected members of different *Nicotiana tabacum* ABP families were overexpressed in tobacco BY-2 cells. From the results of preliminary phenotyping the *Nicotiana tabacum* actin-depolymerizing factor 2 (ADF2) shifted into the focus as most promising candidate (Chen *et al.*, 2002).

1.4.2 Function, structure, and regulation of actin-depolymerizing factors

Actin-depolymerizing factors (ADFs)/cofilins bind to G- and F-actin with a noticeable preference for ADP-G-actin (Carlier *et al.*, 1997; Blanchoin and Pollard, 1999). They disassemble AF by a complex mechanism, which depends on the activity of stabilizing ABP (Ketelaar *et al.*, 2004; Huang *et al.*, 2005).

The activity of ADFs can be modulated by several factors, such as pH (Gungabissoon *et al.*, 2001; Allwood *et al*., 2002), or phosphorylation of a N-terminal serine residue, which leads to a loss of actin-binding when phosphorylated (Allwood *et al.*, 2001). In addition, the phosphoinositide lipid Phosphatidylinositol-4,5-bisphosphate (PIP_2) can specifically inhibit actin-binding ability of ADFs (for review, see Staiger *et al.*, 2010). This inhibition is achieved via an electrostatic interaction of PIP_2 with a positively charged group of amino acids of ADF (Zhao *et al.*, 2010) covering its actin filament binding sites (Figure 1.4 A).

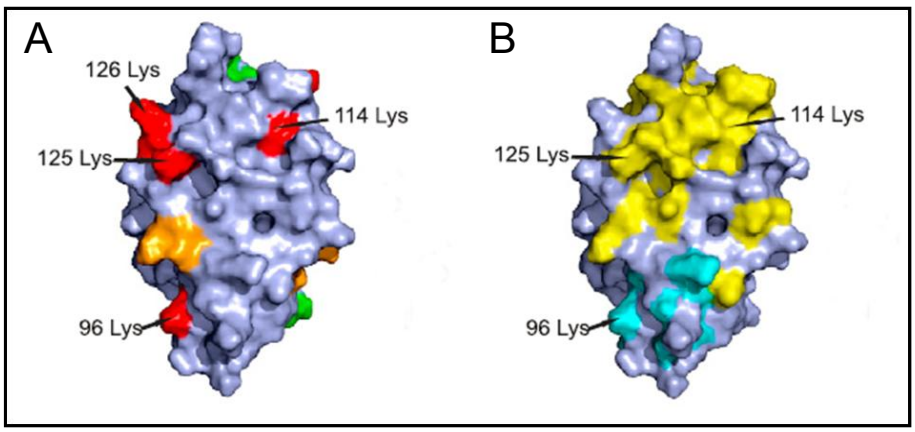

Figure 1.4: (A) Model of the molecular surface of human cofilin-1. The most critical residues in PIP_2 binding are colored in red and other positively charged residues contributing to PIP_2 binding are in orange. The mutated residues (Zhao *et al.*, 2010) that did not display effects on PIP_2 binding are in green. (B) G-actin and F-actin binding sites of cofilin. Residues that are critical for ADF/cofilin interactions with G-actin and F-actin are in yellow. Residues that are critical for interaction with F-actin, but not G-actin, are in cyan. (Zhao *et al.*, 2010)

1.5 Scope of this dissertation

This dissertation can be separated into two main parts. The first section deals with the search for auxin-signal mediators for actin filament re-organziation, whereas the second part is based on the first one and focuses on actin itself. By means of a FP-based approach it was tested, if it is possible to discriminate between differently decorated actin filament sub-populations and their distribution.

1.5.1 The role of actin-binding proteins for auxin-signaling

The incorporation of the actin cytoskeleton in auxin dependent patterning plays a pivotal role in plant patterning. Actin microfilaments undergo a clearly visible re-organization as response to auxin-signaling within minutes. How this signal is mediated, remains still poorly understood. As actin is subject to multiple structural modifications caused by direct or complex-based binding of ABP, it is possible that these proteins are involved in this re-organization process and contribute in this manner to the self-amplification loop between auxin-signaling and AF.

The aim of this dissertation is to investigate the role of representative members of different ABP-families with a focus on the *Nicotiana tabacum* actin-depolymerizing factor 2 (NtADF2) for auxin dependent, patterned cell division in the homologous system. If NtADF2 is part of an auxin-driven feedback loop, it should be possible to manipulate auxin-dependent patterning via manipulation of NtADF2-expression levels in BY-2 cell cultures. In particular, this work is investigating whether overexpression of NtADF2 will impair the polarity of auxin flow. For this purpose, patterned cell division is used as sensitive trait to monitor changes of

polar auxin fluxes. In addition the phenotype of this NtADF2-overexpressing BY-2 cell line is analyzed.

1.5.2 Discrimination and visualization of actin sub-populations

As mentioned before, actin is highly conserved but essential for a plethora of different essential functions, like the polar transport of auxin examined in the first part of this work. All experimental findings led to the assumption, that actin achieves its enormous potential through its various binding proteins resulting in functional actin sub-populations.

The second scope of this dissertation is the visualization and discrimination of diversely decorated actin filament sub-populations by means of novel BY-2 actin-marker lines using the yeast peptide Lifeact, which is, up to now, the ubiquitary actin-binding probe with fewest side effects. Lifeact is fused to a photoswitchable red fluorescent protein (psRFP), or a photoswitchable monomeric fluorescent protein called mIRISFP, respectively. The psRFP forms tetramers and is therefore much bigger than the monomeric Lifeact-mIRISFP. In actin filaments that are heavily decorated by ABP, steric hindrance of the tetrameric psRFP reporter is expected which should lead to differentially labeled subset of actins as evidence for such functional actin filament sub-populations. As this approach reaches the diffraction limit of classical fluorescence microscopy, high resolution PALM-/STORM-microscopy had to be employed for the first time in living plant cells.

1.6 Fluorescent proteins in living plant cells

The second part of the doctoral thesis deals with the visualization of actin filaments using classical fluorescent proteins (FP) fused to different ABP versus the establishment of new BY-2 marker lines containing photoactivatable fluorescent proteins (pa-FP). For a better understanding of the need and the advantages of pa-FP over classical FP it is necessary to illuminate the basics of the techniques and their limitations.

1.6.1 Fluorescent proteins in microscopy

After their discovery and utilization by Osamu Shimomura (Shimomura *et al*., 1962), Martin Chalfie (Chalfie *et al*., 1994) and Roger Tsien (Heim *et al*., 1994; Heim *et al*., 1996; Shaner *et al*., 2004), fluorescent proteins (FP) changed the world of cell biology fundamentally. Their tremendous importance was appreciated in 2008 with the Nobel prize in Chemistry.

The first discovered FP was a green fluorescent protein (GFP) from the jellyfish *Aequorea victoria*. It consists of 238 amino acids with a molecular weight of 26.9 kDa (Prasher *et al*., 1992). An α-helix and 11 anti-parallel β-sheets form a β-barrel containing the covalently

bound chromophore, formed inside of this barrel by cyclization and oxidation reactions from the tripeptide Ser_{65}-Tyr_{66}-Gly_{67} (Ormö *et al*., 1996; Yang *et al*., 1996).

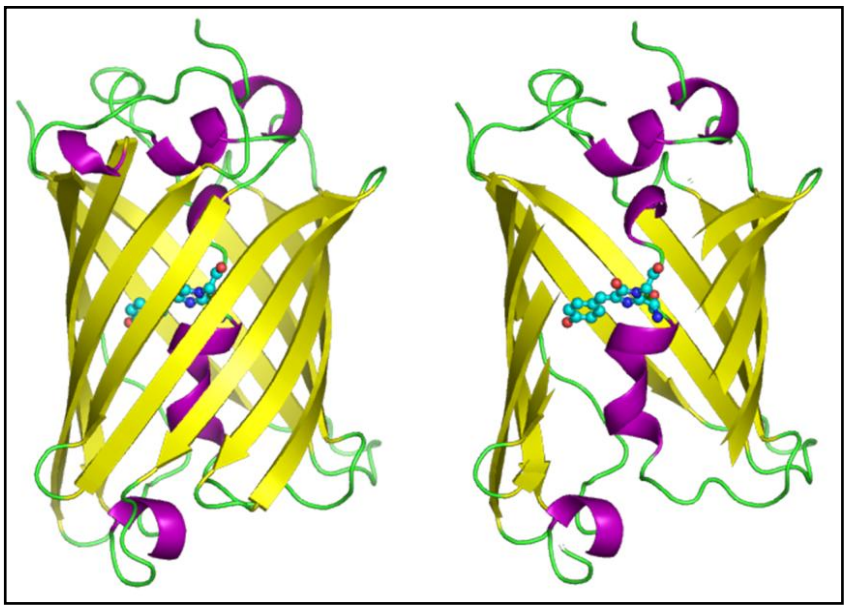

Figure 1.5: GFP molecules in cartoon style (PyMol, http://www.pymol.org/; as of December 2011). Chromophore highlighted as ball and stick (created by Raymond Keller, 2008). Figure 1.5 is basing on the work of Yang *et al.*, 1996. Protein structure information: 1GFL (RCSB Protein Data Bank, http://www.rcsb.org/pdb/, as of December 2011)

GFP as starting point for FP-based microscopy was rapidly followed by molecular modification leading to additional FP with different excitation and emission wavelengths as compared to the original GFP (excitation: 395 nm major, 475 nm minor; emission: 509 nm), which depends on electron-stacking interactions of intra-β-barrel side chains with the chromophore (Heim *et al*., 1994; Heim *et al*., 1996; Shaner *et al*., 2004). FP are non-toxic to cells and therefore feasible for *in vivo* live cell imaging in contrast to fixation- and antibody-based techniques. The possibility to fuse these FP to proteins of interest (POI) enables protein localization studies over a certain period of time depending on bleaching properties of the FP. Constructs of FP-POI fusions are brought into plant cells via ballistic or *A. tumefaciens*-mediated transformation and can be observed under confocal laser scanning microscopes (CLSM) or conventional widefield epifluorescence microscopes.

To visualize the actin cytoskeleton, FP are fused to entire ABP or selected domains of them. The most prominent marker lines in plant cells are based on fusions with the actin-binding domain of mTalin (mTalin), LIM-domain containing proteins or the actin-binding domain 2 of *A. thaliana* fimbrin 1 (FABD2). Since 2008, a new actin-binding probe called Lifeact, a small 17 amino acid peptid from yeast, is considered at the moment as the best available actin marker. This is especially valid for combinations with newest FP resulting in the so far minimal reported side effects. (Riedl *et al*., 2008).

1.6.2 Limitations of classical fluorescent proteins

FP revolutionized cell biology without any doubt, but as usual all new results have to be taken with a pinch of salt. As FP normally cannot bind structures of interest like actin by themselves they need linker proteins and these fusions have to be expressed at a relatively high level to be visible in the cell. This can lead to side effects or artifacts reaching from microfilament bundling (e.g. mTalin overexpression; Ketelaar, 2004; Maisch and Nick, 2007) over false localization pattern due to disproportionate amounts of binding partners or steric hindrance to even mortality of the transformed cells. Even if there are no side effects manifest, it is very important always to keep in mind that the system had to be changed to visualize it.

To reduce artificial effects, experimental procedures based on FP have been subsequently advanced. On the one side the vector systems have been modified, making for example chemical induction of the FP-fusion expression possible. On the other side, the FP themselves had been tailored more precisely to the experimental approaches they are used for. The modification of excitation and emission wavelength made techniques like fluorescent resonance energy transfer (FRET) possible that allowed a better insight in protein interaction in living cells (Campbell *et al.*, 2002). In addition to that improvement, it was possible to alter classical FP in a way that enabled specific time point related expression of FP-fusions. This sort of FP changes its color while aging (Terskikh *et al*., 2000). Despite all modifications one parameter remained unchanged: FP depend on the emission of light and their microscopic detection which binds structural resolution to Abbe's law as optical limit. In the past the only possibility to reach resolution in low nm scale was electron microscopy with all its limitations concerning observation of living cells. However, during the last years, the development of new microscopic techniques like photoactivation localization microscopy (PALM) allowed to circumvent Abbe's law and reach resolutions of 5-20 nm. As conventional FP are not feasible for this approach, new variants had to be found or created that are photoactivatable (pa-FP).

1.6.3 Photoactivation localization microscopy

Photoactivation localization microscopy was developed in 2006 by three independent groups and is now known as PALM (Betzig *et al*., 2006), fluorescence photoactivation localization microscopy (FPALM; Hess *et al*., 2006) or stochastic optical reconstruction microscopy (STORM; Rust *et al*., 2006). All three microscopic techniques work with light-regulated on- and off-switching of single fluorescent molecules (pa-FP, see 1.6.4, p. 12) using short light flashes of adequate wavelength followed by microscopic detection over a certain period of time. The advantage in comparison to conventional fluorescence microscopy, where FP are simultaneously excited and individual signals are not any longer distinguishable, is that these

light flashes are very short or weak and therefore the chance to excite fluorescent molecules adjacent to each other is nearly excluded. This leads to a situation where single fluorescent molecules are excited and emit a specific signal until they are irreversibly bleached. Repeating this step until all molecules have lost their light emitting ability while taking thousands of images, makes it possible to calculate the exact position of every single signal using the mathematical algorithm of the point spread function (Figure 1.6). This technique allows resolutions of single molecules in the range of 5-20 nm in living cells.

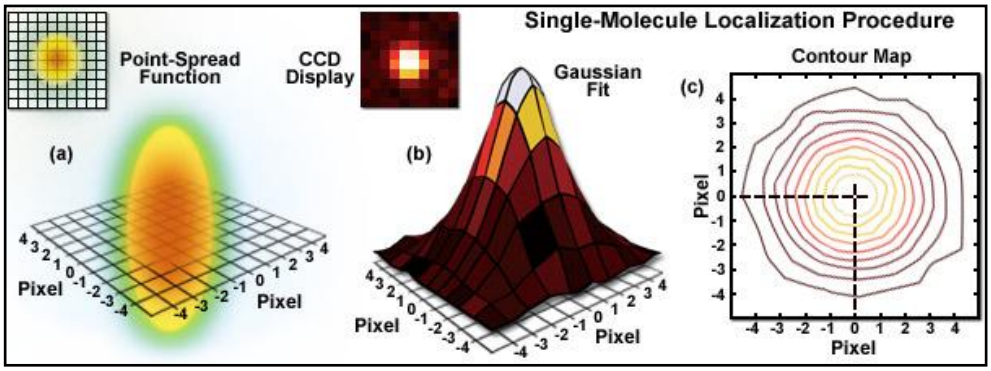

Figure 1.6: Single-Molecule Localization Prodedure of PALM. (A) The point-spread function of a widefield fluorescence microscope is superimposed on a wireframe representation of the pixel array from a digital camera in both two (upper left) and three-dimensional diagrams. The pixelated point-spread function of a single fluorophore as imaged with an EMCCD is shown in the upper left of (B), and modeled by a three-dimensional Gaussian function, with the intensity for each pixel color-mapped in the central portion of (B). (C) A contour map of the intensities. In cases where two contour maps overlap due to emission by fluorophores with a separation distance shorter than the diffraction limit, the centroid for each fluorophore can be individually localized by subtracting the point-spread function of one fluorophore from the other (after it enters a dark state or is photobleached) due to the temporal mapping strategy for generating PALM images.
(http://zeiss-campus.magnet.fsu.edu/articles/super-resolution/palm/introduction.html, as of December 2011)

1.6.4 Photoactivatable fluorescent proteins

Photoactivatable fluorescent proteins (pa-FP) are a subclass of fluorescent proteins. They are able to change their fluorescence emission properties in response to irradiation with light of specific wavelengths and intensity (Adam *et al*., 2008; Fuchs *et al*., 2010).

At the moment pa-FP are used for three kinds of experimental procedures. Super-resolution fluorescent microscopy techniques like photoactivation localization microscopy (PALM) are based upon these probes, enabling the visualization of cellular structures with a level of details never seen before in living cells. In a second approach pa-FP are used for so called pulse-chase experiments, in which a sub-population of fluorescent proteins in a cell can be activated by irradiation and their movements followed over time. The third application is the combination of both approaches using further developed pa-FP (Fuchs *et al*., 2010).

Whether a pa-FP is suited for a given experimental question depends on different parameters like their appearance as proteins. There are obligate tetramers and monomeric

pa-FP both with unique advantages and disadvantages. Tetrameric pa-FP are characterized by a relatively strong fluorescent signal and can be used to label whole cells and organelles. A possible disadvantage is the big size of the tetramer which might disrupt the localization and function of their fusion partner. Compared to tetrameric pa-FP, monomeric pa-FP are smaller and can therefore be used to label and track individual molecules inside a cell (for review, see Lukyanov *et al*., 2005). As a fusion with these proteins carries only one chromophore the signal is in theory weaker. Additional to that, pa-FP are sorted into three main groups according to their modes of photoactivation. A distinction is drawn between reversible photoswitching from a fluorescent to a non-fluorescent state or *vice versa* after photoactivation (photoswitching), and an irreversible change of fluorescent properties, either from a non-fluorescent to a fluorescent state or between two fluorescent states with different emission wavelengths (photoconversion; Lukyanov *et al*., 2005). Into the third group fall pa-FP which combine both mechanisms.

In this dissertation, a photoswitchable red fluorescent protein (psRFP) belonging to the first group of reversible photoswitching from a non-fluorescent to a fluorescent state, and a monomeric IRIS fluorescent protein (mIRISFP; Fuchs *et al*., 2010), combining photoconversion with reversible photoswitching, are fused to Lifeact and are stably expressed in tobacco BY-2 cells to allow a more detailed understanding of the actin cytoskeleton, its polarity and dynamics.

1.6.5 The photoactivatable fluorescent proteins psRFP and mIRISFP

The photoswitchable red fluorescent protein (psRFP)

The photoswitchable red fluorescent protein (psRFP) is a S-143-G mutation of the photoswitchable red fluorescent protein isolated from *Anemonia sulcata var. rufescens* (asRFP) with improved photoswitching properties and was characterized in the group of Prof. Dr. Nienhaus (Institute for applied physics and Center for Functional Nanostructures (CFN), Karlsruhe Institute of Technology (KIT)). Its structure is characterized by four monomers arranged as dimers of dimers, which is typical for FP isolated from anthozoa (Figure 1.7 B). The chromophore of psRFP can be isomerized from its non-fluorescent *trans*-conformation by illuminating with light of a wavelength of 561 nm into its red fluorescent *cis*-conformation (Figure 1.7 A). After illumation with light of wavelength of 450 nm, a clear decrease of fluorescence and a backshift of the chromophore into the non-fluorescent *trans*-conformation can be observed. Because of this mode of switching, the psRFP is sorted into the group of positive switchers. For super-resolution microscopy, this group is preferred over the group of negative switchers, which are switched from their fluorescent to their non-fluorescent state with the excitation light (Stiel *et al.*, 2008).

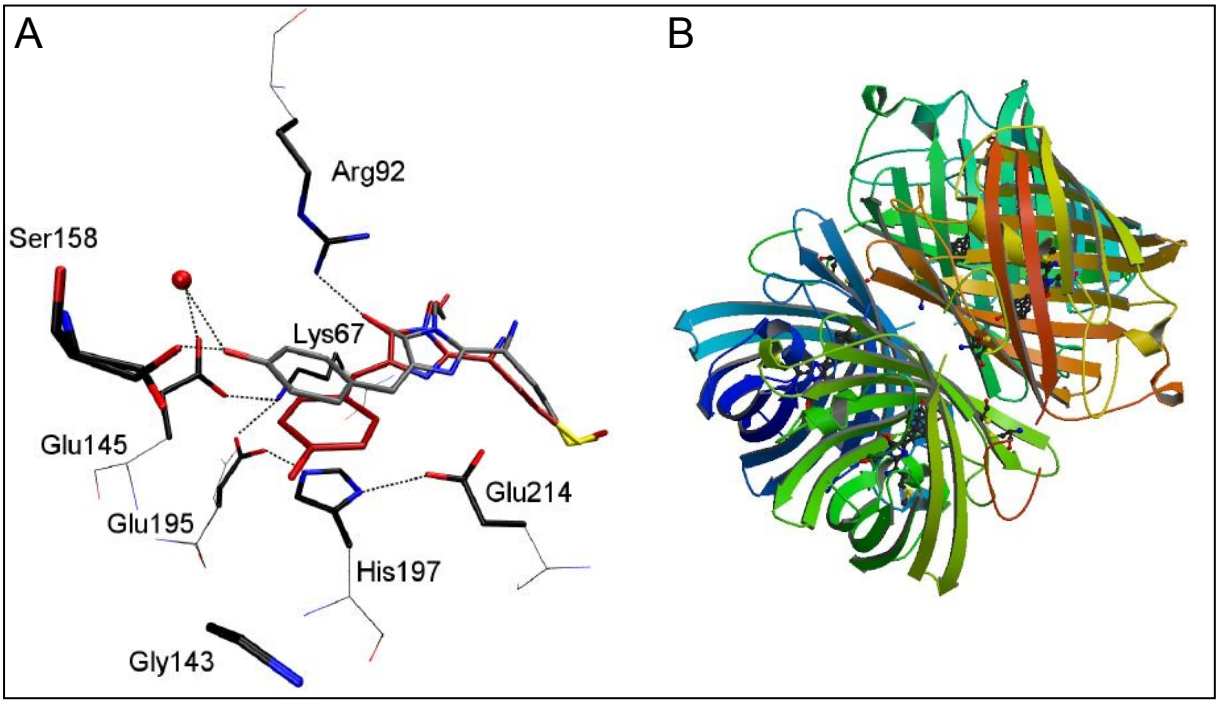

Figure 1.7: (A) The cis (red) and the trans (gray) chromophore of psRFP together with important amino acids in the direct chromophore environment are displayed. Color coding for surrounding residues: black = carbon; red = oxygen; blue = nitrogen. Water molecules are represented by red spheres, hydrogen bonds by dashed lines (Fuchs, 2011). (B) Dimer of dimers of psRFP in its non-fluorescent "off"-state (3CFH, RCSB Protein Data Bank, http://www.rcsb.org/pdb/, as of December 2011)

The monomeric IRIS fluorescent protein (mIRISFP)

This monomeric FP is a further development of IRISFP, a tetrameric pa-FP. It is named after the greek goddess of the rainbow and was characterized in the group of Prof. Dr. Nienhaus (Institute for applied physics and Center for Functional Nanostructures (CFN), Karlsruhe Institute of Technology (KIT)). Tetrameric IRISFP is a F-173-S mutant of tetrameric Eos-FP from *Lobophyllia hemprichii*, which responds to UV-violet-light (380 nm) irradiation with an irreversible photoconversion from a green- to red-emitting state (for review, see Lukyanov *et al*., 2005). The monomeric version mIRISFP differs from monomeric Eos-FP by three additional mutations (A-69-V, F-173-S, K-145-I and Y-189-A), and combines the advantages of monomeric pa-FP with the spectral properties of the tetramer (for review, see Wiedenmann *et al*., 2011). This pa-FP differs strikingly from conventional ones employing a single photoactivation mode and can be used either for pulse-chase experiments as well as super-resolution imaging. The property of photoconversion from a green- to a red-emitting state and the photoswitchablity from an “on” to an “off” state and *vice versa*, in both emitting states, makes a combination of both experimental procedures possible (Fuchs *et al*., 2010).

The peak of emitted fluorescence is at 515 nm (excitation at 486 nm) for the green form and at 578 nm (excitation at 546 nm) for the red form while the chromophores are in the *cis*-conformation. In both non-fluorescent forms, the chromophores are in the *trans*-conformation (Adam *et al*., 2008).

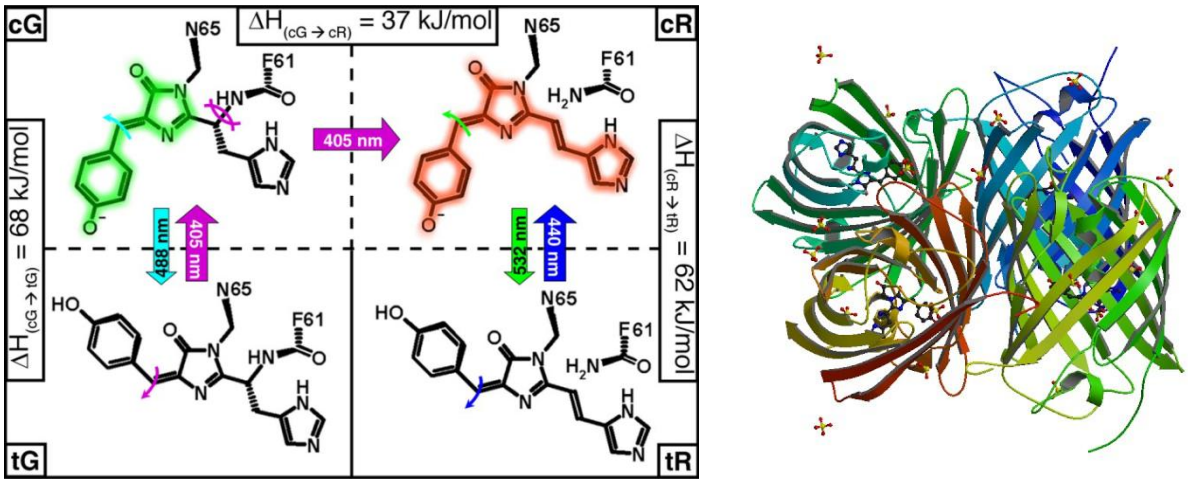

Figure 1.8: Photoinduced transformations in IrisFP. Structural motions induced by light are represented by curved arrows of the same color as those used to represent light illumination at specific wavelengths. cG, *cis*-green Iris; tG, *trans*-green Iris; cR, *cis*-red Iris; tR, *trans*-red Iris (Adam *et al*., 2008). On the right side additional protein structure of the tetrameric green *cis*-conformation (2VVH, RCSB Protein Data Bank, http://www.rcsb.org/pdb/, as of December 2011)

2. Materials and Methods

2.1 Tobacco cell cultures

BY-2 (*Nicotiana tabacum* L. cv BY-2) suspension cell lines (Nagata *et al*., 1992) were cultivated in liquid medium containing 4.3 g/L Murashige and Skoog salts (Duchefa Biochemie, Haarlem, the Netherlands), 30 g/L sucrose, 200 mg/L KH_2PO_4, 100 mg/L inositol, 1 mg/L thiamine, and 0.2 mg/L 2,4-D, pH 5.8. The cells were subcultivated weekly, inoculating 1.0 to 1.5 mL of stationary cells into fresh medium (30 mL) in 100-mL Erlenmeyer flasks. The cells were incubated at 26°C under constant shaking on a KS260 basic orbital shaker (IKA Labortechnik, Staufen, Germany) at 150 rpm. Every three weeks the stock BY-2 calli were subcultured on media solidified with 0.8 % (w/v) agar (Roth, Karlsruhe, Germany). Transgenic cells and calli were cultivated on the same media as non-transformed wild-type cultures (BY-2 WT), but supplemented with corresponding antibiotics (for more details, see **Appendix** 7.8, p. 96). In some experiments, the cell lines were assessed in the absence of selective pressure to exclude possible side effects without any detectable differences in patterning or arrangement of actin filaments.

2.2 Constructs

2.2.1 RNA preparation and reverse transcription

2 mL of cycling BY-2 WT (3 d after subcultivation, 100 mg of cells) were pipetted onto filter paper to remove the liquid medium. The cells were transferred with a spatula into a 2 mL reaction tube, immediately frozen in liquid nitrogen, and ground with a 5 mm steel bead in a TissueLyser (Quiagen, Hilden, Germany). Total RNA was extracted using a RNeasy Plant Mini Kit (Quiagen). Optional on-column digestion of genomic DNA was performed with RNase-free DNAse I (Quiagen) for 30 min at 37°C. Purity and integrity of the RNA-preparation were checked by electrophoresis. For reverse transcription, the Dynamo cDNA Synthesis Kit (Finnzymes, Vantaa, Finland) was used with 1 µg of RNA as template according to the manufacturer's instruction.

2.2.2 Cloning procedure

Plasmids for stable and transient transformation of BY-2 WT cells were constructed using the Gateway®-Cloning technology (Invitrogen Corporation, Paisley, UK). The sequences encoding the genes of interest (**Appendix** 7.1, p. 84) were amplified by PCR (for more details, see **Appendix** 7.4.1, p. 89) using oligonucleotide primers with Gateway®-specific

flanks (**Appendix** 7.3.1, p. 87). The size of the amplicons were verified by electrophoresis and purified via NucleoSpin® Extract II (Machery-Nagel, Düren, Germany) according to the manufacturer's instructions. The resulting gene-regions were inserted into the binary vector pK7WGF2 (Karimi *et al*., 2002; NtADF2, NtADF2, NtVLN1, NtVLN2), pH7WG2 (Karimi *et al*., 2002; Lifeact-psRFP, Lifeact-mIRIS), and pK7FWG2 (Karimi *et al*., 2002; NtWLIM2) following the manufacturer's protocol (**Appendix** 7.5, p. 91). A complete overview of all constructs can be found in the **Appendix** (7.6, p. 92).

The Lifeact-VENUS construct (Era *et al*., 2009) within a binary vector (pGWB2; Nakagawa *et al*., 2007) was a kind gift of Prof. Takashi Ueda (Laboratory of Developmental Cell Biology, University of Tokyo, Japan).

To confirm the accuracy of the sequences, all fusion constructs were verified by restriction digest and sequencing (GATC, Konstanz, Germany).

2.3 Transformation and establishment of tobacco BY-2 cells

2.3.1 Biolistic, transient expression

For biolistic transformation, gold particles (1.5-3.0 µm; Sigma-Aldrich, Taufkirchen, Germany) were coated with the corresponding construct according to a standard manual of BIO-RAD (PDS-1000/He Particle Delivery System manual; for details, see **Appendix** 7.7, p. 95) with the following modifications. Each transformation was performed using gold particles coated with 1 µg plasmid-DNA and placed on macrocarriers (BIO-RAD). Non-transformed BY-2 WT cells (750 µL), collected at different time points after subcultivation (2-5 d), were placed on PetriSlides™ (Millipore, Billerica, USA) containing 2 mL of solid medium. These loaded slides were transferred below a particle gun custom-made according to Finer *et al*. (1992), and bombarded by three shots with a pressure of 1.5 bar at a vacuum chamber of -0.8 bar. Following bombardment, the cells were incubated for 4-24 h in the dark at 26°C, and observed under the fluorescence microscope.

2.3.2 *Agrobacterium*-mediated, stable expression

Stable transformation of non-transformed BY-2 WT cells with the binary vector constructs pK7WGF2-NtADF1, pK7WGF2-NtADF2 and pGWB2-Lifeact-VENUS were achieved according to An (1985) with minor modifications. The constructs were transformed into *Agrobacterium tumefaciens* (strain LBA 4404; Invitrogen Corporation, Paisley, UK) via heatshock (5 min, 37°C). After three days of cultivation on selective medium, a single colony was raised in a 3-mL over-night culture. A 2-mL aliquot of 3-d-old BY-2 WT cells was co-

cultivated for further three days with 150 µl of the *A. tumefaciens* over-night culture at 28°C. Following co-cultivation, the cells were washed three times in liquid medium containing 100 mg/L cefotaxim, and then plated onto solid medium containing 100 mg/L kanamycin and 100 mg/L cefotaxim (pK7WGF2-constructs) or 50 mg/L hygromycin and 100 mg/L cefotaxim (pGWB2-construct). BY-2 calli, which were resistant to the antibiotics, appeared from 21 days of incubation in the dark at 26°C. These calli were transferred onto new plates. After further 21 days, the calli had reached approximately 1 cm in diameter. At this stage, cell-suspension cultures were established from these calli using 25-50 mg/L kanamycin (pK7WGF2-NtADF1, pK7WGF2-NtADF2) or 30 mg/L hygromycin (pGWB2-Lifeact-VENUS) added to the liquid medium for selection. 28 days later, cell lines with clear fluorescence were selected by observation under the fluorescence microscope.

2.3.3 *Agrobacterium*-mediated, stable expression

Stable transformation of non-transformed BY-2 WT cells with the binary vector constructs pK7WGF2-NtVLN1, pK7FWG2-NtWLIM2, pH7WG2-Lifeact-psRFP, pH7WG2-Lifeact-mIRIS, and pOpOff2(kan)-NtADF2 RNAi was achieved according to Buschmann *et al*. (2010) with minor modifications. The preparation of the BY-2 cells started with a subcultivation of 3 mL of a 7-d-old non-transformed tobacco BY-2 cell culture in 60 mL MS-media in a sterile 200 mL flask for three days at standard conditions (see 2.1, p. 16). Thereafter, the cells were washed twice with 200 mL sterile Paul's medium (4.3 g/L Murashige and Skoog salts without vitamins (Duchefa Biochemie, Haarlem, the Netherlands), 10 g/L sucrose, pH 5.8) and resuspended in 10 mL of Paul's media leading to a five-fold concentrated cell density. 1 mL of these concentrated cells was added to *A. tumenfaciens* transformed as described in 2.3.2 and processed as follows. The OD_{600} of the over-night culture was determined and 5 mL of fresh LB-media (plus corresponding antibiotics) were inoculated with these bacteria to an OD_{600} of 0.15. After several hours of growth 1 mL of the transformed *A. tumenfaciens* bacteria was harvested at an OD_{600} of 0.8 by centrifugation at 10000 g (HERAEUS Pico 17 Centrifuge, Thermo Scientific, Langenselbold, Germany) for 1 min in a 1.5 mL reaction tube. The supernatant was removed and the pellet resuspended in 30 µL of Paul's medium. After adding the BY-2 cells to the resuspended bacteria the reaction tube was agitated for 5 min at 100 rpm for a better mixing of the cells. In the next step this mixture was dropped in 100 µL aliquots on plates with Paul's agar (Paul's media solidified with 0.5 % (w/v) Phytagel (Sigma P8169), without antibiotics). After 4 days of incubation at 26°C in the dark the grown cell plaques were transferred and cultivated on new plates with MS agar under selective pressure as described above (see 2.1).

2.4 Visualization of actin filaments by phalloidin-based staining

Actin filaments were visualized by the method of Kakimoto and Shibaoka (1987) modified according to Olyslaegers and Verbelen (1998) as described in Maisch *et al*., 2009. 200 µL of suspended cells were fixed for 10 min in 1.8 % (w/v) paraformaldehyde in standard buffer (0.1 M PIPES, pH 7.0, supplemented with 5 mM $MgCl_2$, and 10 mM EGTA). After a subsequent 10-min fixation in standard buffer, cells were rinsed twice for 10 min with phosphate-buffered saline (0.15 M NaCl, 2.7 mM KCl, 1.2 mM KH_2PO_4, and 6.5 mM Na_2HPO_4, pH 7.2). Then, the resuspended cells were incubated for 35 min with 0.5 mL of 0.66 µM TRITC-phalloidin (Sigma-Aldrich, Taufkirchen, Germany) prepared freshly from a 66 mM stock solution in 96 % (w/v) ethanol by dilution (1:100, v/v) with phosphate-buffered saline. Cells were then washed three times for 10 min in phosphate-buffered saline and observed immediately. The same protocol was used to visualize the colocalization of GFP-NtADF2 with actin filaments. To visualize the colocalization of Lifeact-psRFP with actin filaments the TRITC-phalloidin was exchanged by Alexa-Fluor® 488.

2.5 Quantification of pattern and morphology

All experiments related to division synchrony, mitotic index, cell length and width were observed to be not affected by antibiotic selection.

2.5.1 Determination of frequency distribution, cell length and width

Division synchrony of tobacco BY-2 cells was quantified by collecting 0.5-mL aliquots of cells 4 d after inoculation and immediate observation under an AxioImager Z.1 microscope (Zeiss, Jena, Germany). In addition, the NtADF2 RNAi knockout cell line was induced at inoculation using 10 µM dexamethasone (Roth, Karlsruhe, Germany). Differential interference contrast images were obtained by a digital imaging system (AxioVision; Zeiss). For each picture, the MosaiX module of the AxioVision software was used to cover a 5x5 mm area with 256 single pictures at an overlay of 15 %. Using the stitching-function, frequency distributions over the number of cells per individual file were constructed (Maisch *et al*., 2007). Each data point represents between 921 and 1158 cell files from at least three independent experimental series. Cell length and width were also determined from the central section of the cells using the length function of the AxioVision software according to Maisch *et al*. (2007). Each data point represents mean and standard error from 500 individual cells from three independent experimental series. The results were tested for significance by a Student's t-test at a 95 % confidence level.

2.5.2 Determination of mitotic indices

The mitotic index (MI) of tobacco BY-2 cell suspension was determined following fixation with Carnoy fixative [3:1 (v/v) 96 % (v/v) ethanol:glacial acetic acid, supplemented with 0.25 % v/v Triton X-100]. Nuclei were stained with 1 µg mL^{-1} of Höchst 33258 (2'-(4-hydroxyphenyl)-5-(4-methyl-1-piperazinyl)-2,5'-bi(1H-benzimidazole)-trihydrochloride; Sigma-Aldrich, Taufkirchen, Germany), diluted from a 0.5 mg mL^{-1} filter-sterilized stock solution in distilled water for 5 min. Samples were observed after further 5 min of incubation under an AxioImager Z.1 microscope (Zeiss, Jena, Germany) using the filter set 49 (excitation at 365 nm, beamsplitter at 395 nm, and emission at 445 nm). Mitotic indices were determined as the relative frequency of mitotic cells out of a sample of 500 cells scored for each data point.

2.6 Microscopy and image analysis

For morphological studies, cells were examined under an AxioImager Z.1 microscope (Zeiss, Jena, Germany) equipped with an ApoTome microscope slider for optical sectioning and a cooled digital CCD camera (AxioCam MRm; Zeiss). TRITC-/RFP-, YFP- and GFP-/Alexa-Fluor® 488-fluorescence were observed through the filter sets 43 HE (excitation: 550 nm, beamsplitter: 570 nm, emission: 605 nm), 46 HE (excitation: 500 nm, beamsplitter: 515 nm, emission: 535 nm) and 38 HE (excitation: 470 nm, beamsplitter: 495 nm, emission: 525 nm), respectively (Zeiss). Stacks of optical sections were acquired at different step sizes between 0.4 and 0.8 µm. Images were processed and analyzed using the AxioVision (Rel. 4.8.2) software as described above.

For analysis of division pattern, cells were observed under the same microscope with a 20x objective and differential interference contrast illumination. Images were processed for publication with respect to contrast and brightness using ImageJ (NIH, Bethesda, USA).

For photoactivation localization microscopy (PALM) of Lifeact-psRFP ox BY-2 cells 0.5 mL cells of various days after subcultivation were transferred from their standard cultivation flasks (see 2.1, p. 16) into Chamber Slides™ (4 chambers, Thermo Scientific, Langenselbold, Germany) and observed under the photoactivation localization microscope kindly provided by the lab of Prof. U. Nienhaus (Institute for Applied Physics and Center for Functional Nanostructures - CFN, Karlsruhe Institute of Technology – KIT). The microscope setup for imaging of living Lifeact-psRFP ox BY-2 cells was as follows: 100x objective, 30-50 ms camera exposure time, 300 gain, 4.7x preamp, 5-20 mW 561 nm, <1 mW 473 nm, Andor Solis (Rel. 4.0; http://www.andor.com/software/solis/ as of January 2012). The calculation of the exact position of every single signal using the mathematical algorithm of the point spread

function was performed using an inhouse software written in Matlab R2009b (http://www.mathworks.de/products/matlab/ as of January 2012).

The test for photostability of the Lifeact-psRFP and the RFP-FABD2 BY-2 cell line was performed in the Institute for Applied Physics and Center for Functional Nanostructures by P.N. Hedde. Transgenic cells were taken 3 d after subcultivation and constantly excitated with light of a wavelength of 561 nm at 10 W/cm^2. For 1200 sec every 10 sec an image was taken and the emission intensity measured using the software mentioned above.

2.7 PIP_2, phalloidin, latrunculin B, and auxin treatments

PIP_2 (Phosphatidylinositol 4,5-bisphosphate; Sigma-Aldrich, Taufkirchen, Germany) was added at inoculation from filter-sterilized stocks of 2 µM in chloroform:methanol:0.5 M HCl (10:5:1) to a final concentration of 50 nM, a concentration that had been found in preparatory studies to leave cell division and culture growth unaffected.

Phalloidin from *Amanita phalloides* (Sigma-Aldrich) was added directly to the final concentration of 1 µM into the standard culture medium using a filter-sterilized stock of 1 mM phalloidin dissolved in 96 % (v/v) ethanol.

Latrunculin B from *Latrunculia magnifica* (Sigma-Aldrich) was added directly to the final concentration of 65 nM into the standard culture medium using a filter-sterilized stock of 1 µM latrunculin B dissolved in 96 % (v/v) ethanol.

NPA (1-N-naphthylphthalamic acid; Sigma-Aldrich) was added at inoculation from a filter-sterilized stock of 10 mM in dimethyl sulfoxide to a final concentrations of 10 µM. Auxins were also added directly to the final concentration of 2 µM into the standard culture medium using filter-sterilized stocks of 10 mg/mL IAA (Sigma-Aldrich) and 10 mg/mL 2,4-D (Sigma-Aldrich) dissolved in 96 % (v/v) ethanol, respectively.

Equal aliquots of sterile solvents were added to the control samples as solvent controls.

2.8 Preparation of tobacco BY-2 protoplasts

For preparation of tobacco BY-2 protoplasts 4 mL of Lifeact-psRFP ox cells were taken 3 d after subcultivation according to Kuss-Wymer and Cyr (1992) and Wymer *et al.* (1996). The cells were pipetted into petrislides (diameter 10 cm) together with 4 mL of enzyme solution (sterile filtered 1 % (w/v) cellulase YC, and 0.1 % (w/v) pectolyase Y-23 in 0.4 M mannitol, pH 5.5) and incubated for 6 h at 27°C under constant shaking on an orbital shaker (100 rpm).

In the next step the protoplasts were transferred from the petrislides into 15 mL reaction tubes and sedimented by centrifugation for 5 min at 250 g. The supernatant was discarded. Following this step, the protoplasts were washed three times with washing solution (sterile filtered 4.3 g/L Murashige and Skoog salts (Duchefa Biochemie), 10 g/L sucrose, 100 mg/L inositol, 0.5 mg/L nicotinic acid, 0.5 mg/L pyroxidine-HCl, 0.1 mg/L thiamine in 0.25 M mannitol). After each washing and centrifugation step the protoplasts were resuspended in fresh washing solution.

For regeneration, the washed protoplasts were transferred into small petrislides (diameter 5 cm) with regeneration solution (sterile filtered 4.3 g/L Murashige and Skoog salts (Duchefa Biochemie, Haarlem, the Netherlands), 10 g/L sucrose, 100 mg/L inositol, 0.5 mg/L nicotinic acid, 0.5 mg/L pyroxidine-HCl, 0.1 mg/L thiamine, 0.1 mg/L NAA, 1 mg/L benzylaminopurine in 0.25 M mannitol). The slides were sealed and stored at 27°C in darkness without shaking.

To all used solutions hygromycin in a final concentration of 30 mg/L was added. Observation of the protoplasted Lifeact-psRFP ox BY-2 cells started immediately after the transfer into regeneration solution using an AxioImager Z.1 microscope (Zeiss, Jena, Germany) equipped with an ApoTome microscope slider for optical sectioning and a cooled digital CCD camera (AxioCam MRm; Zeiss), and was repeated every 24 h up to 3 d.

2.9 Determination of actin-binding-protein expression by semi-quantitative RT-PCR

2.9.1 General procedure

The overexpression of the introduced ABP in the corresponding cell line was verified by semi-quantitative RT-PCR in samples of non-transformed BY-2 WT and mTalin overexpressing cells collected at day 4 after subcultivation. The reverse transcription, performed as described in 2.2.1, was followed by a PCR using standard Taq polymerase (NEB, Ipswich, USA) according to the manufacturer's instructions. PCR conditions were chosen as described in **Appendix** (7.4.2, p. 90). To ensure a reproducible quantification, the number of cycles was selected such that the amplification of templates for all primers was in an exponential range (**Appendix** 7.4.2, p.91), and the products were clearly visible on 2 % agarose gels, stained with SYBR Safe (Invitrogen Corporation, Paisley, UK). For detection of ABP cDNA levels in tobacco BY-2, the primers listed in **Appendix** 7.3.2 (p. 88) were used. NtActin (for primers, see **Appendix** 7.3.2, p. 88) and NtGAPD (Hu *et al*., 2010) were used as internal standards. The gels were quantified by grey-value analysis using ImageJ (NIH, Bethesda, USA).

2.9.2 Expression tests after auxin treatment

The expression level of representative ABP of different families was checked after treatment with IAA. Therefore IAA was added to a final concentration of 10 and 30 µM to non-transformed BY-2 WT and mTalin-YFP-overexpressing cells 4 days after subcultivation. Every 15 min a sample of 2 mL was taken from both cell lines up to 2 h. Each sample was processed as described in 2.2.1 followed by a PCR and analyzed as described in 2.8.1 (for primers and PCR protocol, see **Appendix** 7.3.2, p. 88 and 7.4.2, p. 90). All data points represent mean of three independent experimental series.

3. Results

This chapter is separated into three main parts. The generation of new transgenic *Nicotiana tabacum* BY-2 cell lines and expression analysis of selected actin-binding proteins after auxin treatment is described in the first part. The second part focuses on the results dealing with the *Nicotiana tabacum* actin-depolymerizing factor 2 (NtADF2). Finally, the last part deals with photoactivatable fluorescent proteins (pa-FP) in super-resolution microscopy of living plant cells with the aim to discriminate actin filament sub-populations that are differentially decorated with ABP.

3.1 Efficient transformation of BY-2 cells using the TAMBY-2 method

The functional screen of selected ABP requires a transformation protocol that is highly efficient and reliable. Although BY-2 cells are amenable to transformation, the yield has been very low. Therefore, a new method for stable transformation had to be developed. The method of transient *Agrobacterium*-mediated transformation of BY-2 cells (TAMBY-2) was developed by Buschmann *et al*. (2011). In this dissertation the transient method was modified and expanded in order to stably transform BY-2 cells. After the respective ABP homologues had been cloned from the homologous system (BY-2), it was possible to generate ABP overexpressing (ox) BY-2 marker cell lines of several selected families at high efficiency using this method. In addition to the already existing *A. thaliana* fimbrin actin-binding domain 2 ox (GFP-FABD2; Maisch *et al*., 2009), the mTalin ox (mTalin-YFP; Maisch and Nick, 2007) and the WLIM-domain containing protein 1 ox cell line (GFP-WLIM1; Thomas *et al*., 2006), new *Nicotiana tabacum* villin 1 ox (GFP-NtVLN1 ox), *Nicotiana tabacum* WLIM-domain containing protein 2 ox (NtWLIM2-GFP ox), *Nicotiana tabacum* actin-depolymerizing factor 1 ox (GFP-NtADF1 ox), *Nicotiana tabacum* actin-depolymerizing factor 2 ox (GFP-NtADF2 ox), and two Lifeact-based marker lines (Lifeact-psRFP ox; Lifeact-mIRIS ox) could be established during this work. A third Lifeact-based BY-2 cell line with a modified yellow fluorescent fusion protein called VENUS (Lifeact-VENUS ox; Era *et al*., 2009) was produced using the traditional transformation method of An (1982).

These ABP ox cell lines are now available to address the question of this work, if or how representative members of different ABP-families are important for auxin dependent, patterned cell division in the homologous system, as well as for other microfilament-based approaches. From this effort a cell line “library” could be established comprising lines where actin filaments only slightly bundled to lines with heavy bundling. Figure 3.1 shows

exemplarily fluorescence microscopic images of these new transgenic cell lines. As reference a non-transformed WT cell with TRITC-phalloidin stained actin filaments is depicted (Figure 3.1 A).

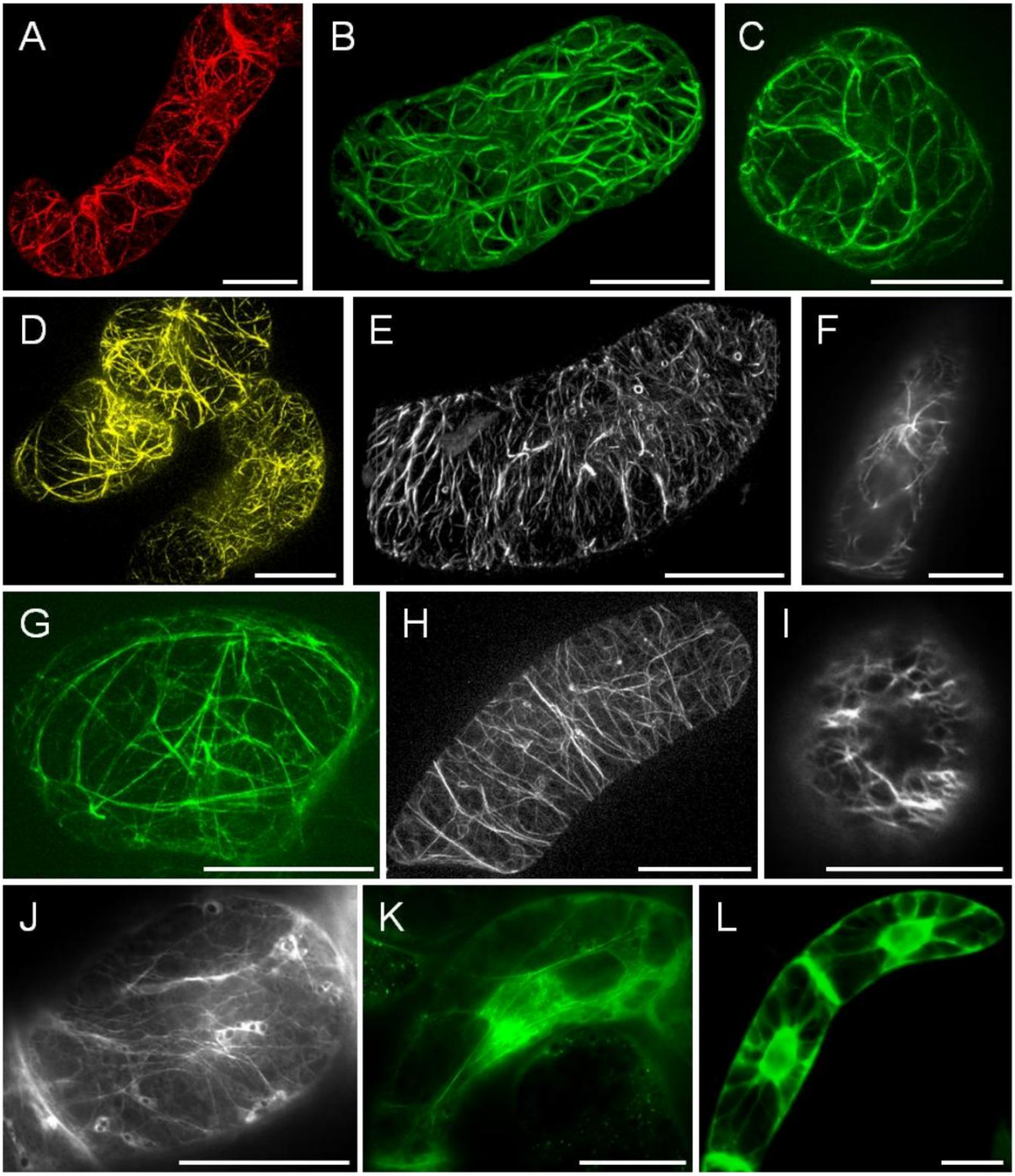

Figure 3.1: Representative Images of TRITC-phalloidin stained non-transformed BY-2 WT cells (A) and transgenic actin marker lines (B-L). (A) 3 d old non-transformed BY-2 WT cells; actin stained with TRITC-phalloidin. (B,C) Transient GFP-NtADF2 ox BY-2 cells. (D) Stable Lifeact-VENUS ox BY-2 cells. (E) Transient Lifeact-psRFP ox BY-2 cell. (F) Stable Lifeact-mIRIS ox BY-2 cell, sub-cortical section. (G) GFP-FABD2 ox BY-2 cell; Maisch *et al*., 2009. (H) Stable NtWLIM2-GFP ox BY-2 cell. (I) Stable Lifeact-mIRIS ox BY-2 cell, cortical section of a cell file tip. (J-L) Stable GFP-NtVLN1 ox BY-2 cells; cortical (J), sub-cortical (K) and central (L) section. Bars: 20 µm.

3.2 Pre-screening of ABP ox BY-2 cell lines revealed promising candidate for auxin-induced pattern formation

A screening for auxin-dependent alterations in the different ABP ox cell lines was performed, focusing on the division pattern (DP), which was known as sensitive monitor for polar auxin flow (Campanoni *et al.*, 2003; Maisch and Nick, 2007). In addition to this parameter also mitotic index and the ratio of cell length over width was checked with more (GFP-NtADF2 ox) or less (other screened ABP) clear differences as compared to the non-transformed BY-2 cell line.

3.2.1 Comparison of division pattern in different ABP ox cell lines

Especially the DP showed distinctive differences between the representatives of ADF (NtADF2), the other ABP ox lines, and the non-transformed BY-2 cell line (Figure 3.2).

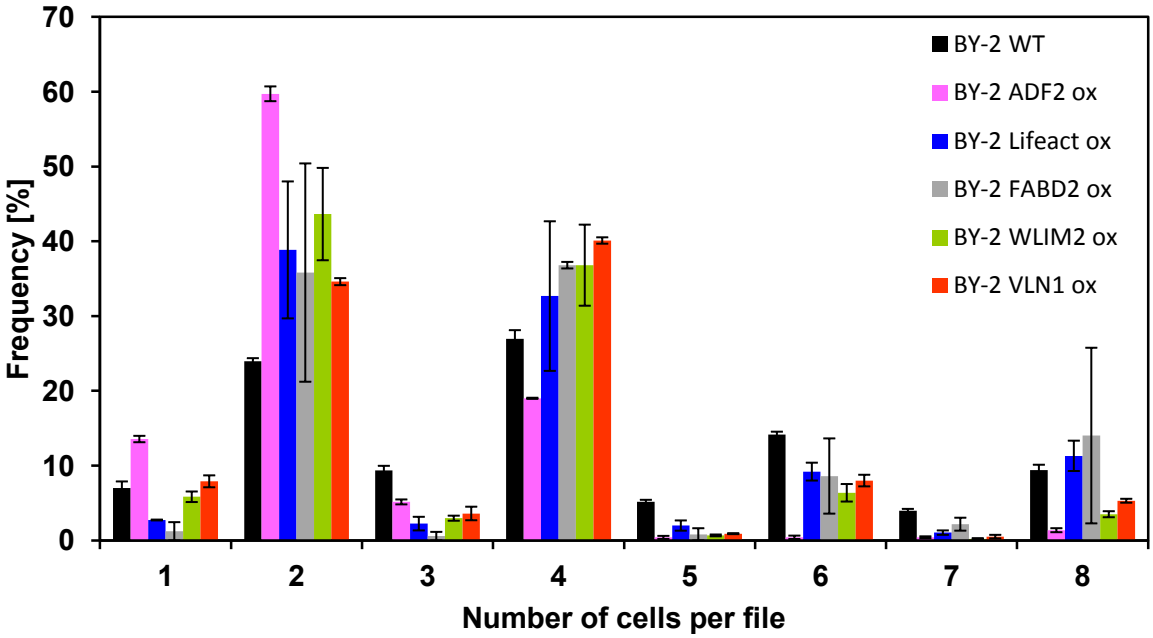

Figure 3.2: Pre-screening of the division pattern of several transgenic BY-2 cell cultures, overexpressing selected representatives of different actin-binding protein families. BY-2 WLIM2 ox and BY-2 VLN1 ox data (Leonhard, 2011). BY-2 Lifeact ox data are derived from Lifeact-Venus ox cell line. All bars represent data of at least 2 independent experimental series. Error bars=SE.

A non-transformed WT BY-2 cell culture was used as control for DP and showed the characteristic pattern with clear peaks at even numbers of cells per file as expected and described in Maisch and Nick (2007). All transgenic cell cultures tested in this pre-screening featured also at least a similar pattern. However, peaks were more pronounced for bicellular (Lifeact ox: +62 %; FABD2 ox: +49 %; WLIM2 ox: +82 %; VLN1 ox: +44 %), and quadricellular (Lifeact ox: +21 %; FABD2 ox: +36 %; WLIM2 ox: +36 %; VLN1 ox: +49 %) and a simultaneously slightly reduced peak for hexacellular files, which is the diagnostic

marker for the efficiency of auxin transport (Lifeact ox: -35 %; FABD2 ox: -39 %; WLIM2 ox: -55 %; VLN1 ox: -43 %). The lines expressing the actin markers Lifeact and FABD2 were closest to the DP of non-transformed cells with even the frequency of octacellular files being at a comparable level. Up to hexacellular files, diagnostic for directional synchrony (Campanoni *et al.*, 2003), also the actin-bundling protein overexpressing cell lines showed only moderate alterations from the characteristic oscillatory behaviour with clear peaks at even cell numbers. However the frequency of octacellular files was clearly reduced by 63 % (WLIM2 ox) and 44 % (VLN1 ox). The GFP-NtADF2 ox cell line behaved completely different from the other ABP ox cell lines with a massively elevated peak of bicellular (+ 149 %), and a clear reduction for quadricellular files (-30 %) accompanied by an almost complete loss of files with more than four cells (-97 % hexacellular files; -86 % octacellular files). This qualitative difference shifted the GFP-NtADF2 ox cell line into the focus. It was therefore decided to characterize this cell line in more detail (see 3.3, p. 29).

3.2.2 IAA does not affect expression level of selected ABP

In parallel to the pre-screening of the transgenic cell lines, an analysis of ABP transcript levels after auxin treatment was performed. For this experimental procedure, auxin was added in different final concentrations (10 µM and 30 µM for up to 1 h) to a mTalin-YFP ox cell line, where actin filaments are constitutively bundled. It was known from Maisch and Nick (2007) that actin filaments are clearly debundled after addition of exogenous auxin within 20 min. If this debundling were mediated by an altered expression level of ABP, it would become detectable by this approach. In a first test a final concentration of 10 µM external IAA was added to the cells and the transcript level checked by qPCR every 15 min. However, it was not possible to detect any significant up- or down-regulations during this experiment (Figure 3.3 A). Even an increased concentration of 30 µM IAA produced no detectable effect during the monitored time frame (Figure 3.3 B).

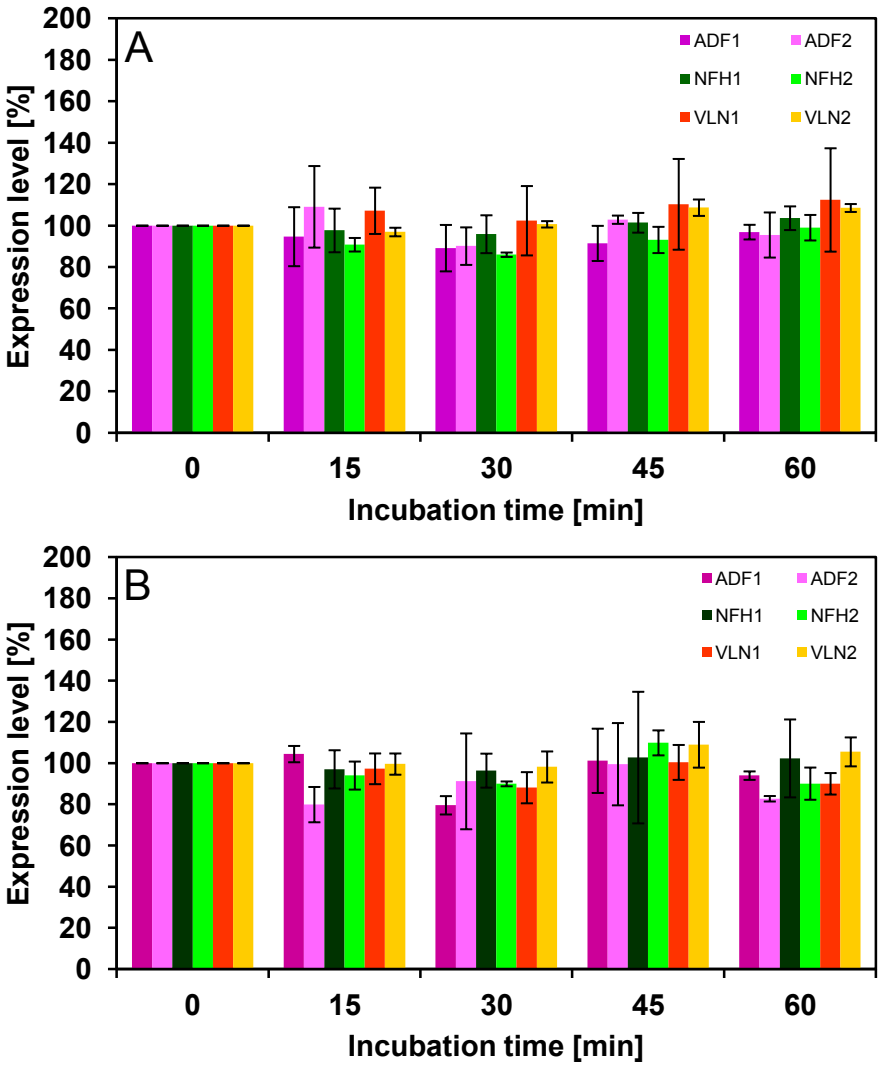

Figure 3.3: Expression analysis of different actin-binding protein family members in BY-2 cell culture after IAA treatment (A) 10 µM final concentration. (B) 30 µM final concentration. All experimental data are derived from three independent experimental series. Error bars=SE.

3.3 *Nicotiana tabacum* actin-depolymerizing factor 2

Nicotiana tabacum actin-depolymerizing factor 2 (NtADF2; NCBI accession number: AAL91667; Chen *et al.*, 2002) was chosen as promising candidate for auxin-dependent actin re-organization from a screen, where tobacco homologues of ABP were investigated for their intracellular localization and the division pattern of the corresponding overexpressing cell lines (see 3.2, p. 26).

3.3.1 NtADF2 – a member of ADF-subgroup 2

Compared to animals, plants harbor numerous ADF/cofilin genes. In 2000 Mun *et al*. classified plant ADF/cofilins into four groups (Figure 3.4) which was supported by further analysis and expansion of the dataset by Maciver and Hussey (2002). For this dissertation, some representatives of important cell biological model plants were selected for each group. Group 1 contains exclusively ADFs of dicots with one exception, an ADF of *O. sativa* (NCBI accession number: NP_001054456) whereas Group 2 and Group 3 combine monocots as well as dicots. The first identified member of Group 4 was ADF3 of *Z. mays* (NCBI accession number: NP_001105474). Southern blot analysis by Danyluk *et al*. (1996) revealed similar sequences only in monocots, leading to the assumption that this group is also exclusive for monocots.

NtADF2 clusters together with NtADF1 into subgroup 2 of plant ADF/cofilin members (Maciver & Hussey, 2002), so far thought to be exclusively present in pollen (Figure 3.4). The nearest non-tobacco homologs are the ADF7 and ADF10 of *A. thaliana.*

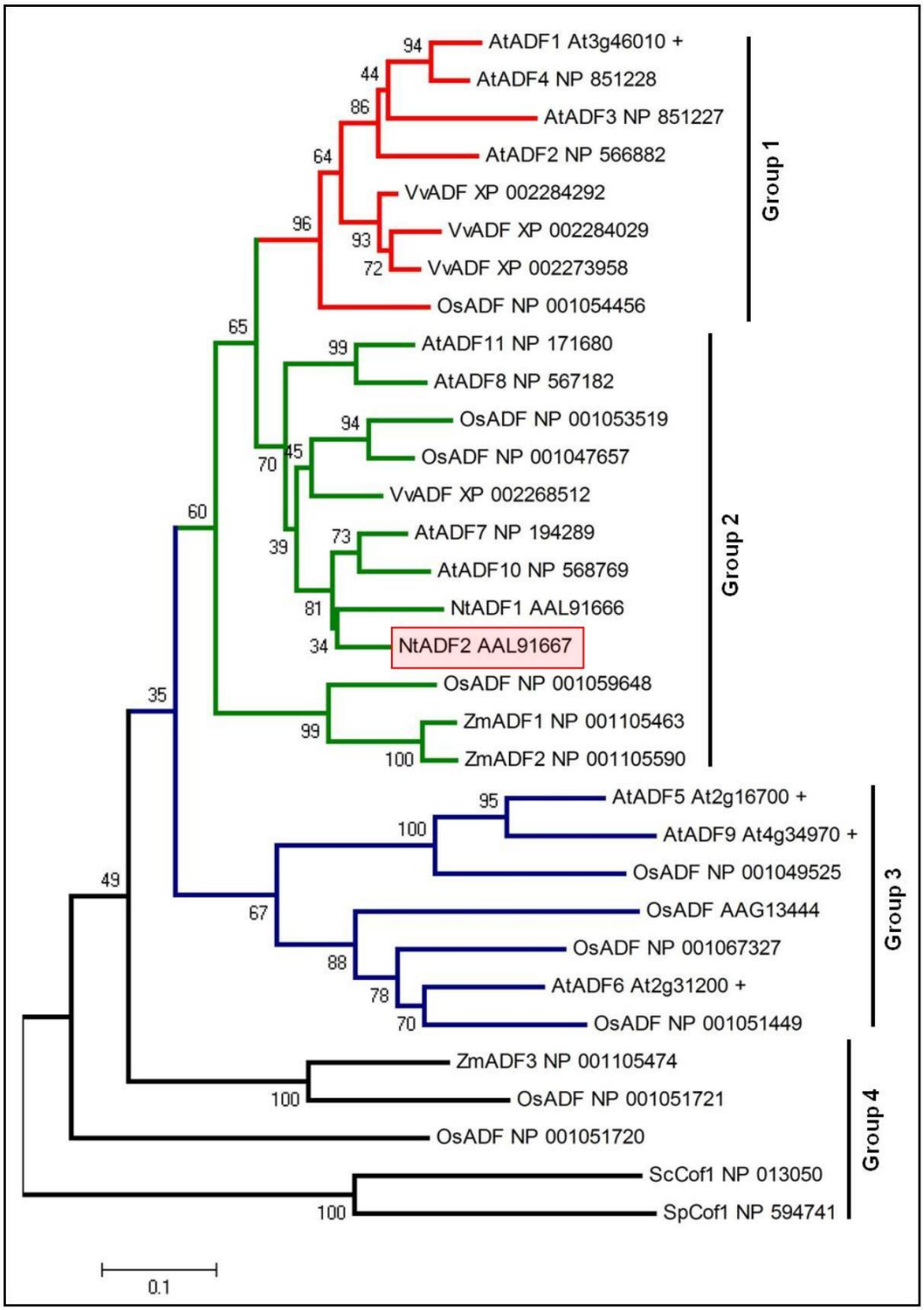

Figure 3.4: A phylogenetic tree of representative model plant ADFs. An alignment of the complete sequences was made with MEGA 4.1 (beta 3); from this data a phylogenetic tree was derived using neighbor-joining method and bootstrapping (1000 reiterations). The output tree was plotted also using MEGA 4.1 (beta 3). All data were taken from published literature and genomic databases. Entries marked with + are listed in the Tree Families Database (Treefam) of the Sanger Institute, all other entries are derived from the National Center for Biotechnology Information database (NCBI). Categorization into 4 groups was performed in accordance with Maciver and Hussey (2002). *Arabidopis thaliana* AtADF; *Vitis vinifera* VvADF; *Oryza sativa* OsADF; *Zea mays* ZmADF; as outgroup cofilin 1 of *Saccheromyces cerevisiae* ScCof1 and *Saccheromyces pombe* SpCof1 was used.

NtADF2 is predicted to consist of 137 amino acid residues with a molecular mass of 15 kD (Chen *et al.*, 2002) and several highly conserved domains. A serine-6 identified as phosphorylation site (Chen *et al.*, 2002) is followed by an actin-binding motif (amino acids 6, 7, 96, 98, 123 and 126). This actin-binding motif is accompanied by a second signature specific for F-actin binding with conserved amino acids 80, 82, 134 and 135. Interestingly, from amino acid 22-28, a predicted nuclear localization sequence is highly conserved in NtADF2 as in all former investigated ADF homologs (Maciver *et al.*, 2002). Moreover, NtADF2 also contains all positively charged amino acids essential for the electrostatic interaction with PIP_2 (Zhao *et al.*, 2010) at position 80 (Lys), 98 (Lys), 109 (Lys), 110 (Arg) suggesting that NtADF2 is able to interact with and can be regulated by PIP_2 (Figure 3.5).

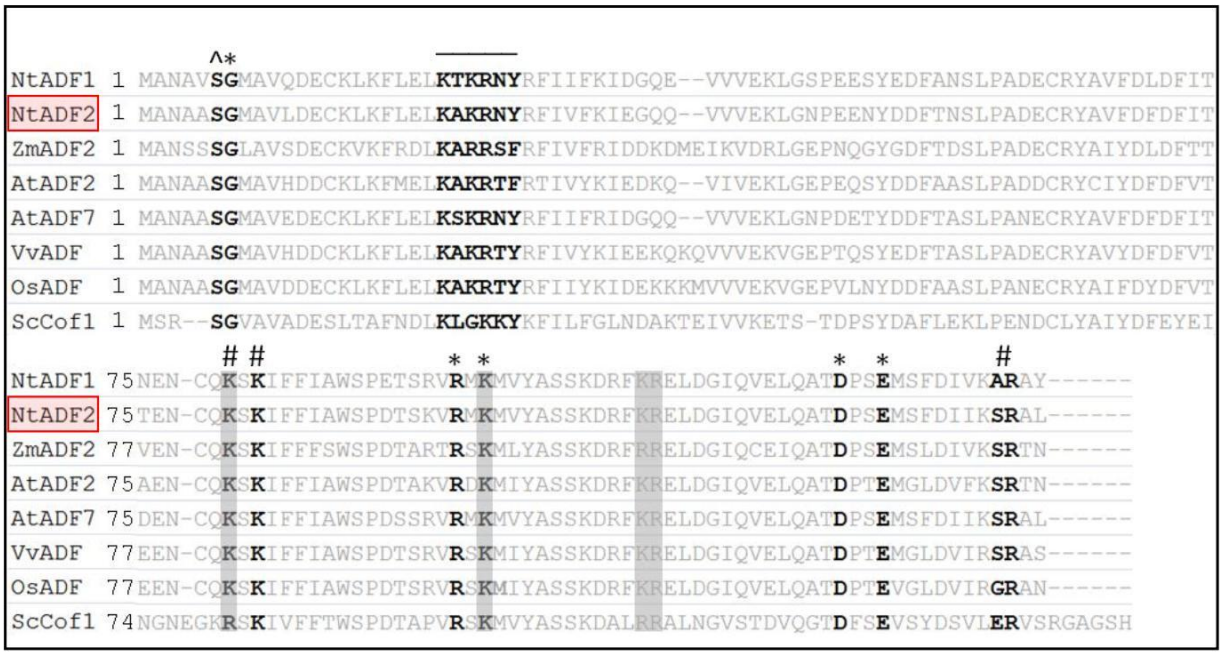

Figure 3.5: An alignment of selected representative model plant ADFs derived from phylogenetic tree analysis of Figure 3.4. As representative protein sequences of *Vitis vinifera* VvADF XP_002284292 and for *Oryza sativa* OsADF NP_001054456 were chosen. All other sequences correspond to Figure 3.5. Black color marks important protein domains: Phosphorylation site *circumflex*; G-actin-binding sites *asterisks*; nuclear localization site *overline*; specific F-actin-binding sites *number sign* (NCBI); PIP_2 interacting sites *grey boxes* (Zhao *et al.*, 2010).

3.3.2 Intracellular localization of NtADF2

To get insight into the role of NtADF2 for actin organization and auxin-dependent patterning, a N-terminal fusion of GFP and the *Nicotiana tabacum* ADF2 (GFP-NtADF2) was overexpressed in the homologous system BY-2, either by transient transformation via particle bombardment (Figure 3.6 A-C) or in a stable manner via *Agrobacterium tumefaciens* followed by selection on kanamycin leading to the GFP-NtADF2 ox cell line (Figure 3.6 D-F).

Figure 3.6 A-C exemplarily shows transiently transformed BY-2 cells 4 h (A), 17 h (B), and 24 h (C) after biolistic transformation. To test for potential changes dependent on the development of the culture, this experiment was performed at different time points. As shown

exemplarily for 3 d (B), 4 d (A), and 5 d (C) after subcultivation, GFP-NtADF2 labeled filamentous structures that resembled actin bundles consistent with observations in transformed pollen tubes (Chen *et al.*, 2002). The fine cortical filaments visualized by other markers such as GFP-FABD2 (Maisch *et al.*, 2009; Figure 3.1 G) or Lifeact-psRFP (Figure 3.1 E) were not observed. Additionally to the bundled filaments, the GFP-signal was found in the nucleus and the cytoplasm, independent of culture stage and incubation time after biolistic transformation.

Cytoplasmic localization was also dominant in the stably transformed tobacco cell line (Figure 3.6 D). However, in a sub-population of stably transformed cells, the GFP marked filamentous (Figure 3.6 E) or fragmented structures (Figure 3.6 F).

To test, whether the filaments visualized by the GFP-marker are AF, the GFP-NtADF2 ox line was stained with TRITC-phalloidin. Since phalloidin and ADF2 share their binding site on actin, they are expected to compete for binding (Nishida *et al.*, 1987; Hayden *et al.*, 1993; Jiang *et al.*, 1997). In fact, in the staining experiment, most cells either showed the GFP-labeled bundles or the TRITC-labeled AF. However, in a sub-population of cells, where the GFP-signal was moderate, dual visualization was successful (as exemplarily shown in Figure 3.6 H, I). Those cells lacked the cortical actin meshwork that can be observed in non-transformed BY-2 WT cells after staining with TRITC-phalloidin (Figure 3.6 J).

Comparison of actin organization revealed clear differences according to the existence of fine AF. Although NtADF2 is overexpressed, the thick actin cables in the transgenic line (Figure 3.6 K1) remained unaltered compared to non-transformed cells (Figure 3.6 J1). In GFP-NtADF2 ox cells the fine actin meshwork was either completely missing (Figure 3.7 B) or highly fragmented (Figure 3.6 F, K2) which was in contrast to non-transformed BY-2 WT cells (Figure 3.6 J2). Interestingly, after pre-treatment with unlabeled phalloidin for three days it was possible to visualize fine AF in GFP-NtADF2 ox cells (Figure 3.6 K3), although non-transformed BY-2 WT cells were only minimally impaired by this treatment (Figure 3.6 J3).

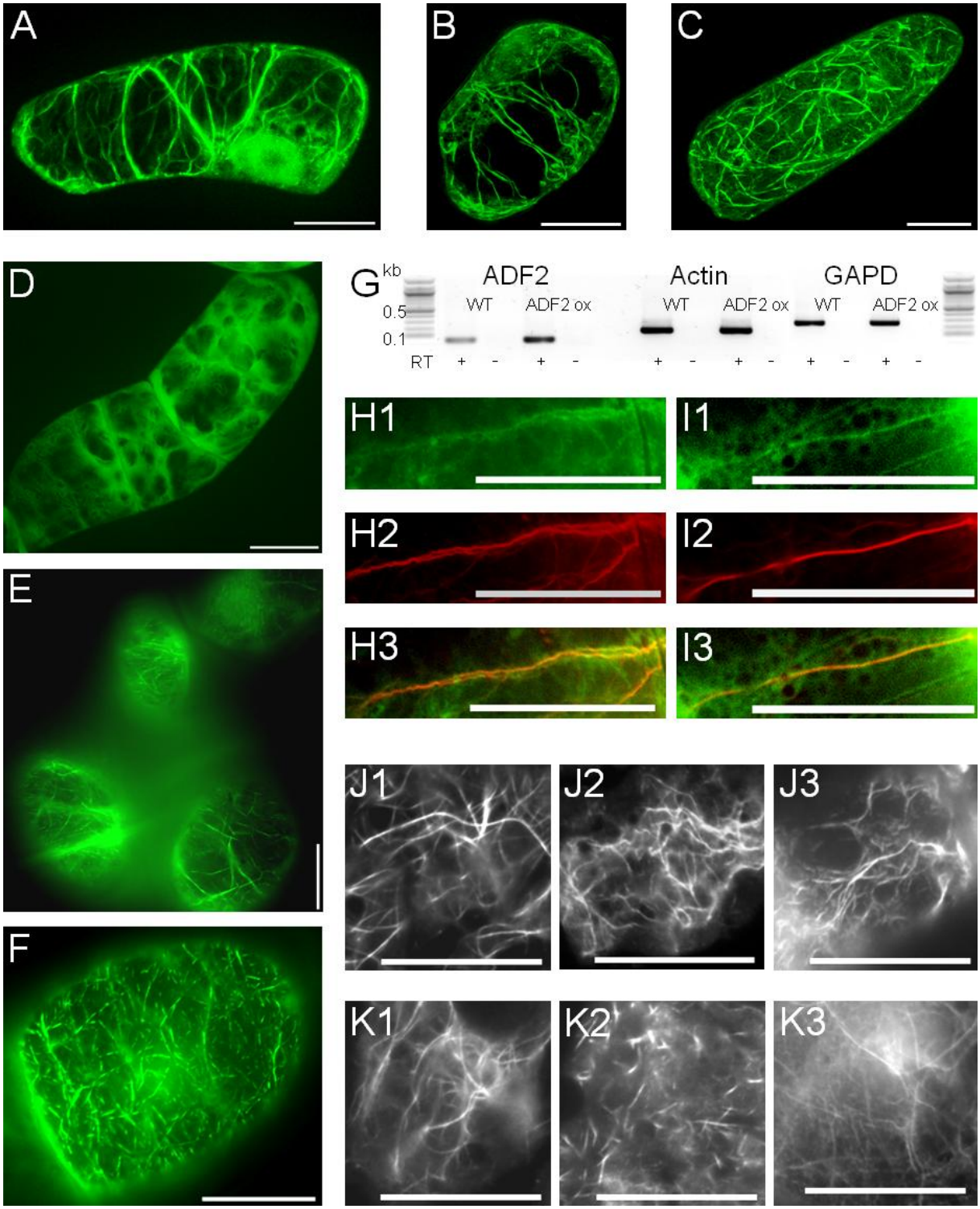

Figure 3.6: Representative fluorescent microscopic images of GFP-NtADF2 ox tobacco BY-2 cells. (A-C) Transient transformed BY-2 cells 4 h (A), 17 h (B) and 24 h (C) after biolistic transformation. Stable transformed GFP-NtADF2 ox BY-2 cells showed a cytoplasmic localized GFP-signal (D) and filamentous structures (H). (E) Semi-quantitative PCR of NtADF2 expression using *Nicotiana tabacum* actin and GAPD as reference genes. Lines marked with *minus* are samples prepared without reverse transcriptase. (H-I) Multi channel confocal images and details of TRITC-phalloidin stained cells: GFP-NtADF2 (1); TRITC-phalloidin (2); Merge (3). (J) Fine actin filaments of TRITC-phalloidin stained non-transformed BY-2 WT and NtADF2 ox BY-2 cells (K) after (3) and without (2) phalloidin pre-treatment. Bars: 20 µm.

To verify the expression of the transgene, a semi-quantitative PCR using cDNA prepared at 4 d after subcultivation was performed. Figure 3.6 G shows an elevation of NtADF2 transcript level in the GFP-NtADF2 ox cell line over the non-transformed BY-2 WT by a factor of about 3. As reference genes, *Nicotiana tabacum* actin and Glyceraldehyde 3-phosphate dehydrogenase (GAPD) were used.

3.3.3 NtADF2 overexpression alters mitosis and cell elongation

To identify possible effects of NtADF2 overexpression on cell morphology a phenotopic analysis was performed. Mitotic Index (MI), cell length, and cell width of the GFP-NtADF2 ox cell line compared to the non-transformed BY-2 WT control were followed through the entire culture cycle. As shown in Figure 3.7, MIs were diminished in the GFP-NtADF2 ox cell line by 20-30 % in comparison to the control from day 1 after subcultivation.

Parallel to the MI, the ratio of cell length and cell width was followed as measure for morphological proportionality, as the cells of the GFP-NtADF2 ox appeared more stunted than the non-transformed control. Since BY-2 WT and GFP-NtADF2 ox did not differ in width (34.6 ± 1.8 µm) throughout the whole cultivation cycle, the impression was exclusively caused by a reduced cell length in the GFP-NtADF2 ox line (13 ± 3 %, Figure 3.7 B).

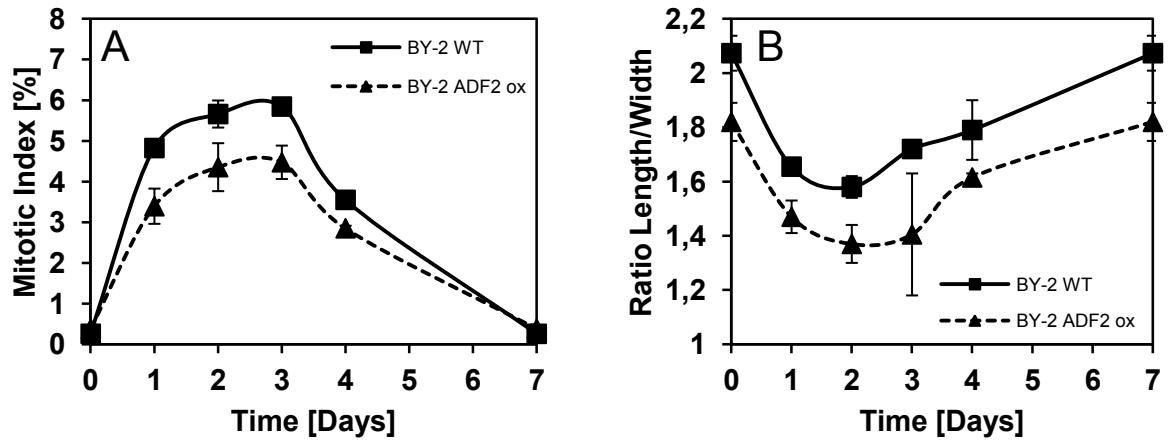

Figure 3.7: Phenotypic analysis of BY-2 WT (filled boxes, continuous curve) and BY-2 GFP-NtADF2 ox (filled triangles, dashed curve) tobacco cell cultures. (A) Mitotic index (mean of n=1500). (B) Cell shape indicated as ratio of cell length over cell width (mean of n≥1000). All experimental data are derived from three independent experimental series; error bars=SE.

3.3.4 NtADF2 overexpression affects division patterns in BY-2 cells

Divisions are synchronized by a polar flow of auxin over a cell file (Campanoni *et al.*, 2003), and this pattern is highly sensitive to perturbations of actin (Maisch and Nick, 2007). Therefore cell-division patterns in the GFP-NtADF2 ox cell line were monitored in comparison with non-transformed controls. In fact, the pattern was altered in the GFP-NtADF2 ox as monitored by frequency distributions over the number of cells within individual files. The non-transformed BY-2 cells showed a characteristic oscillatory behaviour with clear peaks at even cell numbers (Figure 3.8 A). In particular, a clear peak at six cells per file diagnostic for directional synchrony (Campanoni *et al.*, 2003) could be observed. In contrast, this pattern was affected in the GFP-NtADF2 ox. Here, bicellular files were more frequent by 2.5-fold, whereas the frequency of quadricellular files was reduced by almost 30 %. Longer files were almost completely missing (Figure 3.8 A), such that the average number of cells per file dropped to 2.43 (as compared to 4.05 in the non-transformed BY-2 WT cell line). Representative cell files are shown in Figure 3.8 B1, B2. The difference between the lines persisted when the selective pressure on the cell line was removed by omitting kanamycin from the medium (data not shown), confirming that the disturbed pattern was an effect of the transgene and not an effect of the selection pressure.

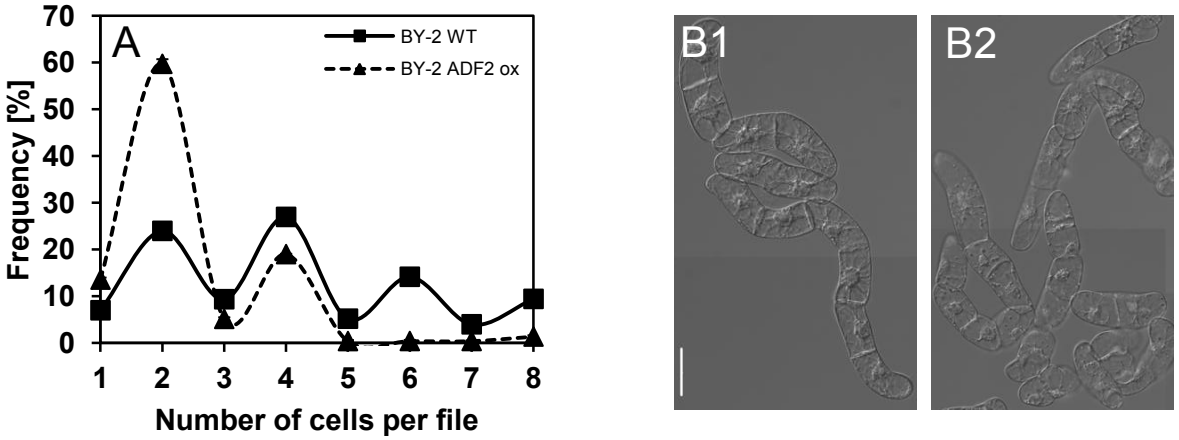

Figure 3.8: Phenotypic analysis of BY-2 WT (filled boxes, continuous curve) and BY-2 GFP-NtADF2 ox (filled triangles, dashed curve) tobacco cell cultures. (A) Division pattern 4 d after subcultivation (mean of n=921 to 1158). All experimental data are derived from three independent experimental series; error bars=SE. (B) Representative cell files of BY-2 WT (B1) and GFP-NtADF2 ox (B2) 4 d after subcultivation. Bar: 20 µm.

3.3.5 Disturbed morphology and division pattern in the GFP-NtADF2 ox can be partially rescued by PIP_2 and phalloidin

As NtADF2 contains a PIP_2 interaction site, and PIP_2 is able to compete with actin for ADF-binding, it was tested, whether the phenotype of the GFP-NtADF2 ox could be rescued by addition of exogenous PIP_2.

PIP_2 was diluted from a 2 µM stock solution to a final concentration of 50 nM in the standard cultivation medium. As control, every experiment was conducted with the same volume of the solvent. These solvent controls showed no detectable effects (data not shown). As illustrated in Figure 3.9 A, it was possible to completely rescue the diminished MI of the GFP-NtADF2 ox cell line. To test for potential negative effects on cell viability, packed cell volume was measured. This test did not reveal any significant difference between treated and untreated cells (data not shown).

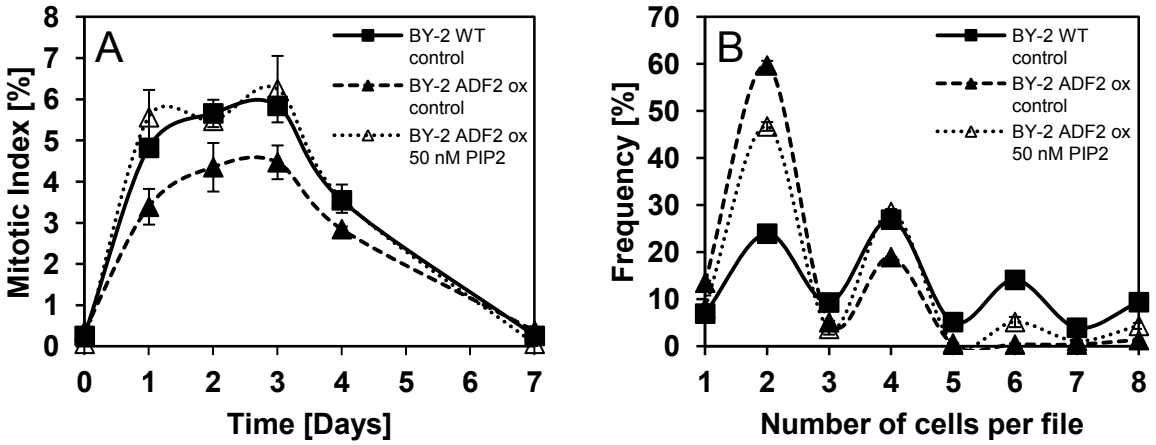

Figure 3.9: Effect of PIP_2 on mitotic indices (A) and division pattern (B). BY-2 WT control (filled boxes, continuous curve), BY-2 GFP-NtADF2 ox control (filled triangles, dashed curve) and BY-2 GFP-NtADF2 ox PIP_2-treated (open triangles, dotted curve) tobacco cell cultures. All experimental data are derived from three independent experimental series; error bars=SE.

With regard to division pattern, assessed at the end of the logarithmic phase, 4 days after subcultivation and addition of PIP_2 to the GFP-NtADF2 ox, a partial rescue could be observed. The strong frequency peak for bicellular files was clearly reduced by 22.0 ± 2.8 % in the treated cell culture. The reduced frequency peak for quadricellular files was completely rescued by 50 nM PIP_2 to the level observed in non-transformed BY-2 WT cells. Most interestingly, the peak at six cells per file, diagnostic for polar auxin transport (Campanoni *et al.*, 2003) and completely eliminated as consequence of ADF2-overexpression, was partially restored (Figure 3.9 B) as well as the peak for files composed of eight cells (frequencies of 5.2 ± 1.1 and 4.4 ± 0.7). The division pattern of non-transformed BY-2 WT cells remained largely unaltered (Figure 3.11 B).

In a second approach, the GFP-NtADF2 ox and the non-transformed BY-2 WT lines were treated with phalloidin at a working concentration of 1 µM, a concentration that in BY-2 causes a mild stabilization of actin without causing toxicity (Berghöfer *et al.*, 2009). For the reduced MI of the GFP-NtADF2 ox, that had been completely rescued by PIP_2 treatment, no effect was detectable. MI remained reduced by 20-30 % throughout the cultivation cycle as compared to the non-transformed BY-2 WT (Figure 3.10 A).

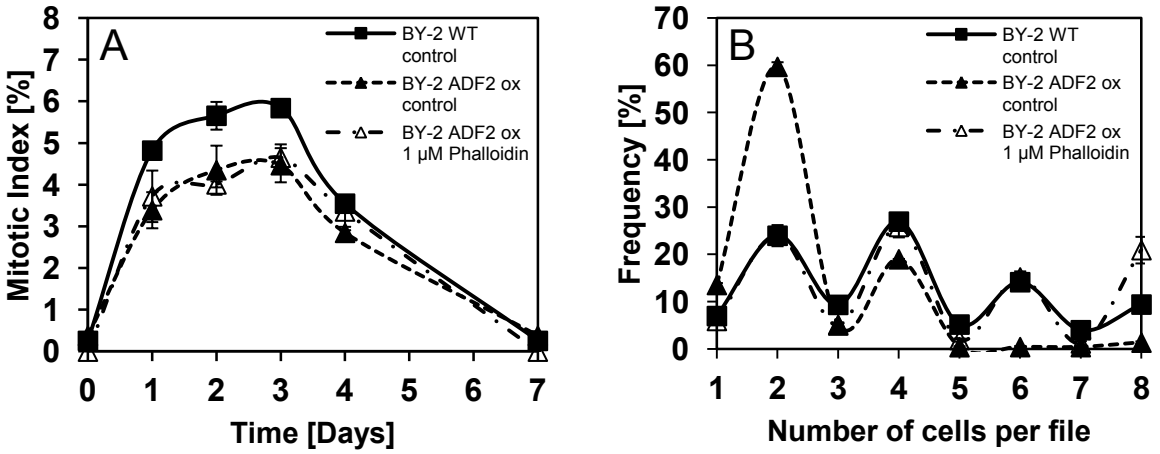

Figure 3.10: Effect of phalloidin on mitotic indices (A) and division pattern (B). BY-2 WT control (filled boxes, continuous curve), BY-2 GFP-NtADF2 ox control (filled triangles, dashed curve) and BY-2 GFP-NtADF2 ox phalloidin-treated (open triangles, dash-dotted curve) tobacco cell cultures. All experimental data are derived from three independent experimental series; error bars=SE.

When the division pattern was scored at the end of the logarithmic phase, 4 days after subcultivation, there was no effect of phalloidin on the non-transformed BY-2 WT. The characteristic oscillatory behaviour with clear peaks at even cell numbers of cells per cell file was maintained (Figure 3.11 A). In contrast, the aberrant division pattern of the GFP-NtADF2 ox was rescued by phalloidin and now became nearly identical to the BY-2 WT pattern. The massive peak at two cells per file was reduced to that of the non-transformed BY-2 WT (Figure 3.10 B).

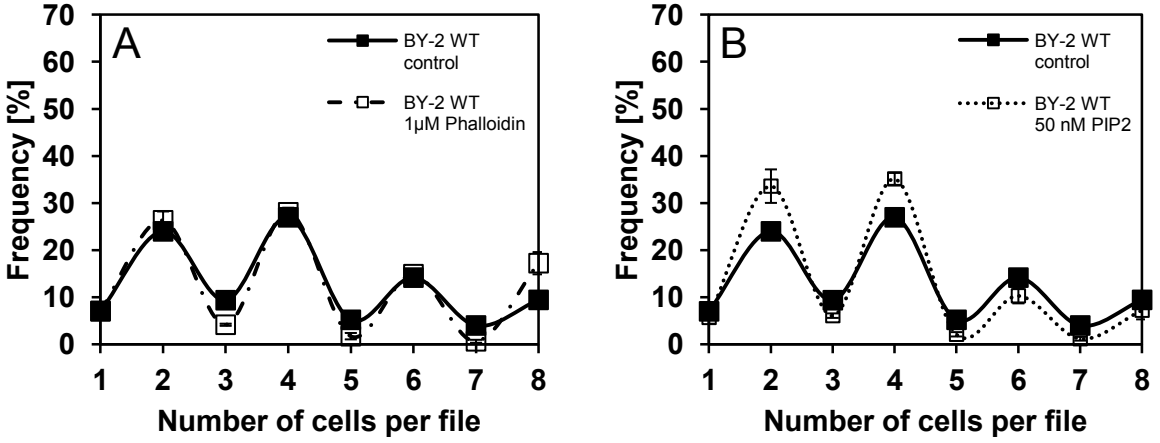

Figure 3.11: Effect of phalloidin (A) and PIP_2 (B) on division pattern. BY-2 WT control (filled boxes, continuous curve), BY-2 WT phalloidin-treated (open boxes, dash-dotted curve) and BY-2 WT PIP_2-treated (open boxes, dotted curve) tobacco cell cultures. All experimental data are derived from three independent experimental series; error bars=SE.

3.3.6 Auxin and auxin-transport inhibitor treatments do not alter the division pattern of the GFP-NtADF2 ox line

Further it was investigated how the pattern of cell division responded to manipulation of auxin transport. Neither treatment with auxins (2 µM IAA, 2 µM 2,4-D; data not shown) nor with NPA (10 µM 1-N-naphthylphthalamic acid), an inhibitor of polar auxin transport, altered the disturbed division pattern of the GFP-NtADF2 ox line significantly (Figure 3.12 A). Conversely, the effect of 65 nM latrunculin B (LatB) in the non-transformed BY-2 WT line was comparable to the affected division pattern of the untreated GFP-NtADF2 ox line (Figure 3.12 B). The DP of non-transformed BY-2 WT cells treated with 10 µM NPA (Maisch and Nick, 2007) is also very similar to the affected division pattern of the untreated GFP-NtADF2 ox line.

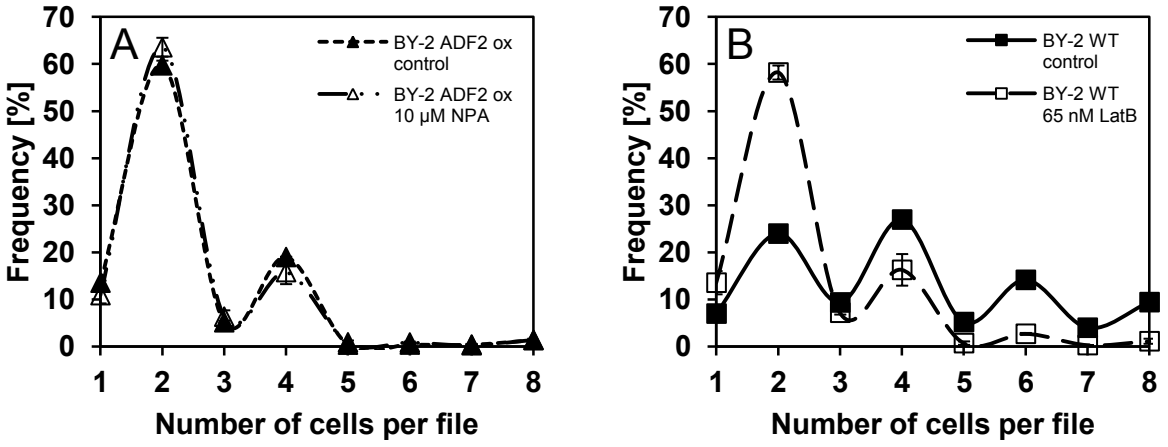

Figure 3.12: Effect of NPA (A) and LatB (B) on division pattern. BY-2 GFP-NtADF2 ox control (filled triangles, dashed curve), BY-2 GFP-NtADF2 ox NPA-treated (open triangles, dash-double-dotted curve), BY-2 WT control (filled boxes, continuous curve) and BY-2 WT LatB treated (open boxes, long-dashed curve) tobacco cell cultures. All experimental data are derived from three independent experimental series; error bars=SE.

3.3.7 Inducible NtADF2 RNAi knockout alters division patterns in BY-2 cells

The phenotyping and complementation experiments indicated an involvement of NtADF2 in auxin-dependent division patterning. To test, whether NtADF2 is necessary for patterning, a second approach was performed in parallel. An inducible NtADF2 RNAi knockout BY-2 cell line was established and characterized in the background of NtADF2 ox results. The only difference in the experiment was the induction of the NtADF2 knockout by adding 10 µM dexamethasone at inoculation. For visualization of a functional knockout the employed pOpOff2(kan) vector harbored a β-glucuronidase (β-Gluc) reporter gene which can be detected by PCR as well as by histochemical staining using 5-bromo-4-chloro-3-indolyl glucuronide (X-Gluc). In the following experiments the first reporter assay was chosen.

Especially the division pattern of this cell line was of major interest. Appropriate controls tested for potential differences in DP in the absence of the dexamethasone inducer (tightness of the promotor) or potential side-effects of the dexamethasone on the cell division (Figure 3.13).

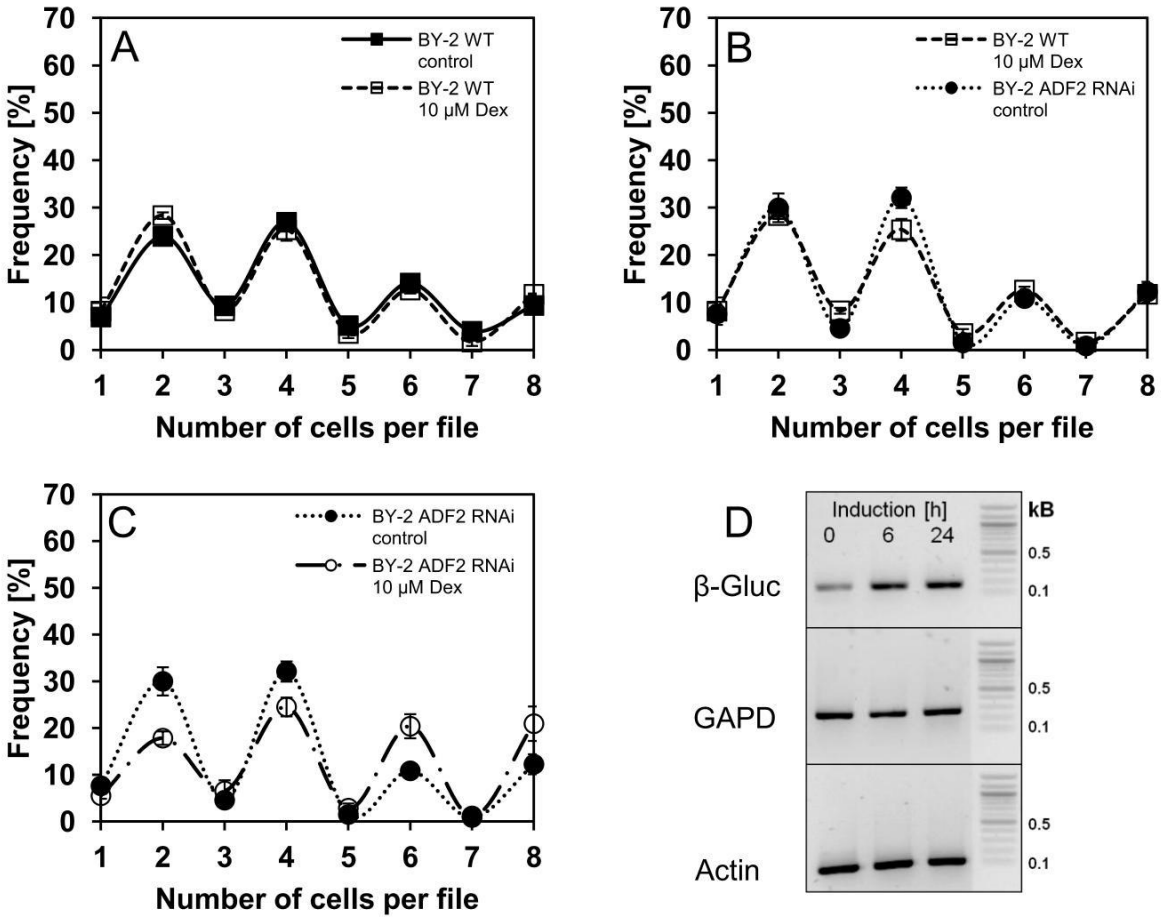

Figure 3.13: Cell division pattern of an inducible NtADF2 RNAi knockout BY-2 cell line 4 d after subcultivation. (A) Control for potential side-effects of dexamethasone induction. Non-transformed BY-2 WT cell culture (filled boxes, continous line), dexamethasone-treated non-transformed BY-2 WT cell culture (open boxes, short dashed line). (B) Control of cell division pattern in the non-induced NtADF2 RNAi knockout cell line (filled circles, dotted line) compared to dexamethasone-treated non-transformed BY-2 WT cell culture (open boxes, short dashed line). (C) Comparison of the cell division pattern of a non-induced (filled circles, dotted line) and an induced NtADF2 RNAi knockout BY-2 cell line (open circles, dash-dotted line). (D) Verification of the NtADF2 knockout using the expression of the GUS-reporter gene. All experimental data are derived from three independent experimental series; error bars=SE.

The DP of the non-induced NtADF2 RNAi knockout cell line was comparable to the non-transformed WT cell culture as well as the DP of the non-transformed WT cell culture was not affected by dexamethasone treatment. After induction at inoculation and analysis 4 d after subcultivation, the DP of the NtADF2 knockout cell line showed a clear shift towards even-numbered cell files comprising six and eight cells. The typical pattern characterized by a prevalence of even-numbered files persisted. The amount of bicellular and quadricellular files was reduced by about 40 % and 24 %, respectively, whereas the frequency of hexacellular and octocellular cell files was increased by about 88 % and 71 %, respectively

(Figure 3.13 C). In other words, the pattern was shifted towards higher ordered even-numbered peaks including the peak at n=6 diagnostic for the efficiency of polar auxin transport.

3.4 Visualization and discrimination of different actin sub-populations using pa-FP and PALM

The first part of this dissertation identified NtADF2 as important mediator of auxin signaling towards actin leading to functional sub-populations of AF within the same cell. The second part of this dissertation posed the question whether it is possible to visualize the proposed sub-populations of actin filaments, which differ in respect to their ABP decoration. For this purpose, a FP-based approach was chosen. The yeast peptid Lifeact, which can ubiquitously bind filamentous actin was used as actin-binding probe and fused to two different FP. The first construct contained a psRFP, which forms tetramers, typical for anthozoan FP (Fuchs, 2011). Due to the molecular size of the tetramer, binding of the Lifeact to actin should be sensitive to steric hindrance by competing ABP, whereas in AF that are not or only scarcely decorated by ABP, binding of psRFP should not be impeded. To verify that the Lifeact marker recognized all AF sub-populations, a second construct comprising the monomeric mIRISFP was selected. Both FP belong to the class of pa-FP and therefore offer the possibility of super-resolution microscopy using photoactivation localization microscopy (PALM). As PALM in living plant cells has never been tested before, the approach at the same time represented a proof-of-principle experiment.

Applying this approach, it was possible to reveal different functional sub-populations of actin filaments in BY-2 cells. In addition, the super-resolution PALM delivered images of actin filaments with a resolution of about 20 nm.

3.4.1 Localization of Lifeact-psRFP differs after transient and stable transformation

Each of the new FP-fusion constructs was tested for functionality by a biolistic transient transformation. In a standard approach 750 µl of cells 3 d after subcultivation were pipetted on a microslide and biolistically transformed with 1 µg of binary plasmid containing the sequence of Lifeact-psRFP and Lifeact-mIRIS, respectively. After 24 h of incubation the slides have been checked for transformants. The two constructs differed clearly in transformation efficiency even though they consisted of the same backbone vector. Numerous (up to 10) of Lifeact-psRFP expressing cells, but only 1-2 Lifeact-mIRIS expressing cells could be scored per transient transformation. In contrast to the difference in

transformation efficiency, the intracellular pattern was nearly identical. Both constructs marked highly specific and distinctive structures with characteristic properties of actin filaments like Y-crossings and cortical arrangements (Figure 3.14 A-C).

After this positive test for functionality both vectors were stably transformed into non-transformed BY-2 WT cell lines using a modified TAMBY-2 method (Buschmann *et al*., 2011). Again, differences in transformation efficiency could be observed. The Lifeact-psRFP approach succeeded instantly, but the Lifeact-mIRIS batch was much more difficult to handle and especially the inhomogeneity of the calli and the transfer from solidified agar plates into liquid medium was difficult and required several attempts to reach success.

In addition, a qualitative difference between both cell lines and the transient pre-test was immediately visible. The Lifeact-mIRIS ox cells displayed again all sub-populations of the plant actin cytoskeleton including the characteristic structures in the cell cortex and the cell center (Figure 3.14 D). In contrast, the stable Lifeact-psRFP ox cells differed from the transient expressors (where transgenes are expressed at higher levels). They did not exhibit even a single red fluorescent filamentous structure in the cell cortex or in transvacuolar strands. Only a tight filamentous basket around the nucleus was labeled by the Lifeact-psRFP construct (Figure 3.14 E). Interestingly, a small sub-population of cells that were obviously undergoing cell death as indicated by an almost complete cessation of cytoplasmic streaming, membrane detachment and deformation in cell shape sometimes displayed a fully decorated actin cytoskeleton comprising both central and cortical arrays (Figure 3.14 F).

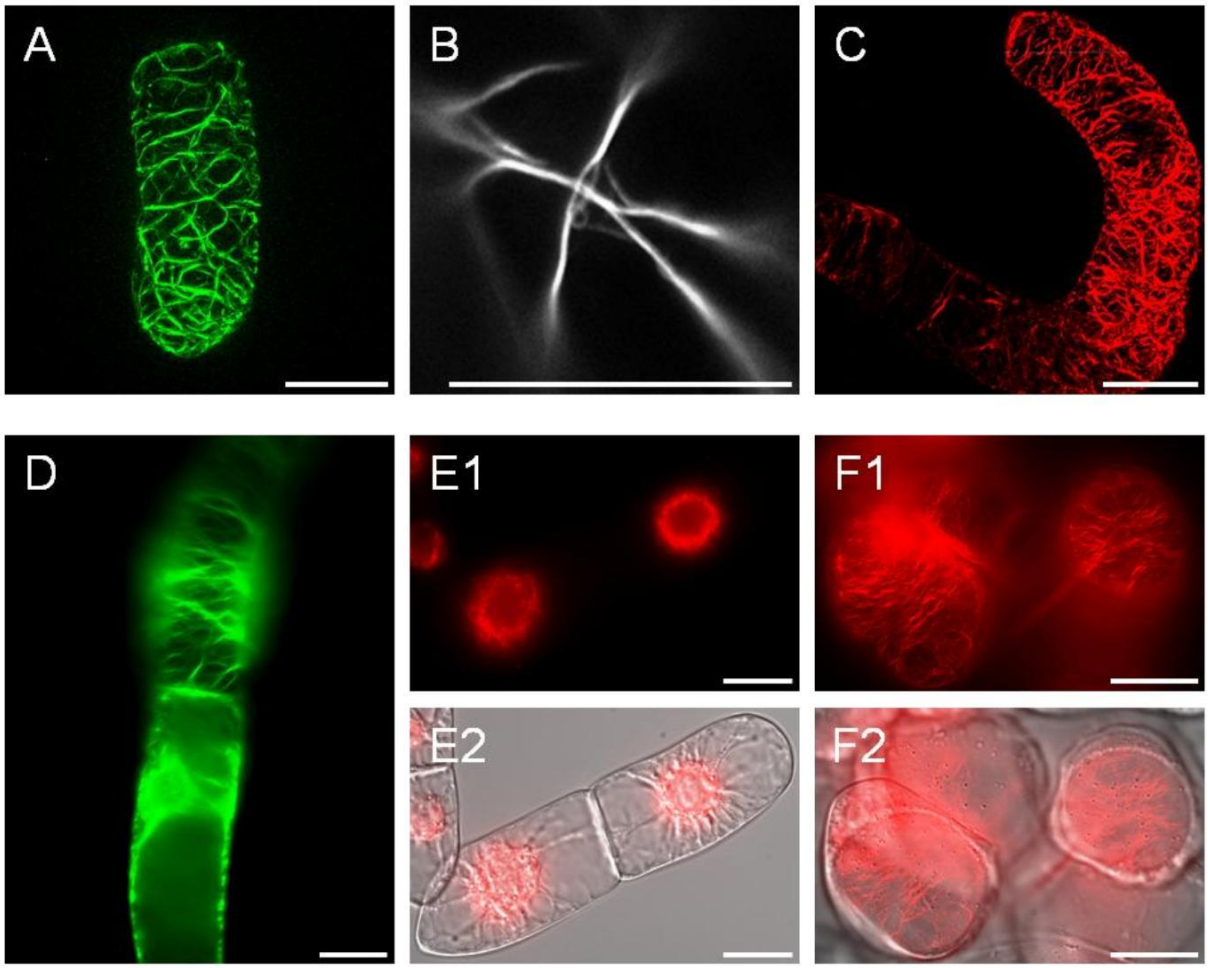

Figure 3.14: Representative images of Lifeact-pa-FP ox BY-2 cells. (A) Transient expression of Lifeact-mIRIS. (B) Specific psRFP-marked filamentous structures in a BY-2 cell after transient transformation; two pairs of filaments forming a needle eye and thread. (C) Transient expression of Lifeact-psRFP. Images of transiently transformed cells were recorded 3 d after subcultivation; 24 h incubation after particle bombardment. (D) Stable Lifeact-mIRIS ox BY-2 cells (lower part: central region; upper part: cortical region). (E) Stable Lifeact-psRFP ox BY-2 cells; RFP-signal nuclear basket exclusive. (F) Extremely stressed stable Lifeact-psRFP ox BY-2 cells at ensuing cell death.(1) RFP-channel (2) merge of RFP-channel and DIC-channel. Bars: 20 µm.

The specific labeling of one actin sub-population (subsequently termed nuclear basket) in the Lifeact-psRFP ox cell line stimulated further analysis of actin conformation, dynamics and localization pattern during cell cycle.

3.4.2 Colocalization of Lifeact-psRFP and AlexaFluor® 488 phalloidin

To understand, why only the perinuclear actin was manifest in the Lifeact-psRFP BY-2 ox cells these cells were PFA-fixed and stained using Alexa-Fluor® 488 labeled phalloidin at day 3 after subcultivation. This approach visualized in addition to the nuclear basket additional actin sub-populations which were not marked via Lifeact-psRFP expression. For the nuclear basket, a clear colocalization of red Lifeact-psRFP (Figure 3.15 A2, B2, C2) and green Alexa-Fluor® 488 (Figure 3.15 A1, B1, C1) resulting in a yellow signal in the merged image (Figure 3.15 A3, B3, C3) could be detected. However, in the cell cortex only the signal from Alexa-Fluor® 488 phalloidin was seen, whereas the Lifeact-psRFP signal was

completely absent (Figure 3.15 B1, C1) leading to the assumption that there should be a difference between actin sub-populations.

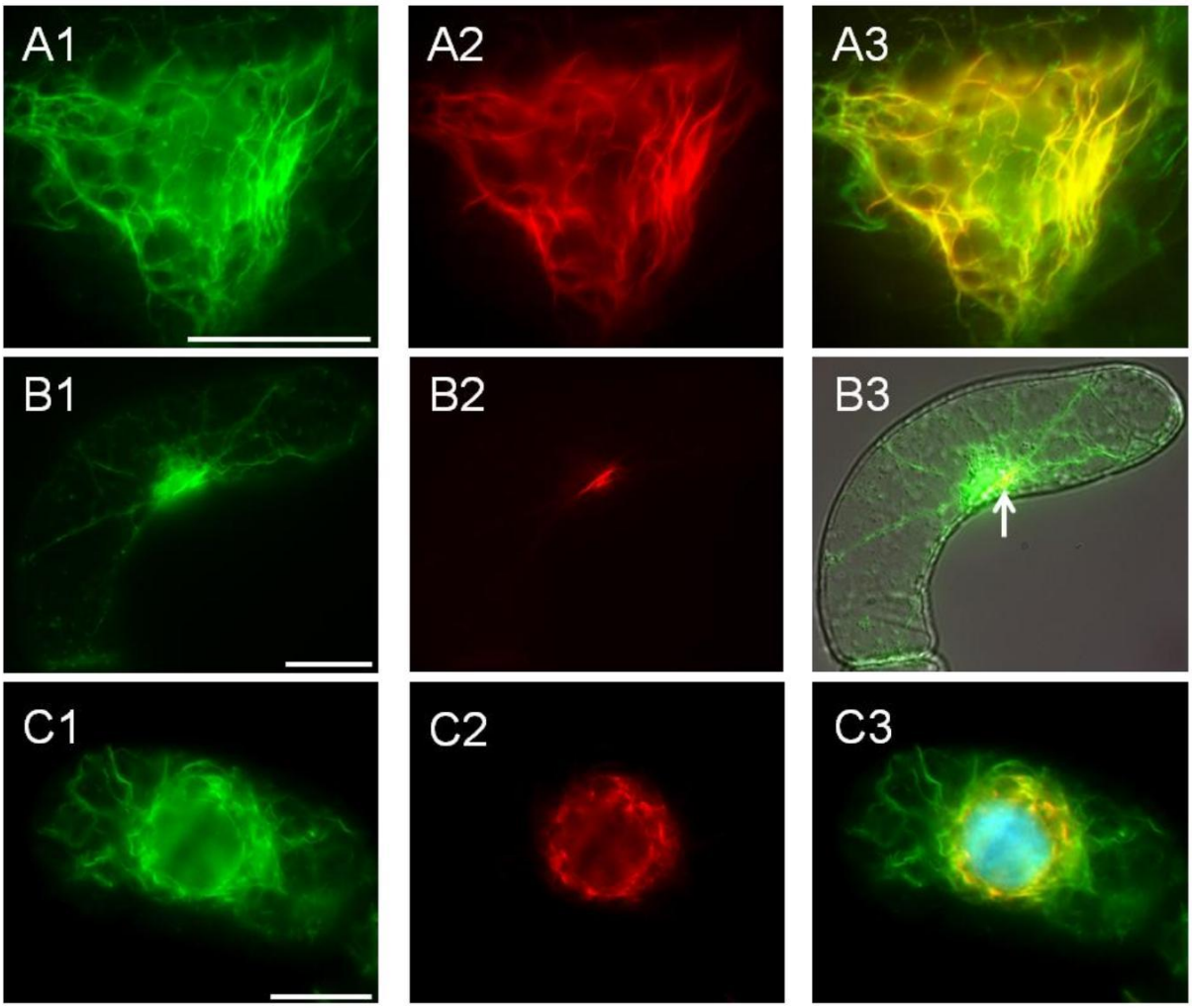

Figure 3.15: Actin staining of fixed Lifeact-psRFP ox BY-2 cells. (A) Nuclear basket; green channel (1) AlexaFluor® 488 phalloidin; red channel (2) Lifeact-psRFP; Merge (3) yellow signal marks colocalization. (B) Whole BY-2 cell; green channel (1) AlexaFluor® 488; red channel (2) Lifeact-psRFP; Merge (3); additional DIC-channel; yellow signal marks colocalization (white arrow). (C) Whole BY-2 cell; green channel (1) AlexaFluor® 488; red channel (2) Lifeact-psRFP; Merge (3); additional blue DAPI-channel (nuclear staining); yellow signal marks colocalization, image recorded by Linda Brochhausen. Bars: 20 µm.

3.4.3 The Lifeact-psRFP ox BY-2 cell culture is sensitive to latrunculin B treatment

In contrast to Lifeact-mIRIS the Lifeact-psRFP fusion protein forms tetramers, which means that one protein complex harbors also four Lifeact peptides for actin-binding. This could cause cross-linking effects of the actin around the nucleus, where the microfilament meshwork is very dense in comparison to the cortical region. Cross-linked AF are stabilized and less sensitive to cytoskeletal drugs like latrunculin B. Therefore sensitivity of the Lifeact-psRFP ox cell line was compared to a non-transformed BY-2 WT cell culture using a dose response assay measuring the effect of different latrunculin B concentrations on packed cell volume.

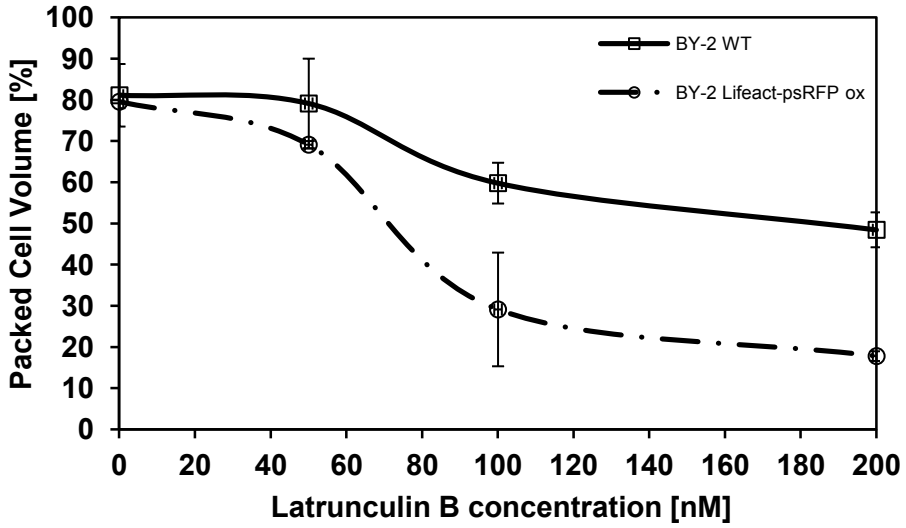

Figure 3.16: Latrunculin B treatment of non-transformed BY-2 WT (open boxes, continous curve) and Lifeact-psRFP ox (open circles, long-dash-dotted curve). Values represent relative cell volume of 15 mL liquid cell culture. All experimental data are derived from three independent experimental series; error bars=SE.

As Figure 3.16 shows, the Lifeact-psRFP ox cell line is not less but even more sensitive to latrunculin B as compared to the non-transformed WT BY-2 cells. Both lines were treated with latrunculin B in different concentrations (50, 100, and 200 nM), incubated for 4 d and evaluated after further 24 h of settling down at 4°C. At a final concentration between 60 and 80 nM latrunculin B the Lifeact-psRFP ox cell volume was already reduced to 50 % compared to the untreated Lifeact-psRFP ox cells, whereas the non-transformed BY-2 WT cell volume was only diminuished by 5-10 % in relation to the control.

In a second approach, Lifeact-psRFP ox BY-2 cells were treated with 10 µM latrunculin B for up to 45 min. This treatment caused a disintegration of the nuclear basket leading to freely floating Lifeact-psRFP marked actin filament fragments in the cytoplasm especially in cells at interphase state. The nuclear basket of cells at or briefly after mitosis were more resistant to

the drug. However, during all cell cycle stages no cortical actin structures seemed to be decorated, even after LatB treatment.

3.4.4 Lifeact-psRFP marks the direction of nuclear migration

The intracellular localization and signal intensitiy of the fusion protein in stably transformed Lifeact-psRFP ox cells persisted through the whole cell cycle (data not shown). Nevertheless, signal intensities and the localization around the nuclear envelop shifted sometimes and formed a gradient. Three main types of gradients could be identified. The most frequent type was a relative homogenous distribution around the whole nucleus. Secondly, a clear gradient towards the nearest cell wall (which in most cases is the wall that has been deposited most recently), and, at comparable frequency, a gradient directed towards the cell center. These gradients of the Lifeact-psRFP signal were correlated with the nuclear migrations characteristic for the cell cycle of vacuolated plant cells (Figure 3.17).

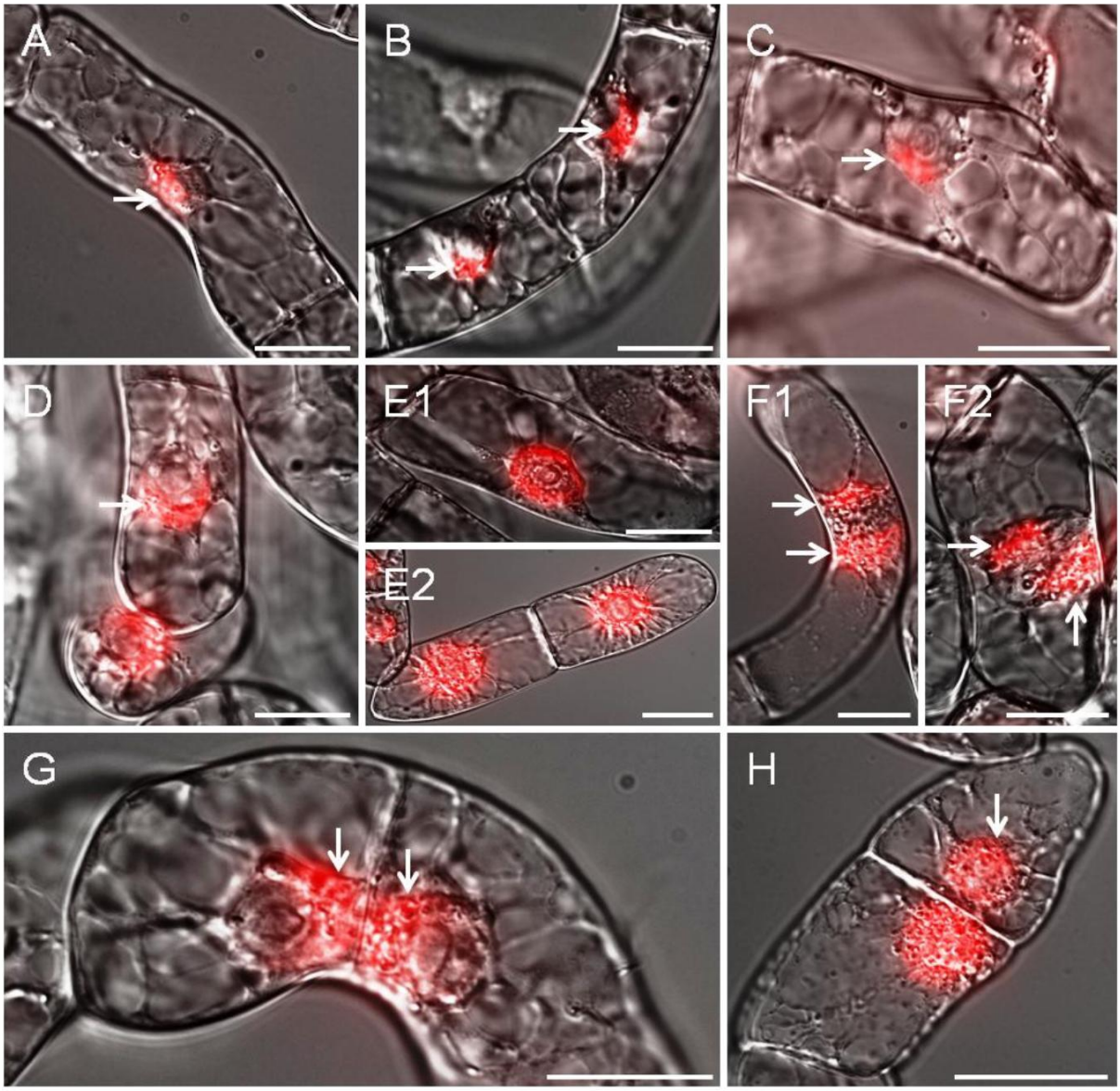

Figure 3.17: Representative images of Lifeact-psRFP ox BY-2 cells during cell cycle. White arrows indicate peaks of Lifeact-psRFP signal gradient. (A) Interphase cell; nucleus is attached to the lateral cell wall, Lifeact-psRFP signal between cell wall and nucleus. (B-D) Interphase cells; nucleus is moving into the center of the cell and prepare for mitosis; Lifeact-RFP signal is oriented towards the cell center. (E1) Interphase cell; nucleus reached cell center; Lifeact-psRFP signal labels whole nuclear basket. (E2) Start of mitosis; nuclei of both cells in prophase; very fine filaments of nuclear basket homogenously marked by Lifeact-psRFP signal. (F) Mitotic cell in anaphase; Lifeact-psRFP signal at both poles of the former nucleus; right cell with abnormal position of division plane leading to insertion of a non-perpendicular new cross wall. (G) End of mitosis; new cell wall has been formed; Lifeact-psRFP signal exclusivly between new cell wall and nuclei. (H) Mitosis completed; nuclei completely sourrounded by Lifeact-psRFP-labeled nuclear basket; upper cell forms gradient towards cell center. Bars: 20 µm.

In Lifeact-psRFP ox BY-2 cells passing through late G1-phase, the psRFP signal was mainly localized between nucleus and the lateral cell wall (Figure 3.17 A). Elsewhere, they formed a tight slightly reduced nuclear basket with preferred orientation to this lateral wall. During movement of the nucleus towards the cell center, the Lifeact-psRFP signal was always strongest at the side of the nucleus oriented to the cell center (Figure 3.17 B-D). Cells, where the nucleus had reached this position, more or less lost the Lifeact-psRFP gradient and the signal was homologously distributed as a nuclear basket (Figure 3.17 E). This conformation

was relatively stable until the end of mitosis. In anaphase, a clear psRFP signal was exclusively localized at the poles of the former nucleus (Figure 3.17 F). Whereas at the end of mitosis in late telophase, the whole Lifeact-psRFP signal was located between new cell wall and nuclei (Figure 3.17 G). Following this stage of cell cycle, a rotation of the whole nuclei, but not a re-orientation of AF around the nuclei could be observed, leading to Lifeact-psRFP gradients in direction of the new cell centers.

In addition to the observation of the entire cell cycle, mitosis was followed in more detail over time in Lifeact-psRFP ox BY-2 cells. As observed during cell cycle, the nuclear basket of Lifeact-psRFP labeled actin filaments was quite stable in mitosis. Until the end of metaphase, the whole structure was contiguous and the filaments were arranged in a fine mesh-like conformation (Figure 3.18 A-C). Starting with anaphase, the AF of the basket became more bundled and a slight gradient of the Lifeact-psRFP signal appeared. Especially during the later mitotic phases, a clear increase of signal intensity in direction towards the cell poles was detectable (Figure 3.18 D, E). Upon completion of mitosis and cytokinesis, the new nuclei migrated to the center of both daughter cells and were completely coated by Lifeact-psRFP marked nuclear baskets (Figure 3.18 F).

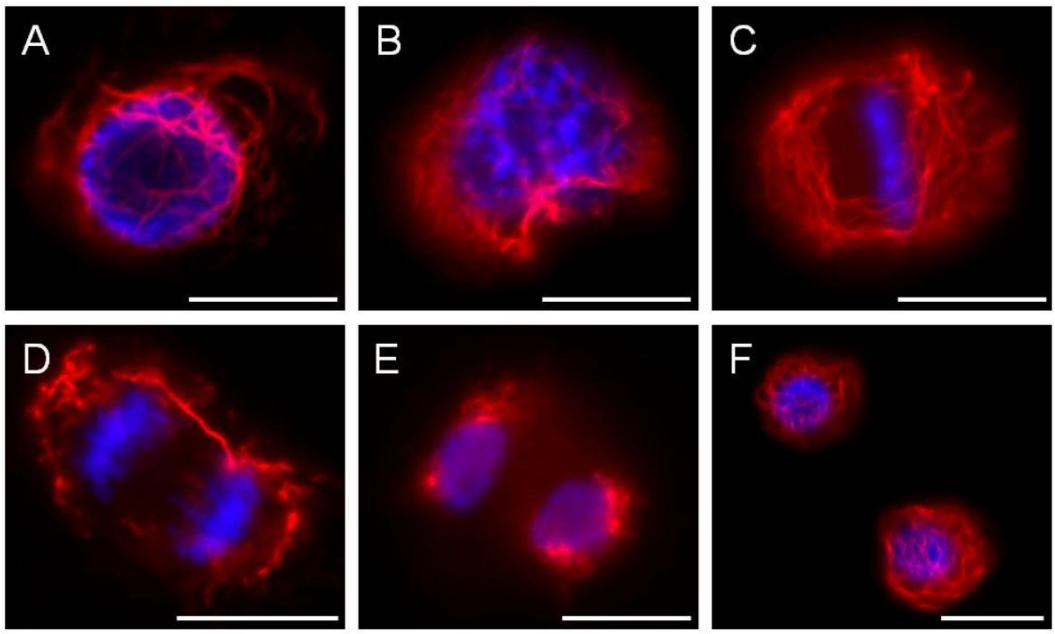

Figure 3.18: Different cell cycle stages in Lifeact-psRFP ox BY-2 cells. Lifeact-psRFP signal: red; Hoechst 33528 stained DNA: blue. (A) (B) Prophase; chromosomes already condensed; fine filamentous nuclear basket intact. (C) Metaphase; chromosomes arranged in the equatorial plane; nuclear basket consists of very fine Lifeact-psRFP marked AF. (D) Anaphase; chromosomes are pulled to the cell poles; nuclear basket reduced to slightly bundeled filaments with moderate gradient towards cell poles. (E) Telophase; new nuclear envelop has been formed and the nucleus becomes round again; clear gradient of the Lifeact-psRFP marked AF towards the cell poles. (F) Two daughter cells short after finished mitosis; nuclei already in center of the cells; very homogenous nuclear actin basket. Bars: 20 µm.

3.4.5 The nuclear basket remains stable evenduring protoplasting

The migration of the nucleus plays a pivotal role in cell division. It is directly connected with cellular events like formation of cell axis and cell polarity. In order to pull (or to push) the nucleus into a new position the anchor point at its envelope has to be established first.

If the nuclear basket decorated by Lifeact-psRFP is relevant for nuclear migration, it should be relatively stable and established early in cell development. A diploma thesis (Zaban, 2010) showed that it is possible to bring BY-2 cells into a *tabula-rasa* state without polarity by chemical digestion of the cell wall (protoplasting). Following this step, the re-orientation and re-organization of the cytoskeleton accompanied by *de-novo* formation of cell axis and polarity can be observed *in vivo* (publication in preparation). An actin meshwork essential for nuclear migration should also exist in this state.

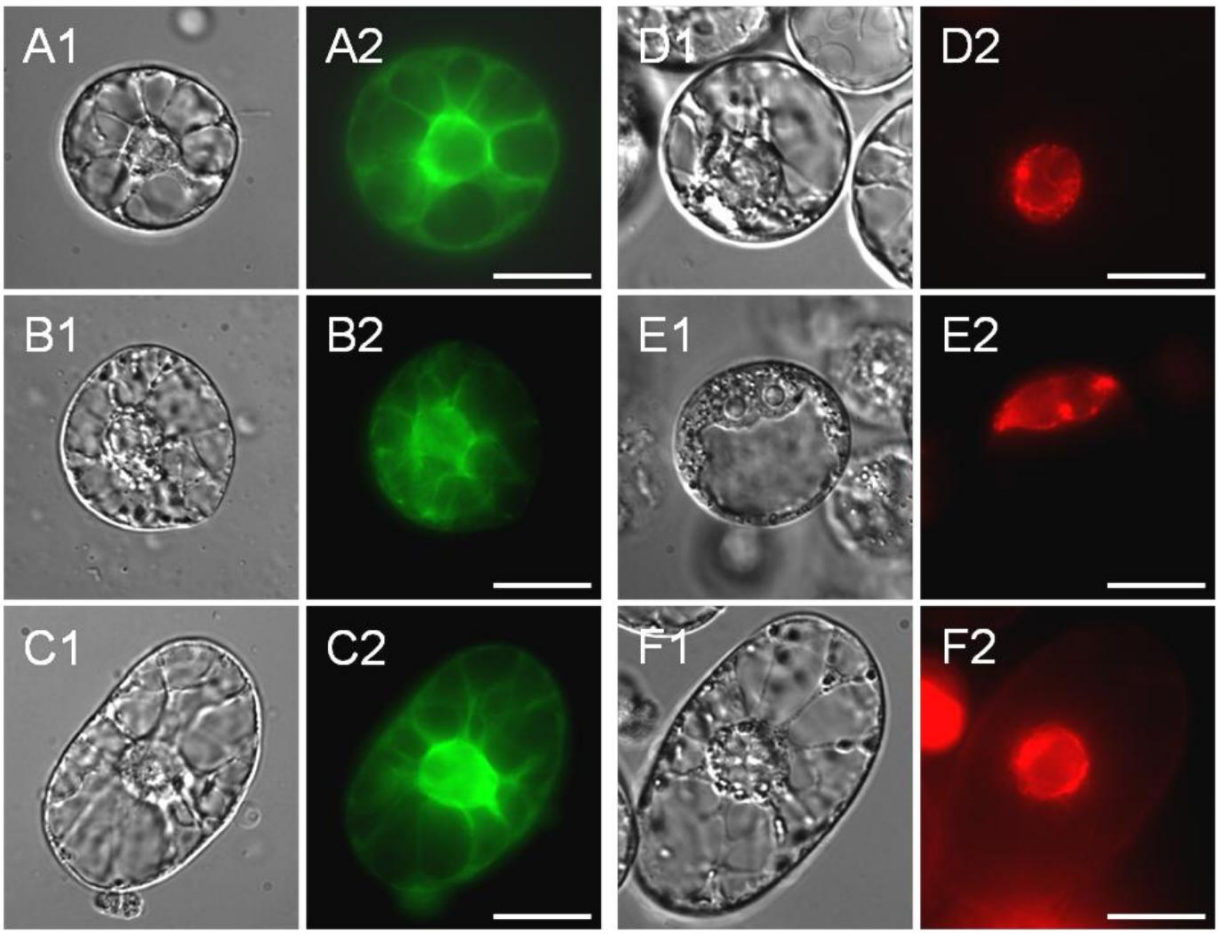

Figure 3.19: Protoplasts of GFP-FABD2 ox (A-C) and Lifeact-psRFP ox (D-F) BY-2 cells. (A) 0 d after protoplasting; cytoplasmic and perinuclear GFP-signal. (B) 1 d after protoplastation; GFP-signal cytoplasmic and perinuclear, but filamentous structures visible in the cortical region. (C) 3 d after protoplasting; nearly regenerated cell with clear axis; GFP-signal around the nucleus, additional GFP-labeled filamentous structures. (D) 0 d after protoplasting; filamentous psRFP-signal exclusively around the nucleus. (E) 1 d after protoplasting; filamentous psRFP-signal around the nucleus, cell was protoplasted at end of mitosis before cytokinesis. (F) 3 d after protoplasting; nearly regenerated cell with clear axis; psRFP-signal exclusive around the nucleus. (1) DIC. (2) FP. Bars: 20 µm.

Up to now it was merely feasible to visualize diffuse actin signals using classical actin marker lines like the GFP-FABD2 ox cell line (Maisch *et al*., 2009) due to the restriction limit and photostability of the FP, making an assertive statement nearly impossible. The observed signal was mainly cytoplasmic but also localized around the nucleus (Figure 3.19 A-C). Therefore, Lifeact-psRFP ox BY-2 cells were protoplasted 3 d after subcultivation and tested for the presence of an actin-based nuclear basket and possible additionally marked structures.

Indeed it was possible to detect a nuclear basket also in Lifeact-psRFP ox protoplasts. Similar to the Lifeact-psRFP ox BY-2 cells no additional signal could be detected except for the specifically labeled fine filaments around the nucleus (Figure 3.19 E-F). Through the regeneration phase of the protoplasts this situation remained stable until day 3, while the diffuse signal of the GFP-FABD2 ox cell line associated slightly more with filamentous actin- towards the cortical region (Zaban, 2010; Figure 3.19 C).

3.4.6 Photoactivation localization microscopy of living Lifeact-psRFP ox BY-2 cells

Additionally to conventional fluorescent microscopic methods, this work aimed to visualize actin filaments of living tobacco BY-2 cells in super-resolution. As promising tools for this approach, the photoactivatable psRFP c-terminally fused to Lifeact was used for photoactivation localization microscopy (PALM). Images of stably transformed Lifeact-psRFP ox BY-2 cells recorded by cofocal laser scanning and epifluorescence microscops always showed a nuclear basket of actin filaments without any signal in the cortical or transvacuolar cell regions. In this experimental approach two questions were of substantial interest. The first issue was directly connected to the microscopic technique PALM itself: Is it possible to do super-resolution microscopy in living plant cells? The second question was linked to the specific localization pattern of the fusion protein which is exclusively visible around the nucleus. For these two questions the lab of Prof. U. Nienhaus (Institute for Applied Physics and Center for Functional Nanostructures - CFN, Karlsruhe Institute of Technology - KIT) kindly provided an adequate microscope for PALM and P.N. Hedde performed PALM imaging.

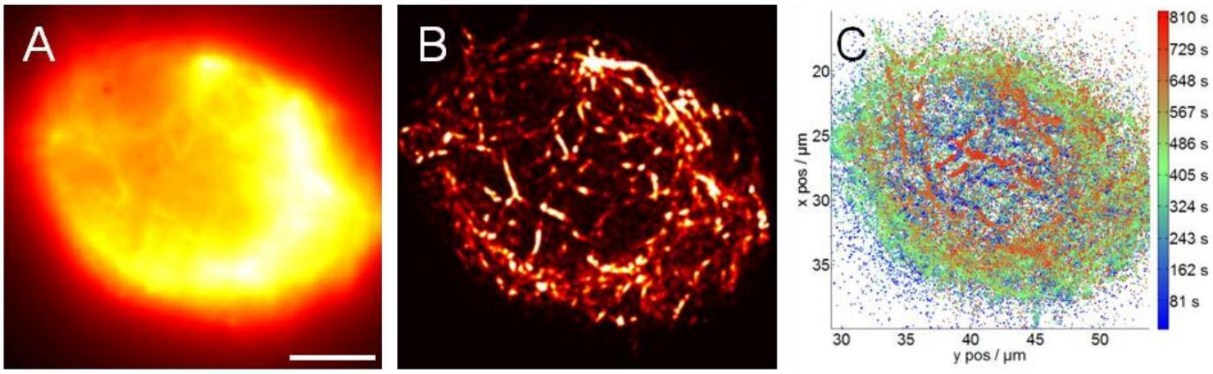

Figure 3.20: PALM analysis of Lifeact-psRFP ox BY-2 cells. (A) Widefield image of a nuclear actin basket. (B) Projection of 27000 single images of 9 sections (each 3000 frames) with distance in z-axis of 2 µm; fine actin filaments are exclusively found around the nucleus after calculating the exact position of every single signal using the mathematical algorithm of the point spread function. (C) mathematical calculation of every single Lifeact-psRFP molecule; color represents time of occurrence and corresponds to z-axis. Microscopic setup: 30 ms camera exposure time, 300 gain, 4.7x preamp, 5 - 20 mW 561 nm, <1 mW 473 nm. Bar: 5 µm.

As shown in Figure 3.20, PALM could be successfully employed in plant cells using the Lifeact-psRFP ox BY-2 cell line. It was not only possible to switch the FP-signal on and off (data not shown), but also to calculate total image projections collected from more than 27000 single images. Additionally, it was possible to combine up to nine independent sections of 3000 frames into a 3D projection. By this way a whole BY-2 nucleus with its nuclear actin basket could be imaged (Figure 3.20 B). The surface of the nuclear basket next to the cell cortex was the starting point of the series, followed by 8 sections (2 µm z-axis distance) towards the central region of the cell. Similar to the results mentioned above

(classical fluorescence microscopy, Figure 3.14 E), again only actin around the nucleus was visualized by the Lifeact-psRFP fusion protein.

The gradient indicating the direction of nuclear migration detected by classical fluorescence microscopy (Figure 3.17) was now analyzed in more detail. Stably transformed Lifeact-psRFP ox cells were checked for the occurrence of this pattern using PALM in combination with 3D projection as described above. For this purpose, 18000 images of six sections (3000 frames each) with a distance of 2 µm were taken and processed. By this approach a clear gradient of the Lifeact-psRFP signal could be detected (Figure 3.21). Through all sections the Lifeact-psRFP signal was oriented towards one favored side of the nucleus.

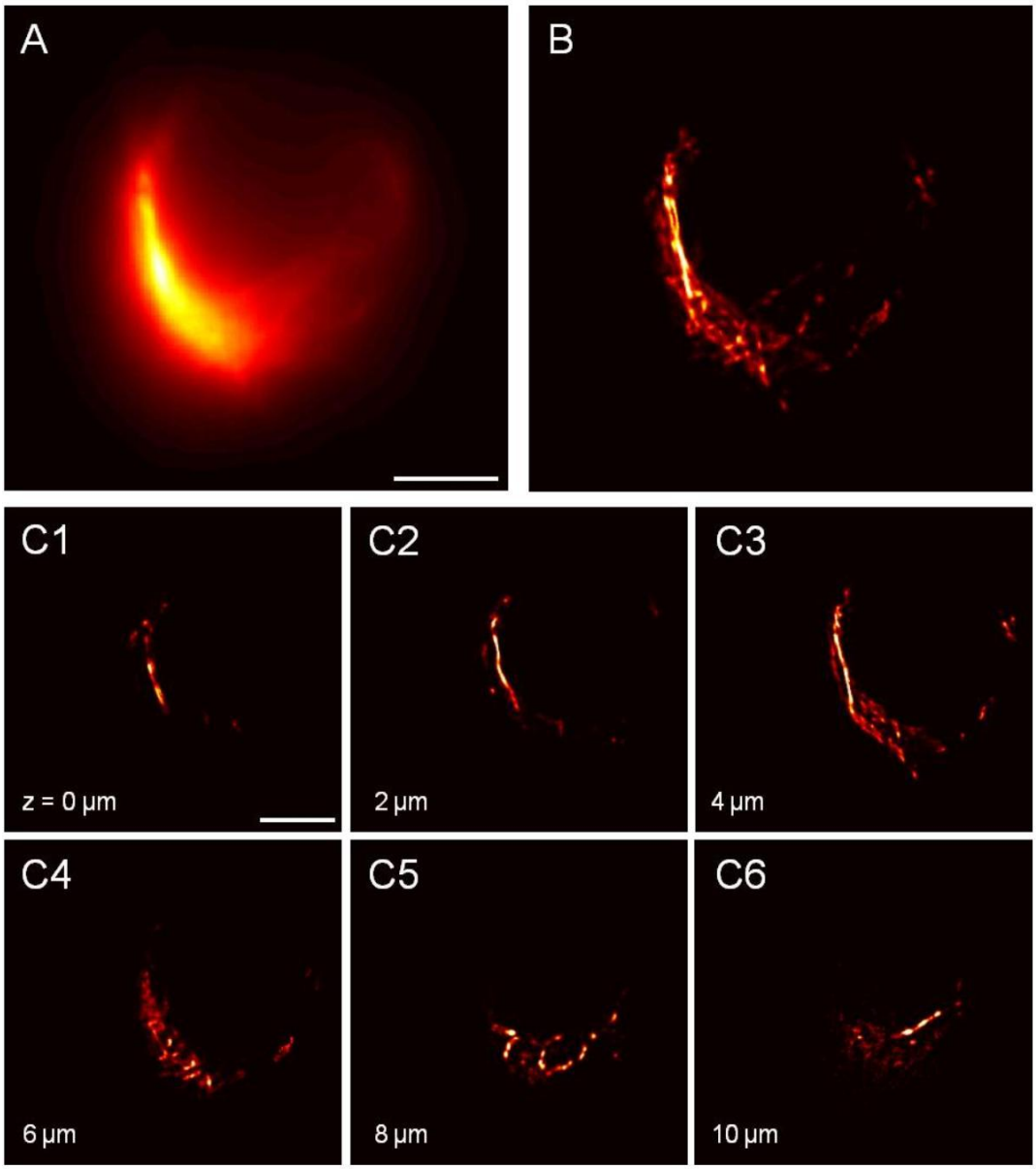

Figure 3.21: PALM analysis of Lifeact-psRFP signal gradient of the nuclear basket in Lifeact-psRFP ox BY-2 cells. (A) Widefield image of a nuclear actin basket. (B) Projection of 18000 single images of 6 sections (each 3000 frames) with a z-axis distance of 2 µm; fine actin filaments exclusive around the nucleus with clear orientation to direction of nuclear migration. Microscopic setup: 30 ms camera exposure time, 300 gain, 4.7x preamp, 5 - 20 mW 561 nm, <1 mW 473 nm. Bars: 5 µm.

3.5 Summary

The prerequisite to investigate the role of actin-binding proteins (ABP) in auxin-dependent pattern formation was the availability of appropriate *Nicotiana tabacum* L. cv. Bright Yellow 2 (BY-2) cell lines expressing tagged variants of these ABP in the homologous system. Therefore, selected ABP were cloned from BY-2, coupled with different fluorescent proteins, and then transformed and expressed in BY-2 using a modified version of the TAMBY-2 method developed by Buschmann *et al.* (2010). This dissertation clearly shows, that the modified version is applicable for stable transformation and provides a good, fast, and reliable alternative superior to the classical transformation procedure established by An (1982).

During the pre-screening of the newly created ABP ox BY-2 cell lines phenotypic parameters like intracellular localization, mitotic index, cell length, cell width, cell proportionality, relative expression level after auxin (IAA) treatment, and cell division pattern were checked to select promising candidates for further investigations. The semi-quantitative PCR after IAA treatment revealed no significant changes of transcript levels, and most cell lines did not reveal obvious phenotypes as compared to the non-transformed BY-2 cell line for most assayed criteria. There was one exception: The division pattern of the *Nicotiana tabacum* actin-depolymerizing factor 2 ox (NtADF2 ox) BY-2 cell line massively differed from the pattern of all other cell lines. Since the division pattern is a highly sensitive monitor for alterations in polar auxin flow (Campanoni *et al*., 2003; Maisch and Nick, 2007), this cell line was investigated in more detail. The mitotic index of this cell line was reduced by around 20 % and the cells were eminently shorter than the non-transformed WT. In addition, cell files with six and eight cells per file, which are diagnostic for polar auxin flow, were nearly totally missing. During localization studies it could be shown, that NtADF2 binds to actin filaments in addition to a diffuse localization. In NtADF2 ox BY-2 cells only a few thick actin bundles and totally disrupted actin filaments could be detected. The next step of investigation comprised complementation experiments which allowed to rescue the impaired division pattern by adding PIP_2 (partially) and phalloidin (complete) as well as the the normal fine actin filaments in the cell cortex (using the stabilizing drug phalloidin). To investigate, whether ADF2 was necessary for actin bundling, a dexamethasone-inducible NtADF2 RNAi BY-2 knockout cell line was created. This cell line, upon induction, behaved antagonistically with respect to the division pattern as compared to the NtADF2 ox line, but was indistinguishable from non-transformed BY-2 cells in the absence of the inducer.

To test, how functionally different sub-populations of actin can coexist in one cell despite a strong conservation of actin, super-resolution microscopy in combination with tetrameric FP reporters were used to distinguish between differentially ABP-decorated actin filament sub-

populations. Establishment and analysis of transgenic BY-2 cell lines expressing fusions of the photoactivated fluorescent proteins psRFP or mIRISFP with Lifeact on the one hand revealed that especially psRFP is a powerful tool for super-resolution microscopy. On the other hand it turned out that there are obviously different functional actin sub-populations within the plant actin cytoskeleton. To test the usability of the tetrameric psRFP construct in PALM applications of living cells, it was possible to acquire images of actin filaments with a brilliant resolution in the range of a few nm. In addition, the signal was that stable that even z-stacks could be produced resulting in one of the first three-dimensional PALM images in plant cell biology. Using classical fluorescence microscopy as well as PALM, central actin filaments structures could be visualized forming a basket around the nucleus. This basket was very stable and marked the leading edge of nuclear migration that accompanies mitosis in vacuolated plant cells.

4. Discussion

In contrast to animals, where patterns and polarity are mostly bound to the whole entity, every single plant cell is characterized by an own polarity, leading to an interaction with neighboring cells to generate an overall polarity and pattern. As a result of their sessile lifestyle plants are eminently dependent on rapid and adequate reactions with respect to exogenous alteration. These reactions reach from transcription to cytoskeletal re-organization.

Previous work could show, that tobacco cell lines such as VBI-0 (*Nicotiana tabacum* L. cv. Virginia Bright Italia 0; Campanoni *et al*., 2003) and BY-2 (*Nicotiana tabacum* L. cv. Bright Yellow 2; Maisch and Nick, 2007) constitute minimal systems capable of pattern formation. Campanoni *et al.* (2003) demonstrated a weak coupling between the divisions of neighboring cells, leading to a clear pattern with elevated frequencies of files composed of an even number of cells. This minimal pattern could later be linked to actin organization by Maisch and Nick (2007). Inhibition experiments identified the polar flow of the phytohormone auxin as responsible signal. In addition to this signal a pivotal role was played by the conformation of filamentous actin culminating in a model, which combined actin conformation with a self-amplifying auxin feedback loop.

These results raised new issues, which were the motivation of the first part of this doctoral thesis. Do actin-binding proteins (ABP) play a role in the mediation of polarly transported auxin-signal and the mentioned self-amplifying feedback loop? Is the conformation of actin necessary and sufficient to maintain the division pattern in BY-2 cell files? The experimental approaches led to a model on patterned cell division in respect to actin, auxin and ABP, which will be discussed below.

In the second part of this work the following questions were in the center: Is it possible to discriminate between different actin sub-populations characterized by a different actin-binding protein (ABP) decoration? Is it possible to use photoactivatable fluorescent proteins (pa-FP) for high resolution PALM-/STORM-Microscopy in living plant cells which could deliver new insights into the configuration of the actin cytoskeleton and its dynamics? The new microscopical techniques not only allowed to discriminate and visualize actin filaments in the low nm-scale, they also led to a model on the function and appearance of intracellular actin sub-populations, which will be discussed in the second part of this chapter.

4.1 Usability of TAMBY-2 for stable BY-2 transformation

The availability of accordant *Nicotiana tabacum* L. cv. Bright Yellow 2 (BY-2) cell lines overexpressing these ABP was the pre-condition to investigate the role of actin-binding proteins (ABP) for auxin-dependent patterning in the homologous system. Therefore, selected ABP were cloned from BY-2, fused to different fluorescent proteins, transformed and expressed in BY-2 cells applying a modified version of the TAMBY-2 method developed by Buschmann *et al.* (2010). As BY-2 cells react definitely sensitive to alterations of the cytoskeleton caused by modifications of the abundance of cytoskeleton-modifying proteins, the correct expression level of the ABP in the transgenic BY-2 cell cultures overexpressing ABP is eminently important to maintain viability. Therefore transformation failures are the norm rather than an exception. To obtain a transgenic BY-2 cell culture overexpressing ABP in an expression level which leaves the cells viable, can last quite a long period of time and require many repeats. To reduce the lag time to reach a functional cell line, a method for transient BY-2 transformation (Buschmann *et al.*, 2010) was modified to meet the requirements for stable transformation. During this work it could clearly been shown that the modified method is not only suitable for stable transformation, but even superior to the classical transformation procedure established by An (1982). The method of An contains some tricky steps which can reduce the transformation rate to zero. Wounding the BY-2 cells for better transformation efficiency by *A. tumefaciens* without killing them and plating the co-cultivated cells with the correct cell density on the selection plates needs not only a lot of experience, but also luck. All these steps are much simpler in the modified TAMBY-2 protocol and even consume considerably less time. As positive side-effect the number of paralleles can be easily raised in the TAMBY-2 method (Buschmann *et al.*, 2010) over the classical protocol raising the probability for successful transformation. Further advantage of the new method is that positive transformants already grow on selection medium. They form calli and are already separated at the initial stage from cell populations without a successful transformation event. Thus, a subsequent separation becomes obsolete, and the positive calli can be transferred immediately into liquid medium saving at least four additional weeks of re-cultivation after screening which was inevitable using the method of An (1982).

4.2 Pre-screening of ABP ox BY-2 cell lines revealed NtADF2 as promising candidate

After establishment of all transgenic ABP ox BY-2 cell cultures, a fluorescent microscopic and a molecular biological analysis followed. On the one side, intracellular localization of the FP-tagged ABP, mitotic index, cell width, cell length and the division pattern of the transgenic cell lines were investigated. On the other side, the expression level of ABP transcripts was

followed by semi-quantitative PCR in response to auxin. These pre-screening experiments supported the work of Maisch and Nick (2007), which showed the incorporation of actin in synchronized cell division in BY-2, as well as a promising candidate (*Nicotiana tabacum* actin depolymerizing factor 2) could be identified playing an essential role in auxin-signaling pathway.

4.2.1 IAA does not affect transcript levels of selected ABP

The initial question of this work was whether an auxin-signal can directly affect actin filament (AF) re-organization through ABP. Therefore, as a first step a semi-quantitative PCR was performed and the transcript levels of selected ABP from different ABP-families were analyzed after treatment with 10 and 30 µM IAA. In the non-transformed BY-2 WT cell culture auxin did not cause any alterations of transcipt levels (data not shown). As additional test, the auxin response in a line with constitutively bundled actin (mTalin ox BY-2 cell culture; Maisch and Nick, 2007) was performed. If there is an effect at all, it should be most readily detectable in this cell line. However, even after increasing the IAA concentration to 30 µM no significant alteration of the expression level of any tested ABP was observable.

The observed re-organization of AF after adding exogenous IAA (Kusaka *et al.*, 2009) starts immediately and is finished after about 20 min. An alteration of ABP expression level should be visible in the tested period of time of about 60 min, whereas a regulation via protein *de novo* synthesis and degradation is not fast enough for the observed actin re-organization (Guilfoyle, 2009). A much faster mode of regulation, for example a kinase-dependent phosphorylation or a transient inhibition of protein function by covering binding-sides, would be much more conceivable. The result of the semi-quantitative PCR supported the assumption that the re-organization of AF is not regulated by the transcription of ABP genes. In addition, the result emphasized the need to search for protein domains in ABP making a fast regulation possible (see 4.3.1, p. 59).

The results of this screening seemed to be clear but there is one point, which should be kept in mind. Due to relatively high similarity of the ABP homologs it is possible that the selected primers had also a certain affinity to several members of the tested family. Under normal restricted conditions the PCR could work as intended and the correct sequence is amplified. As reaction to the auxin treatment the relation of the expression level of different ABP family members could be shifted towards one member while others could be downregulated. The lower affinity for the “false” family member could be still big enough for an amplification as result of the modified abundance of the single homologues and by this way a reaction after auxin treatment could be covered.

4.2.2 Division pattern in ABP ox BY-2 cell lines

The division pattern (DP) of the transgenic BY-2 cell cultures in comparison to that of the non-transformed BY-2 WT cell line was the most important screening parameter during this study. It was known that this pattern is the most sensitive sensor known so far for alterations in polar auxin flow (Campanoni *et al*., 2003; Maisch and Nick, 2007) and can be monitored quite easy by means of frequency distributions.

A non-transformed WT BY-2 cell culture was used as control for DP and showed the characteristic pattern with clear peaks at even numbers of cells per file as expected and described in Maisch and Nick (2007). All transgenic cell cultures tested in this pre-screening featured at least a similar pattern. They possessed higher peaks at bicellular, quadricellular and a slightly reduced frequency of hexacellular files. Both lines expressing the actin markers Lifeact and FABD2 were most comparable in their DP to non-transformed cells. Even the frequency of octacellular files was at a comparable level (Figure 3.2, p. 26). This was not that surprising because both binding proteins used as actin-probes harbor only binding and no bundling functions. They are therefore used as state-of-the-art actin markers and they only marginally stabilize AF by decorating them (Sano *et al.*, 2005). However this mild stabilization seemed to have a positive effect on the division pattern of the accordant actin marker lines such that a slight but clearly visible higher peak of octacellular cell files could be detected. Due to the mild stabilization of actin filaments their dynamic or innate turnover might be slightly slowed down making the filaments a longer time accessible for transport processes. The slight increase in the range of auxin-signaling in these two actin marker lines as compared to the non-transformed BY-2 WT is consistent with a role of actin in this process (Maisch and Nick, 2007) and indicated the importance of filament stability in this background. Up to hexacellular files that are diagnostic for directional synchrony of cell division (Campanoni *et al.*, 2003), also the transgenic cell lines overexpressing ABP showed only moderate alterations in comparison to the characteristic oscillatory behaviour (Figure 3.2 p. 26) with clear peaks at even cell numbers. However, the frequency of octacellular files was clearly reduced in the WLIM2 ox and the VLN1 ox lines. This result is in accordance with the findings of Maisch and Nick (2007) that due to the overexpression of mTalin the AF were constitutively heavily bundled which abolished the division pattern. In contrast to mTalin, the LIM-domain containing (Thomas *et al.*, 2006), and the villin proteins (for review, see Staiger *et al.*, 2010) are only weak actin bundlers, such that an impaired but still coordinated cell division is conceivable resulting in the observed pattern.

These findings strongly support the role of actin organization and especially the role of fine AF for division synchrony and pattern.

During the screening for altered division patterns it turned out that one candidate, the *Nicotiana tabacum* actin-depolymerizing factor 2 ox (NtADF2 ox) BY-2 cell line differed qualitatively from the other ABP ox cell lines by a massive increase of bicellular, a clear reduction of quadricellular, and an almost complete loss of files with more than four cells. Especially the lack of files with six cells is relevant, as this peak is diagnostic for directional weak coupling of cell division and cannot be explained by any other model (Campanoni *et al.*, 2003). One of the already known functions of actin depolymerizing factors (for review, see Staiger *et al.*, 2010) is the binding and depolymerizing of AF. This would comply with the assumption that an overexpression of NtADF2 leads to an abnormal increase of AF depolymerization resulting in hindered auxin-signal mediation and an impaired cell division pattern. The observed division pattern where cell files with more than four cells per file were absent would be a natural consequence of actin depolymerization. Therefore, the subsequent work was centered on this cell line and NtADF2 itself.

4.3 NtADF2 is involved in auxin-dependent patterning

In this section the localization and potential function of NtADF2, a member of the ADF/cofilin-family, will be analyzed and discussed in more detail. During this work the first stable NtADF2 ox BY-2 cell line was created, which enabled the visualization of intracellular localization of NtADF2 *in vivo* in the context of patterned cell division. It was possible to detect a link between ADF function, the stability of fine AF, and auxin-dependent division patterning in BY-2 cell files. This NtADF2 ox cell line allowed to study ADF functions in the homologous system and to rescue the altered cell division pattern of this cell line chemically with PIP_2 and phalloidin. In addition, further ABP overexpressing BY-2 cell lines as well as a NtADF2 RNAi knockout BY-2 cell line could be established also supporting the results obtained from observations of the NtADF2 ox BY-2 cell line.

4.3.1 Phylogenetic and protein domain analysis of the ADF/cofilin family

Phylogenetic analysis using representative plant homologues of selected model plants revealed that NtADF2 contains all characteristic domains of the ADF/cofilin family including a PIP_2 interaction side and clusters together with NtADF1 into subclass II of the plant ADF phylogenetic tree (Figure 3.4, p. 30) described by Mun *et al.* (2000) and extended by Maciver *et al.* (2002). This subclass II is defined as “pollen exclusive expressed“. Since the isolation of two “pollen-specific” paralogs of ADF (Chen *et al.*, 2002), no additional ADF had been reported for *Nicotiana tabacum*. This is quite untypical for plants, which normally possess more ADF homologs than animals (Maciver *et al.*, 2002). Since the source of the NtADF2

cloned in this work was a non-transformed BY-2 line, this is the first report that this ADF isoform is expressed in vegetative cells.

It is necessary to revisit the characteristic protein domains of the ADF/cofilin family. As mentioned before, the re-organization of AF is a very fast process and therefore the regulation has also to be very rapid. The ADF/cofilin family and especially the NtADF2 protein sequence harbors some very interesting domains. The possibility of regulation NtADF2 function by phosphorylation of a serine-6 residue (Allwood *et al.*, 2001) and masking of the binding side for filamentous actin by PIP_2 (for review, see Staiger *et al.*, 2010) resulting in a loss of function offers at least in theory two ways of fast regulation which would be advantageous for a rapid reaction on an auxin signal. In addition to that, Lanteri *et al.* (2008) could show a rapid and transient accumulation of PIP_2 after IAA treatment. Subsequently, more PIP_2 interacts with ADF, blocking its filamentous actin binding site, which would lead to an altered level of active ADF and a modified rate of AF depolymerization.

4.3.2 Actin cytoskeleton is impaired by NtADF2 overexpression

A closer look on the AF of the NtADF2 ox BY-2 cell culture revealed that only thick actin bundles could be detected both after transient transformation (Figure 3.6, p. 33) and TRITC-phalloidin staining (Figure 3.6 H, I), whereas fine filaments were totally absent or fragmented (Figure 3.6 F). This shift towards the bundled conformation would be expected when ADF preferentially acted on the more dynamic fine AF. ADF binds at the pointed-end and twists the filament leading to an enhanced decay (for review, see Bamburg, 1999). In contrast, thick filaments are stabilized by actin-bundling proteins, and AF that are bundled by mTalin (Ketelaar *et al.*, 2004) or *Arabidopsis*-villin (Huang *et al.*, 2005) persist the depolymerizing activity of ADF *in vitro*. The thick AF observed after transient transformation probably persisted because they were protected from depolymerization due to their bundling. Due to the artificial stabilization of AF by phalloidin pre-treatment, fine AF could be protected from decay in the NtADF2 ox line (Figure 3.6 K3). In addition to bundled actin cables a strong cytoplasmic and nuclear GFP-signal was detectable (Figure 3.6 D), probably due to the high affinity of ADFs for G-actin (Carlier *et al.*, 1997; Blanchoin & Pollard, 1999). To test for potential effects of overexpression or cell cycle, different incubation times and cell ages were checked, without any significant effects on localization (Figure 3.6 A-C). The absence of fine filaments was confirmed by the observation of the stable transformant (Figure 3.6 E), and is congruent with findings published for pollen tubes (Chen *et al.*, 2002).

4.3.3 NtADF2 overexpression affects cell growth and division pattern

The phenotypic characterization revealed clear differences between non-transformed and NtADF2 ox cell culture. NtADF2 ox cells were significantly shorter and exhibited a reduced MI (Figure 3.7, p. 34), indicating that, due to the overexpression of NtADF2, there are no fine filaments left or stable enough to fulfill their role in intracellular trafficking, affecting growth and mitosis. Similar results have been shown by Chen *et al.* (2002) for tip growth in tobacco pollen tubes and by Dong *et al.* (2001) for longitudinal growth of *Arabidopsis thaliana* cotyledons, hypocotyls, and roots at the seedling stage.

Non-transformed BY-2 cells grow in files up to eight cells per file with an enhanced amount of even-numbered cells per file before decay into shorter even-numbered files. This synchronized file growth is, as mentioned before, dependent on polar flow of auxin (Maisch and Nick, 2007; Nick *et al.*, 2009; for review see Nick, 2010). The NtADF2 ox cell line behaved significantly different. Files with more than four cells were hardly detectable (Figure 3.8, p. 35). Thus, the depolymerization of fine AF, caused by overexpression of NtADF2, interfered with the auxin-dependent synchrony of cell division. This synchrony should be, at least partially, restored when fine AF are protected from depolymerization via exogenous PIP_2 which competes with F-actin binding of NtADF2 reducing the depolymerizing activity of NtADF2. In fact, it was possible to partially restore the division pattern by exogenous PIP_2 (Figure 3.9 B, p. 36) demonstrating the participation of NtADF2.

In addition to this direct complementation of NtADF2 functional upregulation by adding exogenous PIP_2, a chemical complementation downstream of NtADF2 was tested. The question was, whether a rescue can be achieved by reducing actin dynamics *per se*. If the missing existence of stable fine filaments is the reason for the impaired division synchrony, the stabilization of the fine AF should decrease ADF depolymerizing activity and rescue the normal division pattern in the NtADF2 ox line as well. To test this reasoning, the NtADF2 ox BY-2 cell line was treated with phalloidin at a low concentration that was not causing toxicity even for prolonged treatments. Indeed, the phalloidin treatment resulted in a complete rescue of division pattern in the NtADF2 ox BY-2 cell line (Figure 3.10 B, p. 37) at a concentration that did not cause a significant effect on the non-transformed control culture (Figure 3.11 A, p. 37). This observation correlates with the findings described above (see 4.3.2, p. 60), where due to the artificial stabilization of AF by phalloidin pre-treatment fine AF could be protected from decay in the NtADF2 ox line and visualized by TRITC-phalloidin staining (Figure 3.6 K3, p. 33).

In the work of Maisch and Nick (2007), the altered division pattern could be rescued by adding IAA, which led to a debundling of the AF in the mTalin ox BY-2 cell culture.

Fluorescent microscopy of the NtADF2 ox BY-2 cell line showed also thick strains of bundled AF. Therefore it could be possible that the missing fine filaments were not depolymerized but just bundled and that this effect is responsible for the similar division pattern of the NtADF2 ox and mTalin ox BY-2 cell lines. This interpretation could be tested with a simple experiment. If only the bundles of AF are the reason for the impaired division pattern, the addition of IAA should lead to a recovery of the DP in the NtADF2 ox BY-2 cell line but it failed to do so (data not shown).

This finding supported the suggestion that the stability of fine filamentous actin plays a pivotal role in auxin-dependent patterning supported by the results of the phenotypic characterizations of additional actin marker lines overexpressing actin-bundling proteins like NtVLN1 or NtWLIM2 (Figure 3.2, p. 26), and LatB treatment of non-transformed BY-2 WT cells (Figure 3.12 B, p. 38), respectively. In the latter approach it was possible to phenocopy the NtADF2 ox BY-2 DP phenotype by treating the non-transformed BY-2 WT cells with a low concentration of LatB.

4.3.4 Inducible NtADF2 RNAi knockout BY-2 cell line supports NtADF2 ox BY-2 phenotype

As nearly all results were derived from ABP overexpressing BY-2 cell lines where side-effects might obscure interpretation, a dexamethasone inducible NtADF2 RNAi knockout BY-2 cell line was established and investigated with respect to patterning. Control experiments verified that the division pattern of the non-transformed BY-2 WT was not affected by the inducer dexamethasone (Figure 3.13 A, p. 39), and that the NtADF2 RNAi knockout BY-2 cell line behaved as the non transformed line in the absence of the inducer (Figure 3.13 B). A clear shift from cell files with fewer cells towards files with six and eight cells could be observed when the RNAi lines were induced with dexamethasone (Figure 3.13 C). This phenotype was antagonistic to that observed in the NtADF2 ox BY-2 cell line, which supports the notion that the observed DP of the transgenic cell line is NtADF2-specific and not a side-effect of transformation *per se*. Moreover, the stability and abundance of fine filamentous actin seems to be crucial for auxin-dependent signaling. Nevertheless the results of the NtADF2 RNAi cell line have to be taken with a pinch of salt. To fulfill the requirements of the pOpOff vector the whole sequence of the NtADF2 was chosen as probe. As indirect proof of functionality the β-glucuronidase marker gene transcript level was tested. An additional test for downregulation of the NtADF2 has to be performed at the protein level. Keeping in mind, that the high level of ADF identity could also lead to off target effects.

4.3.5 Model of auxin signaling towards actin

Summing up all derived data of the different transgenic BY-2 cell lines and experiments, the observations can be integrated into a first working model comprising a putative pathway from auxin signaling via actin re-organization to synchronized cell division with NtADF2 as pivotal player. The working model is composed of four interdigitated regulatory mechanisms:

I.) (Figure 4.1, cyan) Auxin passes the cell membrane via diffusion or transmembrane proteins (Lanková *et al.*, 2010) activating several auxin-dependent pathways, among others, ADF-related events. Here, one of the first steps is the alteration of the PIP_2-level in the inner membrane layer causing a rapid and transient accumulation of PIP_2 (Lanteri *et al.*, 2008). Subsequently, more PIP_2 interacts with ADF, hindering its actin binding site. This leads to a reduced depolymerization activity of ADF. Additional to this interaction, ADF is able to inhibit the activity of PLC (Gungabissoon *et al.*, 1998), thus raising the PIP_2 level even further.

II.) (Figure 4.1, yellow) A second regulatory mechanism is based on the phosphorylation state of ADF. This phosphorylation at serine-6 is mediated by a yet unidentified Ca^{2+}-dependent kinase (CDPK), which, in turn, is affected by Rac/Rop GTPases (Smertenko *et al.*, 1998; Allwood *et al.*, 2001; Chen *et al.*, 2003). Phosphorylated ADF is not able to depolymerize actin and was long thought to be a completely inactive form of the protein. However, Han *et al.* (2007) could show a direct stimulation of PLD activity for phosphorylated ADF/cofilin which is again linked to a Calcium-dependent protein kinase (CDPK) via phosphatidic acid (PA) signalling (Farmer & Choi, 1999).

III.) (Figure 4.1, red) In interaction with other ABP like profilin, capping proteins (for review, see Staiger *et al.*, 2010), or actin-related proteins (for review, see Bernstein & Bamburg, 2010), ADF affects actin dynamics and conformation by modulation of the equilibrium between polymerized F-actin and cytoplasmic G-actin. Both forms of actin are able to interact directly with PLD to control their intracellular amount. G-actin inhibits PLD-activity, whereas F-actin is stimulating (Pleskot *et al.*, 2010), such that ADF-phosphorylation rate can be regulated via this pathway (see regulatory mechanism II).

IV). (Figure 4.1, green) Downstream of the three described regulatory mechanisms, the auxin signal transmitting pathway is dependent on the actin conformation. Bundled AF impair intracellular transport and, thus, interfere with the proper localization of PIN-formed proteins, that are essential for auxin export (for review, see Nick, 2010).

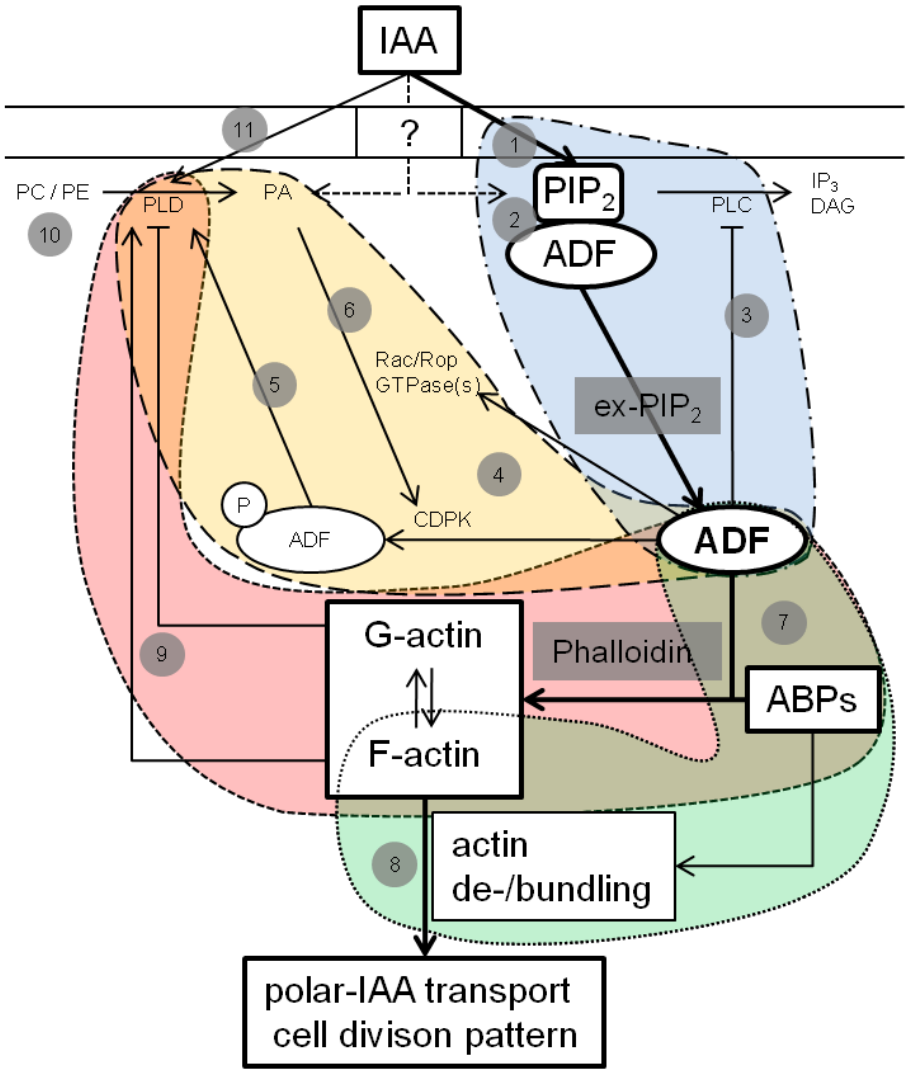

Figure 4.1: Model of the putative pathway from auxin signaling via actin re-organization to synchronized cell division (arrows in bold). References: (1) Lanteri *et al*., 2008; (2) Van Troys *et al*., 2008; (3) Gungabissoon *et al*., 1998; (4) Lin *et al*., 2004; (5) Chen et al., 2003; (6) Bernstein and Bamburg, 2010; (7) Farmer and Choi, 1999; (8) Campanoni and Nick, 2005, Maisch and Nick, 2007; (9) Bernstein and Bamburg, 2010, Staiger *et al*., 2010; (10) Pleskot *et al*., 2010; (11) Wang, 2000; (12) Lanteri *et al*., 2008.

4.4 Conclusion (NtADF2)

In conclusion, actin-binding proteins in general and actin-depolymerizing factor 2 in particular fullfill an important role in auxin-signal mediation. The results of this dissertation were consistent with the work of Maisch and Nick (2007) and Nick *et al.* (2009), in which they could decipher the incorporation of actin filaments in auxin-dependent synchronized cell division in BY-2 and in rice, by artificial actin-bundling due to massive overexpression of mTalin in combination with rescue experiments. Especially the stable overexpression of actin-binding proteins like the *Nicotiana tabacum homologs* of Villin 1 and WLIM 2 in BY-2 with moderate actin-bundling properties (for review, see Thomas *et al.*, 2009), whose phenotypes could be sorted in between the extreme pattern of the mTalin ox BY-2 cell

culture and the characteristic natural division pattern in non-transformed BY-2 WT cell cultures. It was possible to identify a relation between actin-bundling intensity and the impaired division pattern of the cell cultures. Additionally to this already expected correlation, the identification of the *Nicotiana tabacum* actin-depolymerizing factor 2 as a pivotal key protein for a predicted auxin-signal pathway represents the first attempt to link an actin-binding protein to this auxin-driven phenomenon of actin re-organization. In combination with the results from overexpression and complementation, this work clearly indicate, that abundance and activity of NtADF2 control the stability of fine AF as prerequisite for functional auxin-dependent signalling with respect to synchronized cell division (Campanoni and Nick, 2005; Maisch and Nick, 2007). In addition, the stability of fine AF is involved in keeping the mentioned actin-auxin oscillator running.

4.5 Outlook (NtADF2)

The present dissertation contributed to the understanding of the complex system of auxin-dependent patterning while leading to further questions related to auxin-signal perception, mediation and actin organization, which should be in focus of future research:

Combining the already known information about interaction partners of actin-depolymerizing factors like profilins or capping proteins (for review, see Staiger *et al.*, 2010) with results of this work (partial complementation after PIP_2 treatment) implicates that the non-linear and dynamic activity of NtADF2 in the regulation of actin organization is expected to involve complexes with other ABPs. To identify possible interaction partners connected to this auxin-induced actin re-organization, titration of complex composition through genetic engineering would be a logical next step.

In addition to this first point, it is crucial to have a closer look at the first border the auxin-signal has to cross – the plasma membrane. Besides ion channels (especially Ca^{2+}; phosphorylation of ADF is directly affected by a Ca^{2+}-dependent protein kinase; Allwood *et al.*, 2001), and recently identified influx carriers like AUX/LAX (Petrášek and Friml, 2009; Friml, 2010), further actin-binding proteins could play an essential role in this system as well. During the last years, the formins were put in the focus of attention (Yang *et al.*, 2011). Due to their localization next to the cell membrane, their role as anchor points for actin filaments, and further functions like actin polymerization (Cvrcková *et al.*, 2004; Michelot *et al.*, 2005, 2006; Blanchoin and Staiger, 2010), they could be of elementary importance for auxin-signaling. First cloning approaches of two *Nicotiana tabacum* homologues have already been initiated.

In parallel to ABPs (like the formins), also the role of the phospholipases C and D should be investigated in more detail. Both are located in the zone of initial contact with the auxin-signal. While phospholipase C is directly connected to PIP_2-level regulation in the membrane and affected by cytoplasmic ADF, phospholipase D can directly bind actin filaments (Bernstein and Bamburg, 2010), and microtubules (Gardiner *et al.*, 2001). Microtubules are, with respect to auxin-dependent patterning, quite unattended but probably important as shown in the work of Heisler *et al.* (2010) for the correlation of microtubule orientation and PIN1 (auxin efflux carrier and responsible for polar flow of auxin) polarity.

A very promising method to address these complex mechanisms in the future is the technique of RNA interference, which gives the opportunity to silence single components of the system and enables the observation of possible effects for example in transgenic BY-2 cultures. Nevertheless, the cellular mechanisms responsible for silencing and their potential side-effects are still far from being completely understood. Thus, it is of elemental need to critically examine every single result.

In addition to the before mentioned experimental approaches to auxin-signal perception and signaling, a closer look on the BY-2 cell culture itself is of major interest. The division pattern of this cell line has been successfully used as reporter for auxin signaling and several regulatory circuits could be identified. However, the disintegration of cell files into single cells is still a promising topic. NtADF2 ox BY-2 cell files only possessed a low number of cells per file at the point of examination with a high amount of bicellular files, the smallest regular unit. But also non-transformed tobacco cell files disintegrate during their cell cycle into even-numbered cell files with fewer cells and this pair-cell rule can be disrupted by inhibitors of polar auxin transport (Qiao *et al.*, 2010). Even though the polar transport of auxin obviously plays an important role, the processes linked to auxin habituation or the dampening of this flow are also far from being understood. Therefore, beside the formation of cell files also their decay has to be investigated.

As last point of this section it is necessary to mention that ABP as possible mediators of auxin-dependent patterning probably cooperate with additional factors such as reactive oxygen species that can be modulated by pathogens or stress leading to actin re-organization. Not only BY-2 cells, but also “real” plants respond to these signals by cytoskeletal bundling (for recent review, see Smertenko and Franklin-Tong, 2011) or disruption (Qiao *et al.*, 2010).

4.6 Visualization and discrimination of different actin sub-populations

The second aim of this work was the visualization and discrimination of different actin sub-populations. Actin has to fulfill many various different tasks while its isoforms are highly conserved even between different species (Meagher *et al.*, 1999a, 1999b). Therefore, structural differences between actin isotypes can be excluded as factor controling functional differentiation between AF sub-populations. In fact, it is the different subsets of actin-binding proteins and their complexes that are responsible for the functional variability of the single filaments. This raised the question whether it is possible to discriminate between different sub-populations of actin filaments, which differ in respect to their ABP decoration. In this work, a FP-based strategy was designed. The yeast peptid Lifeact, binding to an ubiquitous motif in filamentous actin was used as actin-binding probe and fused with two different FP. For the first construct a psRFP, which forms tetramers, typical for anthozoan FP (Fuchs, 2011), was used. Due to its molecular size a binding of the Lifeact motif to actin should be sensitive to steric hindrance in case of a dense decoration with ABP. As control, a second construct consisting of the monomeric mIRISFP was selected, which is comparable in size to the classical GFP and should therefore bind actin filaments without steric hindrance. There was an additional reason for selecting these two FP. Both belong to the class of pa-FP and offered the possibility of super-resolution microscopy using photoactivation localization microscopy (PALM), a technology that so far, to our knowledge, has never been applied in living plant cells.

Indeed, this “steric-hindrance approach” revealed different functional sub-populations of actin filaments in BY-2 cells and the super-resolution PALM delivered images of actin filaments with a resolution of about 20 nm, both discussed in the following in more detail.

4.6.1 Differences in localization pattern of Lifeact-psRFP after transient and stable transformation

As routinely done with all newly cloned constructs, the fusion of Lifeact and psRFP was tested for functionality by transient transformation using the ballistic method of a particle gun (Figure 3.14, p. 42). The efficiency of the transformation was at a moderate level compared to other constructs produced in this work (e.g. GFP-NtADF2), and the Lifeact-psRFP signal labeled filamentous structures very clearly. As it was expected that the Lifeact peptide would bind filamentous actin, the observed localization of the psRFP-signal was not surprising. The psRFP belongs to the group of positive switchers (Fuchs, 2011), which means that the ground state of the FP is its “off”-mode. Therefore, screened areas had to be illuminated first

with light of 561 nm wavelength. This procedure helped to localize the transgenic cells in the population much faster. The filaments labeled by Lifeact-psRFP as well as by Lifeact-mIRISFP were homogenously distributed through the entire cell. A difference in localization could not be observed.

The constructs seemed to be functional and the next logical step was the stable transformation into BY-2 cells because the transient transformed cells could not be used for PALM anyway, as the number of transformed cells was too small. As mentioned before, a second Lifeact-fusion with the pa-FP mIRIS was also generated and tested. The localization was identical to the Lifeact-psRFP signal, but the transformation efficiency was much lower. This was not that spectacular but it was a first small difference between the two selected FP for the Lifeact-fusions. However, after stable transformation, more conspicuous differences between the two constructs emerged. Whereas in the Lifeact-mIRISFP expressing cells, similar to the transient approaches, filamentous structures were labeled throughout the entire cell, in the Lifeact-psRFP expressing cells, only a basket-like structure around the nucleus was marked (Figure 3.14 E, p. 42). A control staining with Alexa-Fluor® 488 phalloidin revealed that the structures marked by the Lifeact-fusions were indeed filamentous actin including the basket-like structure around the nucleus. This control staining showed further that there are additional sub-populations of filamentous actin existent in Lifeact-psRFP expressing cells, which are not labeled by the probe (Figure 3.15, p. 43) but only by Alexa-Fluor® 488 phalloidin.

This finding, in combination with the Lifeact-mIRISFP data, exclude the possibility that the observed localization was nuclear basket specific. But this also meant that it was possible to specifically label different sub-populations of actin within a cell. The sole difference between both probes was the nature of the FP label. Thus, the Lifeact-psRFP expressing BY-2 cells clearly reveal a difference between central and cortical actin filaments with respect to the availability of the Lifeact binding side. As pointed out in the introduction (see 1.3, p. 5), stability and dynamics of filamentous actin are controlled by actin-binding proteins (ABP) and their complexes. Since actin isoforms are very conserved, it is straightforward to assume that the decoration with different ABP differentiates functionally different sub-populations of actin. The sub-population constituting the nuclear basket might be accessible for the Lifeact-psRFP fusion protein, because they are more scarcely decorated with ABP, whereas the cortical filaments are densely covered impeding the access of the tetrameric probe (Figure 4.2).

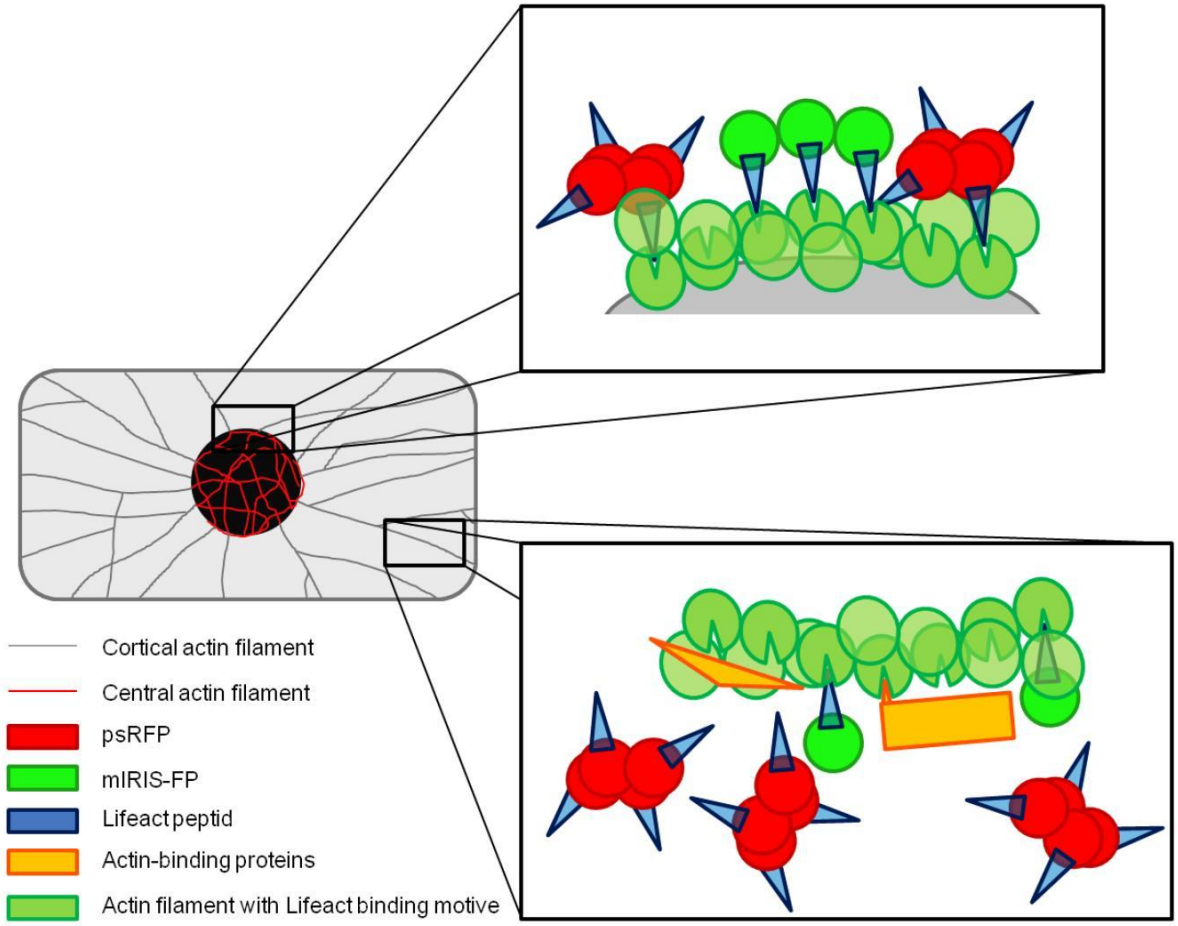

Figure 4.2: Model of the putative Lifeact-psRFP and Lifeact-mIRISFP binding to the nuclear actin basket and to cortical or transvacuolar actin filaments. The Lifeact-mIRISFP construct is able to bild both sub-populations of actin, whereas the tetrameric Lifeact-psRFP is excluded at the small binding sites left freely accessible by ABP decoration. The FP and especially the tiny Lifeact peptide are not true to scale for better visibility.

This model is supported by the observation that cortical AF are labeled in cells going to die, such that the functionality of cortical actin is expected to be disrupted. These cells may have ceased their regulated decoration and the Lifeact-psRFP binding motif became freely accessible.

The observed complete decoration of actin filaments in transiently transformed BY-2 cells can be explained in a similar way: In transient transformation only the cells with the highest level of expression are detected. These cells are not viable in the long term, but are extremely stressed due to functional disruption of the cytoskeleton as consequence of overexpression. In stable transformation, only those cells will survive where the expression of the probe does not impair cellular functions leading to natural selection of physiological levels of the probe.

4.6.2 The nuclear basket of Lifeact-psRFP expressing BY-2 cells alters during cell cycle

The Lifeact-psRFP signal around the nucleus was very stable (data not shown), but varied through the cell cycle (Figure 3.17, p. 46). A clear cell cycle-dependent gradient could be observed. In BY-2 cells at the onset of mitosis, the nucleus was positioned in the cell center, and the psRFP-labeled actin filament basket was very homogenous and formed a tight meshwork around the nucleus. In contrast, nuclei, which moved towards the cell center in preparation of mitosis, showed a clear signal-gradient towards their direction of migration. During mitosis, the labeled actin filaments moved to the poles of the new daughter nuclei and subsequently formed a homogeneous meshwork around the nuclei (Figure 3.18, p. 47). After cytokinesis, the Lifeact-psRFP signal was exclusively found between the new cell wall and the daughter nuclei. It was possible to observe, how whole nuclei were turned, without re-orientation of the labeled actin filaments, and pulled into the new center of the cell. The signal of the nuclear basket was observed to be most intense at the “anchor” points (see supplementary movie on DVD) of transvacuolar cytoplasmic strands that are maintained by actin filaments and microtubules. These observations clearly show that the labeled actin filaments are actively regulated by the cell.

This raised the question for the reason of this regulation. Eventually, the open epitope, which could be labeled by the psRFP tetramer is a kind of an intracellular signal. An indication for binding proteins or complexes is imaginable. This question could not be answered in this work, but without any doubt, the labeled actin basket was characterized by a clearly visible stability and stability is definitely advantageous for saving informations. The nuclear basket and its polarity could probably function as a spatial memory for cell polarity.

4.6.3 Nuclear actin basket - a spatial memory for cell polarity

The questions how cell polarity is inherited from the mother to the daughter cell, the role of the cytoskeleton as spatial memory during cell division, and how nuclear position and migration affect this process are essentiall but poorly understood. Until now unidentified signals have to be responsible to maintain growth direction and formation of polarity after cell division. The stability and orientation of the nuclear basket observed in Lifeact-psRFP expressing BY-2 cells could be a part in this re-formation of cell polarity.

To exclude a stabilization caused by mere overexpression, the Lifeact-psRFP expressing BY-2 cell line was tested for its drug sensitivity. The chosen drug latrunculin B (LatB), which binds and irreversibly sequesters G-actin, leads to an elimination of actin filaments depending on their innate turnover. Stable actin bundles require a longer action or higher

concentrations of the inhibitor, dynamic actin filaments are rapidly eliminated (Coué *et al.*, 1987). Therefore, LatB sensitivity can be used to monitor actin filament stability. If the expression of Lifeact-psRFP would have led to a raised stability of actin filaments *per se*, the cell culture should be less sensitive. The packed cell volume would have been in this case at least at the same level compared to LatB-treated non-transformed BY-2 WT control cells. However, the clear opposite was observed (Figure 3.16, p. 44). The Lifeact-psRFP expressing cells were even more sensitive to LatB treatment, indicating that there is no general stabilization of actin filaments. Nevertheless, data of a recent bachelor thesis (Brochhausen, 2011) showed a slightly delayed nuclear migration compared to the non-transformed BY-2 WT short before mitosis. A similar effect was described by Frey *et al*. (2010) for BY-2 cells, where a kinesin with the calponin-homology domain (KCH) from *Oryza sativa* had been overexpressed. Actin filaments, microtubules and KCH seem to cooperate in the premitotic nuclear migration (Frey, 2011; Klotz and Nick, 2012).

Although every visualization alters and impairs the marked system, the participation of the Lifeact-psRFP labeled actin basket in nuclear migration is consistent with the nuclear pulling model worked out for the KCH kinesins (Frey *et al.* 2010; Klotz and Nick, 2012).

If the stability and orientation of the nuclear basket observed in Lifeact-psRFP expressing BY-2 cells plays a pivotal role in the establishment of cell polarity in cells after mitosis, the basket should be a kind of starting scaffold for cytoskeletal re-formation. Therefore, Lifeact-psRFP expressing cells had been protoplasted to mimick the loss of polarity following mitosis. Due to protoplasting BY-2 cells are transferred into a non-polar state, in which the cytoskeleton does not possess any special predominant direction. After re-organization of the cytoskeleton in combination with nuclear movement, a new polarity develops in the cell providing the direction of growth. The persistence of the nuclear basket during this *tabula rasa* state (Figure 3.19, p. 48) and its clear gradient during the cell cycle (Figure 3.17, p. 46) stimulates a model where the nucleus itself or rather its actin basket already harbor a basic polarity. This polarity could be inherited to the daughter cells and trigger the establishment of the cell polarity.

4.6.4 Super-resolution microscopy in living plant cells using photoactivation localization microscopy (PALM)

In comparison to animal cells, in which super-resolution microscopy already led to enormous progress in comprehension of the cytoskeleton, microscopy in plant cells is limping behind. One of the reasons is the cell wall. Because of its thickness an intact cell wall renders methods like total internal reflection microscopy (TIRF) impossible in plant cells without protoplastation. A second problem are autofluorescent compounds such as chlorophyll or

secondary plant metabolites. The development of photoactivation localization microscopy (PALM) along with the discovery and further development of photoactivated fluorescent proteins (pa-FP) enables an insight in living plant cells never seen before. Due to the combination of an improved protocol for plant cell transformation, the usage of pa-FP instead of classical FP, and computer-based signal localization of the PALM technique it became possible for the first time to perform super-resolution microscopy in living plant cells with intact cell wall, and at a low nm scale. This dissertation shows not only the feasibility of a stably expressed Lifeact-psRFP fusion for PALM in plant cells, but also the possibility to reconstruct three-dimensional images out of several planes constructed from thousands of individual frames. As PALM was used before only for solitary sections, this is an important step towards application of super-resolution microscopy in cell biology in general, and in plant cells in particular. The results of super-resolution PALM supported and extended the findings observed by classical fluorescence microscopy in the transgenic Lifeact-psRFP expressing BY-2 cell line.

PALM of living Lifeact-psRFP ox BY-2 cells

Additional target of this work, in addition to the interesting insights into nuclear migration and polarity, was to test the applicability of psRFP for super-resolution imaging applying PALM in living plant cells. As shown in Figure 3.14 (p. 42), it was possible to stably transform BY-2 cell cultures with Lifeact-psRFP and Lifeact-mIRISFP fusions, which was the first step on the way to super-resolution images of actin filaments in plants. The mIRISFP expressing cells were only used as control cell line for the nuclear basket labeling of the Lifeact-psRFP expressing BY-2 cells and were not tested for PALM imaging. On the one hand, it was possible to depict the nuclear actin basket with a resolution in the low nm-scale. On the other hand, the excellent photostability of the psRFP-signal allowed to visualize several z-stacks of one individual nuclear basket, which could be used for reconstruction of the complete three-dimensional structure (Figure 3.20 B, p. 50). This represents an advance of the PALM technique, because super-resolution was limited to a single focal layer (e.g. **Appendix** 7.9, p. 98 shows single sections typical for PALM). Especially plant cells possess a distinct three-dimensional structure stabilized by the cell wall, posing a further challenge to microscopic imaging as compared to the flat adhering animal cells. There are several possible reasons for this observed photostability. The fluorescent molecule could be either more resistant to bleaching in general or the signal stability could be connected to the maturation of the chromophore. Both possibilities should be investigated in future work.

4.7 Conclusion (super-resolution microscopy)

It was possible to visualize and discriminate between different functional actin sub-populations by means of the Lifeact-psRFP construct expressing BY-2 cell culture. The psRFP-labeled nuclear actin basket seemed to have a stabilizing function on the nucleus additional to its presumed role for nuclear migration. In contrast to animals, plants do not have intermediate filaments - at least up to now they could not be demonstrated, despite considerable effort. Intermediate filaments maintain the nuclear structure in animal cells. The localization of the Lifeact-psRFP revealed a sub-population of actin filaments which might represent the functional plant analogue of intermediate filaments. The discovery of a sterically different AF population in the nuclear basket expands existing models on nuclear migration, even though the whole mechanism is still far from being understood.

Independent of these findings, it was possible to use super-resolution PALM in living plant cells and resolve cytoskeletal structures at a scale of about 20 nm. In this doctoral thesis it could be demonstrated, that the BY-2 cell culture as well as the psRFP fused to Lifeact (or other proteins of interest) is amenable to get a better understanding of cellular processes in plant cell biology.

4.8 Outlook (super-resolution microscopy)

To gain and expand knowledge, applicability is the ultimate goal of technical progress in any field of science. Therefore, it is necessary to put technical developments into practice under defined conditions and specific questions. PALM and psRFP have been successfully employed in living plant cells to address the question of functionally different actin sub-populations. In this approach, the imaging velocity of the PALM setup and the photostability of the psRFP were crucial for image acquisition at the low nm-scale. The relative low dynamics of the actin filament basket enabled the sequential imaging of 3000 single frames at 30 ms excitation. Highly dynamic structures are still a serious challenge for super-resolution microscopy, which is the starting point of further development. It would be a great benefit, if the imaging speed of the microscopes could be improved, for example by shorter excitation periods of advanced fluorescent proteins or by increasing the sensitivity of signal detection. In parallel, the ongoing search for new fluorescent proteins or engineered variants of FPs already in use has great potential.

In case of psRFP, this engineering would comprise the breakage of the tetrameric structure into monomers by introducing sequence mutations comparable to the development of mIRISFP based on its tetrameric precursor. As this procedure is not that easy as it sounds, a larger period of time has to be scheduled. Not only the identification of the structurally

relevant amino acids is time-consuming, but also problems linked to monomerization can pose challenges leading for example to unintended localization of the fluorescent protein in the cell. After successful engineering, the localization of the monomeric version of the psRFP would be an ultimate proof of the presumed reasons for the localization of the tetrameric psRFP used in this work.

A very fundamental question in cell biology is the question, how actin-binding proteins are targeted to the filaments and locations in the cell they are designed for? There are no membrane encased compartments in the cytoplasm. Are the ABP translated and subsequently transported to their area of activity, or are they synthesized directly at their site of activity? If the first assumption is correct and they are synthesized next to the nucleus, how does the protein find the correct filament? All these questions probably could be answered by labeling single ABP using photoactivatable fluorescent proteins like Eos-FP, photoswitching subpopulations of the FP-tagged ABP at defined cellular regions, and following their localization over time. To construct a vector system based on the Gateway® technique and a pa-FP instead of a conventional FP will be a future project. For this purpose, a monomeric Eos-FP and the monomeric IRISFP will be choosen (both FP are developed by the group of Prof. U. Nienhaus, Institute for applied physics and Center for Functional Nanostructures (CFN), Karlsruhe Institute of Technology (KIT)). The monomeric IRISFP would additionally enable super-resolution imaging beside its pulse-chase possibility and combine both powerful tools.

5. Acknowledgments

The author thanks:

Dr. Monika Dieterle (Center de Recherche Public-Santé, Val Fleuri, Luxembourg) for the GFP-WLIM1 ox BY-2 cell line.

Prof. Takashi Ueda (Laboratory of Developmental Cell Biology, University of Tokyo, Japan) for the Lifeact-VENUS construct.

Dr. Jan Maisch (Botanical Institute I, Karlsruhe Institute of Technology, Germany) for the fimbrin actin-binding domain 2 ox and the mTalin ox BY-2 cell lines.

Dr. Petra Hohenberger (Botanical Institute I, Karlsruhe Institute of Technology, Germany) for the pDONR-NtADF1 and pDONR-NtADF2 constructs.

This work was supported by the Center for Functional Nanostructures, CFN, Project E1.5, and Sino-German Center for Science Funding, Programme GZ614.

6. References

Adam, V., Lelimousin, M., Böhme, S., Desfonds, G., Nienhaus, K., Field, M.J., Wiedenmann, J., Mc Sweeney, S., Nienhaus, U. and Bourgeois, D. (2008) Structural characterization of IrisFP, an optical highlighter undergoing multiple photo-induced transformations. *Proc. Natl. Acad. Sci. USA* **105**, 18343-18348.

Allwood, E.G., Smertenko, A.P. and Hussey, P.J. (2001) Phosphorylation of plant actin-depolymerising factor by calmodulin-like domain protein kinase. *FEBS Lett.* **499**, 97-100.

Allwood, E.G., Anthony R.G., Smertenko, A.P., Reichelt, S., Drobak, B.K., Doonan, J.H., Weeds, A.G. and Hussey, P.J. (2002) Regulation of the pollen-specific actin-depolymerizing factor LlADF1. *Plant Cell* **14**, 2915-2927.

An, G. (1985) High Efficiency Transformation of Cultured Tobacco Cells. *Plant Physiol.* **79**, 568-570.

Bamburg, J.R., McGough, A. and Ono, S. (1999) Putting a new twist on actin: ADF/cofilins modulate actin dynamics. *Trends Cell Biol.* **9**, 364-370.

Berghöfer, T., Eing, C., Flickinger, B., Hohenberger, P., Wegner, L.H., Frey, W. and Nick, P. (2009) Nanosecond electric pulses trigger actin responses in plant cells. *Biochem. Biophys. Res. Commun.* **387**, 590-595.

Berleth, T. and Sachs, T. (2001) Plant morphogenesis: long-distance coordination and local patterning. *Curr. Opin. Plant Biol.* **4**, 57-62.

Bernard, P., Couturier, M. (1992) Cell killing by the F plasmid CcdB protein involves poisoning of DNA-topoisomerase II complexes. *J. Mol. Biol.* **226**, 735-745.

Bernstein, B.W. and Bamburg, J.R. (2010) ADF/Cofilin: a functional node in cell Biology. *Trends Cell Biol.* **20**, 187-195.

Betzig, E., Patterson, G.H., Sougrat, R., Lindwasser, O.W., Olenych, S., Bonifacino, J.S., Davidson, M.W., Lippincott-Schwartz, J. and Hess, H.F. (2006) Imaging intracellular fluorescent proteins at nanometer resolution. *Science* **313**, 1642-1645.

Blanchoin, L. and Pollard, T.D. (1999) Mechanism of interaction of *Acanthamoeba* actophorin (ADF/cofilin) with actin filaments. *J. Biol. Chem.* **274**, 15538-15546.

Blanchoin, L. and Staiger, C.J. (2010) Plant formins: diverse isoforms and unique molecular mechanism. *Biochim. Biophys. Acta* **1803**, 201-206.

Brochhausen, L. (2011) Funktionelle Analyse eines Markers für perinukleäres pflanzliches Aktin. Bachelor thesis.

Bünning, E. (1965) Die Entstehung von Mustern in der Entwicklung von Pflanzen. In *Handbuch der Pflanzenphysiologie* (Ruhland W, ed). Springer: Berlin, pp. 383-408.

Buschmann, H., Green, P., Sambade, A., Doonan, J.H. and Lloyd C.W. (2011) Cytoskeletal dynamics in interphase, mitosis and cytokinesis analysed through Agrobacterium-mediated transient transformation of tobacco BY-2 cells. *New Phytol.* **190**, 258-267.

Bushman, W., Thompson, J.F., Vargas, L. and Landy, A. (1985) Control of directionality in lambda site specific recombination. *Science* **230**, 906-911.

Campanoni, P., Blasius, B. and Nick, P. (2003) Auxin transport synchronizes the pattern of cell division in a tobacco cell line. *Plant Physiol.* **133**, 1251-1260.

Campanoni, P. and Nick, P. (2005) Auxin-dependent cell division and cell elongation: NAA and 2,4-D activate different pathways. *Plant Physiol.* **137**, 939-948.

Campbell, N.A. and Reece, J.B. (2003) In *Biologie*. Spektrum Akademischer Verlag: Heidelberg Berlin.

Carlier, M.F., Laurent, V., Santolini, J., Melki, R., Didry, D., Xia, G.X., Hong, Y., Chua, N.H. and Pantaloni, D. (1997) Actin depolymerizing factor (ADF/cofilin) enhances the rate of filament turnover: implication in actin-based motility. *J. Cell Biol.* **136**, 1307-1322.

Chen, C.Y., Wong, E.I., Vidali, L., Estavillo, A., Hepler, P.K., Wu, H. and Cheung, A.Y. (2002) The Regulation of Actin Organization by Actin-Depolymerizing Factor in Elongating Pollen Tubes. *Plant Cell* **14**, 2175-2190.

Chen, C.Y., Cheung, A.Y. and Wu, H.M. (2003) Actin-depolymerizing factor mediates Rac/Rop GTPase–regulated pollen tube growth. *Plant Cell* **15**, 237-249.

Cvrcková, F., Novotny, M., Pícková, D., Zársky, V. (2004) Formin homology 2 domains occur in multiple contexts in angiosperms. *BMC Genomics* **5**, 44.

Danyluk, J., Carpentier, E. and Sarhan, F. (1996) Identification and characterization of a low-temperature regulated gene encoding an actin-binding protein from wheat. *FEBS Lett.* **389**, 324-327.

Davies, P.J. (2010) The Plant Hormones: Their Nature, Occurrence, and Functions. In *Plant Hormones: Biosynthesis, Signal Transduction, Action* (Davies PJ, ed). Springer: Heidelberg, pp. 1-15.

Dong, C.H., Xia, G.X., Hong, Y., Ramachandran, S., Kost, B. and Chua, N.H. (2001) ADF Proteins Are Involved in the Control of Flowering and Regulate F-Actin Organization, Cell Expansion, and Organ Growth in Arabidopsis. *Plant Cell* **13**, 1333-1346.

Era, A., Tominaga, M., Ebine, K., Awai, C. Saito, C. Ishizaki, K., Yamato, K.T., Kohchi, T., Nakano, A. and Ueda T. (2009) Application of Lifeact Reveals F-Actin Dynamics in *Arabidopsis thaliana* and the Liverwort, *Marchantia Polymorpha. Plant Cell Physiol.* **50**, 1041-1048.

Farmer, P.K. and Choi, J.H. (1999) Calcium and phospholipid activation of a recombinant calcium-dependent protein kinase (DcCPK1) from carrot (*Daucus carota* L.). *Biochem. Biophys. Acta* **1434**, 6-17.

Finer, J.J., Vain, P., Jones, M.W. and McMullen, M.D. (1992) Development of the particle inflow gun for DNA delivery to plant cells. *Plant Cell Rep.* **11**, 323-328.

Frey, N. (2011) DYNAMIC BRIDGES - An Unconventional Rice Kinesin Links Actin and Microtubules. *Doctoral thesis*.

Frey, N., Klotz, J. and Nick, P. (2009) Dynamic bridges - a calponin-domain kinesin from rice links actin filaments and microtubules in both cycling and non-cycling cells. *Plant Cell Physiol.* **50**, 1493-1506.

Friml, J. (2010) Subcellular trafficking of PIN auxin efflux carriers in auxin transport. *Eur. J. Cell Biol.* **89**, 231-235.

Fuchs, J., Böhme, S., Oswald, F., Hedde, P.N., Krause, M., Wiedenmann, J. and Nienhaus, U. (2010) A photoactivatable marker protein for pulse-chase imaging with superresolution. *Nat. Methods* 7, 627-630.

Fuchs, J. (2011) Characterization and Application of Photoswitchable Fluorescent Proteins for Nanoscopy. *Doctoral thesis*.

Gardiner, J.C., Harper, J.D.I., Weerakoon, N.D., Collings, D.A. Ritchie, S., Gilroy, S., Cyr, R.J. and Marc, J. (2001) A 90-kD Phospholipase D from Tobacco Binds to Microtubules and the Plasma Membrane. *Plant Cell* **13**, 2143-2158.

Guilfoyle, T.J. (1999) In *Biochemistry and Molecular Biology of Plant Hormones* (Libbenga, K.L., Hall, M., Hooykaas, P.J.J., eds). Elsevier, Leiden, pp. 423-459.

Gungabissoon, R.A., Jiang, C.J., Drobak, B.K., Maciver, S.K. and Hussey P.J. (1998) Interaction of maize actin-depolymerizing factor with actin and phosphoinositides and its inhibition of plant phospholipase *C. Plant J.* **16**, 689-696.

Gungabissoon, R.A., Khan, S., Hussey, P.J. and Maciver, S.K. (2001) Interaction of elongation factor 1α from *Zea mays* (ZmEF-1α) with F-actin and interplay with the maize actin severing protein, ZmADF3. *Cell Motil. Cytoskeleton* **49**, 104-111.

Han, L., Stope, M.B., Lopez de Jesus, M., Weernink, P.A.O., Urban, M., Wieland, T., Rosskopf, D., Mizuno, K., Jakobs, K.H. and Schmidt, M. (2007) Direct stimulation of receptor-controlled phospholipase D1 by phospho-cofilin. *EMBO J.* **26**, 4189-4202.

Hartley, J.L., Temple, G.F. and Brasch, M.A. (2000) DNA cloning using *in vitro* sitespecific recombination. *Genome Research* **10**, 1788-1795.

Hayden, S.M., Miller, P.S., Brauweiler, A. and Bamburg, J.R. (1993) Analysis of the interactions of actin depolymerizing factor with G- and F-actin. *Biochem.* **32**, 9994-10004.

Heisler, M.G., Hamant, O., Krupinski, P., Uyttewaal, M., Ohno, C., Jönsson, H., Traas, J. and Meyerowitz, E.M. (2010) Alignment between PIN1 Polarity and Microtubule Orientation in the Shoot Apical Meristem Reveals a Tight Coupling between Morphogenesis and Auxin Transport. *PLoS Biol.* **8**, e1000516.

Hess, S.T., Girirajan, T.P.K. and Mason, M.D. (2006) Ultra-high resolution imaging by fluorescence photoactivation localization microscopy. *Biophys. J.* **91**, 4258-4272.

Holweg, C., Suslin, C. and Nick, P. (2004) Capturing *in vivo* dynamics of the actin cytoskeleton stimulated by auxin or light. *Plant Cell Physiol,* **45**, 855-863.

Hu, T.X., Yu, M. and Zhao, J. (2010) Comparative transcriptional profiling analysis of the two daughter cells from tobacco zygote reveals the transcriptome differences in the apical and basal cells. *BMC Plant Biol.* **10**, 167-183.

Huang, S., Robinson, R.C., Gao, L.Y., Matsumoto, T., Brunet, A., Blanchoin, L. and Staiger, C.J. (2005) *Arabidopsis* VILLIN1 Generates Actin Filament Cables That Are Resistant to Depolymerization. *Plant Cell* **17**, 486-501.

Jiang, C.J., Weeds, A.G. and Hussey, P.J. (1997) The maize actin-depolymerizing factor, ZmADF3, redistributes to the growing tip of elongation root hairs and can be induced to translocate into the nucleus with actin. *Plant J.* **12**, 1035-1043.

Kakimoto, T. and Shibaoka, H. (1987) Actin filaments and microtubules in the preprophase band and phragmoplast of tobacco cells. *Protoplasma* **140**, 151-156.

Karimi, M., Inze, D. and Depicker, A. (2002) Gateway vectors for *Agrobacterium*-mediated plant transformation. *Trends Plant Sci.* **7**, 193-195.

Ketelaar, T., Anthony, R.G. and Hussey, P.J. (2004) Green fluorescent protein mTalin causes defects in actin organization and cell expansion in *Arabidopsis* and inhibits actin depolymerizing factor's actin depolymerizing activity in vitro. *Plant Physiol*. **136**, 3990-3998.

Kusaka, N., Maisch, J., Nick, P., Hayashi, K. and Nozaki, H. (2009) Manipulation of Intracellular Auxin in a Single Cell by Light with Esterase-Resistant Caged Auxins. *Chembiochem* **10**, 2195-2202.

Kuss-Wymer, C.L. and Cyr, R.J. (1992) Tobacco protoplasts differentiate into elongate cells without net microtubule depolymerization. *Protoplasma* **168**, 64-72.

Laňkova, M., Smith, R.S., Pešek, B., Kubeš, M., Zažimalova. E., Petrašek, J. and Hoyerova, K. (2010) Auxin influx inhibitors 1-NOA, 2-NOA, and CHPAA interfere with membrane dynamics in tobacco cells. *J. Exp. Bot*. **61**, 3589-3598.

Lanteri, M.L., Laxalt, A.M. and Lamattina, L. (2008) Nitric Oxide Triggers Phosphatidic Acid Accumulation via Phospholipase D during Auxin-Induced Adventitious Root Formation in Cucumber. *Plant Physiol.* **147**, 188-198.

Leonard, A. (2011) Functional analysis of two plant actin-binding proteins. Bachelor thesis.

Lomax, T.L., Muday, G.K. and Rubery, P.H. (1995) Auxin transport. In *Plant Hormones: Physiology, Biochemistry, and Molecular Biology* (Davies, P.J., ed). Kluwer: Dordrecht, pp. 509-530.

Lukyanov, K.A., Chudakov, D.M., Lukyanov, S. and Verkhusha, V.V. (2005) Innovation: Photoactivatable fluorescent proteins. *Nat. Rev. Mol. Cell Biol.* **6**, 885-891.

Maciver, S.K. and Hussey, P.J. (2002) The ADF/cofilin family: actin remodeling proteins. *Genome Biology* **3**, 3007.1-3007.12.

Maisch, J. (2007) Auxin, Actin, and Polar Patterning in Tobacco Cells. *Doctoral thesis*.

Maisch, J. and Nick, P. (2007) Actin is involved in auxin-dependent patterning. *Plant Physiol.* **143**, 1695-1704.

Maisch, J., Fišerova, J., Fischer, L. and Nick, P. (2009) Actin-related protein 3 labels actin-nucleating sites in tobacco BY-2 cells. *J. Exp. Bot.* **60**, 603-614.

Mattsson, J., Sung, Z.R. and Berleth, T. (1999) Responses of plant vascular systems to auxin transport inhibition. *Development* **126**, 2979-2991.

Meagher, R.B., McKinney, E.C. and Kandasamy, M.K. (1999a) Isovariant dynamics expand and buffer the responses of complex systems: the diverse plant actin gene family. *Plant Cell* **11**, 995–1006.

Meagher, R.B., McKinney, E.C. and Vitale, A.V. (1999b) The evolution of new structures: clues from plant cytoskeletal genes. *Trends Genet.* **15**, 278–284.

Michelot, A., Guérin, C., Huang, S., Ingouff, M., Richard, S., Rodiuc, N., Staiger, C.J. and Blanchoin, L. (2005) The formin homology 1 domain modulates the actin nucleation and bundling activity of Arabidopsis FORMIN1. *Plant Cell* **17**, 2296–2313.

Michelot, A., Derivery, E., Paterski-Boujemaa, R., Guérin, C., Huang, S., Parcy, F., Staiger, C.J. and Blanchoin, L. (2006) A novel mechanism for the formation of actin-filament bundles by a nonprocessive formin. *Curr. Biol.* **16**, 1924–1930.

Mun, J.H., Yu, H.J., Lee, H.S., Kwon, Y.M., Lee, J.S., Lee, I. and Kim, S.G. (2000) Two closely related cDNA encoding actin-depolymerizing factors of *Petunia* are mainly expressed in vegetative tissues. *Gene* **257**, 167-176.

Nakagawa, T., Kurose, T., Hino, T., Tanaka, K., Kawamukai, M., Niwa, Y., Toyooka, K., Matsuoka, K., Jinbo, T. and Kimura T. (2007) Development of Series of Gateway Binary Vectors, pGWBs, for Realizing Efficient Construction of Fusion Genes for Plant Transformation. *J. Biosci. Bioeng.* **104**, 34-41.

Nagata, T., Nemoto, Y. and Hasezawa, S. (1992) Tobacco BY-2 cell line as the ‘‘Hela’’ cell in the cell biology of higher plants. *Int. Rev. Cytol.* **132**, 1-30.

Nick, P. (2006) Noise yields order: auxin, actin and polar patterning. *Plant Biol.* **8**, 360-370.

Nick, P. (2010) Probing the actin-auxin oscillator. *Plant Signal Behav.* **5**, 4-9.

Nick, P., Han, M. and An, G. (2009) Auxin stimulates its own transport by actin re-organization. *Plant Physiol.* **151**, 155-167.

Nishida, E., Iida, K., Yonezawa, N., Koyasu, S., Yahara, I. and Sakai, H. (1987) Cofilin is a component of intranuclear and cytoplasmic actin rods induced in cultured cells. *Proc. Natl. Acad. Sci. USA* **84**, 5262-5266.

Normanly, J., Slovin, J.P. and Cohen, J.D. (2010) Auxin Biosynthesis and Metabolism. In *Plant Hormones: Biosynthesis, Signal Transduction, Action* (Davies, P.J., ed). Springer: Heidelberg, pp. 36-62.

Olyslaegers G, Verbelen JP (1998) Improved staining of F-actin and colocalization of mitochondria in plant cells. *J. Microsc. Oxford* **192**, 73-77.

Petrášek, J. and Friml, J. (2009) Auxin transport routes in plant development. *Development* **136**, 2675–2688.

Pleskot, R., Potocky, M., Pejchar, P., Linek, J., Bezvoda, R., Martinec, J., Valentova, O., Novotna, Z. and Žarsky, V. (2010) Mutual regulation of plant phospholipase D and the actin cytoskeleton. *Plant J.* **62**, 494-507.

Qiao, F., Chang, X. and Nick, P. (2010) The cytoskeleton enhances gene expression in the response to the Harpin elicitor in grapevine. *J. Exp. Bot.* **61**, 4021-4031.

Reinhard, D., Mandel, T. and Kuhlemeier, C. (2000) Auxin regulates the initiation and radial position of plant lateral organs. *Plant Cell* **12**, 507-518.

Rust, M., Bates, M. and Zhuang, X. (2006) Sub-diffraction-limit imaging by stochastic optical reconstruction microscopy (STORM). *Nat. Methods* **3**, 793-796.

Sachs, T. (2000) Integrating cellular and organismic aspects of vascular differentiation. *Plant Cell Physiol.* **41**, 649-656.

Sano, T., Higaki, T., Oda, Y., Hayashi, T. and Hasezawa, S. (2005) Appearance of actin microfilament 'twin peaks' in mitosis and their function in cell plate formation, as visualized in tobacco BY-2 cells expressing GFP-fimbrin. *Plant J*. **44**, 595–605.

Simon, S. and Petrašek, J. (2011) Why plants need more than one type of auxin. *Plant Sci.* **180**, 454-460.

Smertenko, A.P. and Franklin-Tong, V.E. (2011) Organisation and regulation of the cytoskeleton in plant programmed cell death. *Cell Death Differ.* **18**, 1263–1270.

Smertenko, A.P., Jiang, C.J., Simmons, N.J., Weeds, A.G., Davies, D.R. and Hussey, P.J. (1998) Ser6 in the maize actin-depolymerizing factor, ZmADF3, is phosphorylated by a calciumstimulated protein kinase and is essential for control of functional activity. *Plant J.* **14**, 187-193.

Staiger, C.J., Poulter, N.S., Henty, J.L., Franklin-Tong, V.E. and Blanchoin, L. (2010) Regulation of actin dynamics by actin-binding proteins in pollen. *J. Exp. Bot.* **61**, 1969-1986.

Stiel, A.C., Andresen, M., Bock, H., Hilbert, M., Schilde, J., Schönle, A., Eggeling, C., Egner, A., Hell, S. W. and Jakobs, S. (2008) Generation of monomeric reversibly switchable red fluorescent proteins for far-field fluorescence nanoscopy. *Biophys. J.* **95**, 2989-2997.

Thomas, C., Hoffmann, C., Dieterle, M., Van Troys, M., Ampe, C. and Steinmetz, A. (2006) Tobacco WLIM1 Is a Novel F-Actin Binding Protein Involved in Actin Cytoskeleton Remodeling. *Plant Cell* 18, 2194-2206.

Thomas, C., Tholl, S., Moes, D., Dieterle, M., Papuga, J., Moreau, F. and Steinmetz, A. (2009) Actin bundling in plants. *Cell Motil. Cytoskeleton* **66**, 940–957.

Van Troys, M., Huyck, L., Leyman, S., Dhaese, S., Vandekerkhove, J.I. and Ampe, C. (2008) Ins and outs of ADF/cofilin activity and regulation. *Eur. J. Cell. Biol.* **87**, 649-667.

Waller, F. and Nick, P. (1997) Response of actin microfilaments during phytochrome-controlled growth of maize seedlings. *Protoplasma* **200**, 154-162.

Waller, F., Riemann, M. and Nick, P. (2002) A role for actin-driven secretion in auxin-induced growth. *Protoplasma* **219**, 72-81.

Wang, X. (2000) Multiple forms of phospholipase D in plants: the gene family, catalytic and regulatory properties, and cellular functions. *Prog. Lipid Res.* **39**, 109-149.

Wiedenmann, J., Gayda, S., Adam, V., Oswald, F., Nienhaus, K., Bourgois, D. and Nienhaus, G.U. (2011) From EosFP to mIrisFP: structure-based development of advanced photoactivatable marker proteins of the GFP-family. *J. Biophot.* **4**, 377-390.

Wielopolska, A., Townley, H., Moore, I., Waterhouse, P. and Helliwell, C. (2005) A high-throughput inducible RNAi vector for plants. *Plant Biotechnol. J.* **3**, 583-590.

Wymer, C.L., Wymer, S.A., Cosgrove, D.J. and Cyr, R.J. (1996) Plant Cell Growth Responds to External Forces and the Response Requires Intact Microtubules. *Plant Physiol.* **110**, 425-430.

Yang, F., Moss, L.G. and Phillips, G.N. Jr. (1996) The molecular structure of green fluorescent protein. *Nat. Biotechnol.* **14**, 1246-1251.

Yang, W., Ren, S., Zhang, X., Gao, M., Ye, S., Qi, Y., Zheng, Y., Wang, J., Zeng, L., Li, Q., Huang, S. and He, Z. (2011) BENT UPPERMOST INTERNODE1 Encodes the Class II Formin FH5 Crucial for Actin Organization and Rice Development. *Plant Cell* **23**, 661-680.

Zaban, B. (2010) Tabula rasa - Polarität bei der Regeneration von Protoplasten. Diploma thesis.

Zhao, H., Hakala, M. and Lappalainen, P. (2010) ADF-Cofilin Binds Phosphoinositides in a Multivalent Manner to Act as a PIP_2-Density Sensor. *Biophys. J.* **98**, 2327-2336.

7. Appendix

7.1 Coding sequences of actin-binding proteins

7.1.1 NtADF1 gene (Accession number NCBI database: AAL91666)

MANAVSGMAVQDECKLKFLELKTKRNYRFIIFKIDGQEVVVEKLGSPEESYEDFANSLPADEC
RYAVFDLDFITNENCQKSKIFFIAWSPETSRVRMKMVYASSKDRFKRELDGIQVELQATDPSE
MSFDIVKARAY-

7.1.2 NtADF2 gene (Accession number NCBI database: AAL91667)

MANAASGMAVLDECKLKFLELKAKRNYRFIVFKIEGQQVVVEKLGNPEENYDDFTNSLPADEC
RYAVFDFDFITTENCQKSKIFFIAWSPDTSKVRMKMVYASSKDRFKRELDGIQVELQATDPSE
MSFDIIKSRAL-

7.1.3 NtNFH1 gene (Accession number NCBI database: AAF24496)

MLSSSFFFFLLLFSATVSATNRRVLHHPFFPVDSQPPSPSPTGTTTPKYPFDSSTTPNNNNYN
NNTPFFPFPPPPPPSPSAFASFPANISTLILPHSAKSKPLSSKLIATAIICVVAAVLVLSLAV
FLHIRKRRNQAASTSDAKTQRSNSSTHFNYSNANSNNGNNSSSGNRSHIPKLQRPSQTSSEFL
YLGTMVSSHGGIDGPHNPPQRRRSGNVTSVPASRKMDSPEIHPLPPLLGRNLSQNYGNNNDNN
NNADVISGRTEEDEEFYSPRGSLDGRESSIGTGSVSRRAFAAVEVENFGGGSRSSSSSSYSSS
SSCSGSPARSVSLSISPPVSLSPKSLMPKSPELVAIHTAPPPQYSPPPPPPPLPPRANFVPIL
VMGNESDSPSPPSSSSPERYSSRSIDSSPRSFNVWDQNLESPARITNQIQQIEPVSVASPPPP
PPPLSISIPASVPPPPPPPPCKNWDSPKTLTPPTSKPPVLVTPLRPIALESPVLISPMDQLPS
NSEPIEKNEQKIENEETPKPKLKTLHWDKVRASSDRETVWDQLKSSSFKLDEEMIETLFVVKT
PTSNPKETTRRAVLPSQSQENRVLDPKKSQNISIQLRALSVTVEEVCEALLEGNADALGTELL
ESLLKMAPSKEEERKLKEYKDDSPFKLGPAEKFLKAVLDIPFAFKRVDAMLYISNFDSEVDYL
KKSFETLEASCEELRSNRMFLKLVEAVLKTGNRLNVGTNRGDAHAFKVDTLLKLADVKGADGK
TSFLHFVVQEIIRLQAVESVAMSLVKEITEYFHGNSAREEAHPFRIFMVVRDFLMVLDRVCKE
VGMINERTIVSSAHKFPVPVNPTLQPAIGGLTAIRQHSFSDDDSSSP-

7.1.4 NtNFH2 gene (Accession number NCBI database: AAF24497)

MVFPFFFFLLFLFCSTHCISFAAVSAHNRRVLHESFFPIDSPPPSQPPIPAPPAPPTPYPFQP
STPDNNNPFFPTYRSPPPPPPPPSPSSLVSFPANISDINLPNTSKSKHVSSKLIITAITCVLA
AIIVLSIAICLHAKKRRRHFNDPKTQRSDNSNRLNHGSSKNDGNTNNSIPKLQQPSQTSSEFL
YLGTIVNSHGGINSGSNPDTAPSSRKMASPELRPLPPLNGRNLSQNYRNTRNDDDFYSTEESV

GYIESSFGAGSLSRRGFAAVEVNKFVGSSLSGSDSSSSSGSGSPNRSVSLSISPPVSVSPKRE
SCSRPKSPELIAVVTPPPPQRPPPPPPPFVHGPQVKVTANESPVLISPMEKNDQNVENHSIEK
NEEKSEEILKPKLKTLHWDKVRASSDCEMVWDQLKSSSFKLNEEMIETLFVVKNPTLNTSATA
KHFVVSSMSQENRVLDPKKSQNIAILLRVLNGTTEEICEAFLEGNAENIGTELLEILLKMAPS
KEEERKLKEYKDDSPFKLGPAEKFLKAVLDIPFAFKRIDAMLYISNFDYEVDYLGNSFETLEA
ACEELRSSRMFLKLLEAVLKTGNRMNVGTNRGDAHAFKLDTLLKLVDVKGADGKTTLLHFVVQ
EIIKSEGARLSGGNQNHQQSTTNDDAKCKKLGLQVVSNISSELINVKKSAAMDSEVLHNDVLK
LSKGIQNIAEVVRSIEAVGLEESSIKRFSESMNRFMKVAEEKILRLQAQETLAMSLVKEITEY
VHGDSAREEAHPFRIFMVVKDFLMILDCVCKEVGTINERTIVSSAQKFPVPVNPNLQPVISGF
RAKRLHSSSDEESSSP-

7.1.5 NtVLN1 gene (Accession number NCBI database: CAE17316)

MEGGGKIEVWRINGSAKTPVPGDDIGKFYSGDCYIVLYTYHCNDRKEDYYLCWWIGKDSVEED
QNMAAKLASTMCNSLKARPVLGRVYQGKEPPQFVAIFQPMLVLKGGLSSGYKSYIADKGLNDE
TYTADSVALIRLSGTSVHNNKAVQVDAVATSLNSNECFLLQSGSSVFSWHGNQSTYEQQQLAA
KVAEFLKPGVTVKHAKEGTESSTFWFALGGKQSYTSKKVASEVARDPHLFAYSFNKGKFEIEE
IYNFSQDDLLTEDVLLLDTHAEVFVWVGQSSDPKEKQSSFEVGQKYIEMAASLEGLSPHVPLY
KVMEGNEPCFFTTFFSWDPAKAIAHGNSFQKKVMLLFGVGHASENQQRFNGTNQGGATQRASA
LAALNSAFSSSPAKSSSAPRSAGKSPGSQRAAAIAALSSALSAEKKQPPEGGSPLRLSRTSSV
DAIAPGNEVSTAEIEDSKEVPERKEIETVEPAETDGEDVGPKPEPEQDETGNDSSQTTFSYER
LKAKSENPVTGIDLKRREAYLSDEEFESVLEMTKEAFYKLPKWKQDIHKKKVDLF-

7.1.6 NtVLN2 gene (Accession number NCBI database: CAE17317)

MREDYYLCWWIGKDSIEEDQSMAARLASTMCNSFKGRPVLGRVFQGKEPPQFVAIFQPMLVLK
GGLSSGYKNYIADKGLNDETYAADSVALIRLSGTSVHNNKAVQVDAVPASLNSNECFLLQSGS
SIFSWHGNQSTYEQQQLAAKVAEFLKPGATVKHTKEGTESSAFWFAVGGKQSYTSKKVATEVS
RDPHLFAYSFNKGKFEVEEIYNFSQDDLLTEDVLLLDTHAEVFVWIGQSADSKEKQSAFDVGQ
KYVEMAASLEGLSPNVPLYKVTEGNEPCFFTTFFSWDPAKASAHGNSFQKKVMLLFGVGHASE
NQQRSNGSGGPTQRASALAALNSAFSPSPPKSSSATRPAGTSSASQRAAAIAALSGVLTAEKK
QSSEGGSPVRSNRSSPVRSSRSSPVRSADSGPTENDLSTAEVQDSEKASEPKEIVEPAESNGS
EPKPEAEQDEGGNESGQAIFSYEQLKAKSDNPVTGIDFKRREAYLSDEEFESVLGMKKEAFYK
LPKWKQDMHKRKVDLF-

7.1.7 NtWLIM2 gene (Accession number NCBI database: AAD56951)

MSFIGTQQKCKACEKTVYPVELLSADGVNYHKSCFKCSHCKGTLKLSNFSSMEGVLYCKPHFE
QLFKESGNFNKNFQSPAKSAEKLTPELTRSPSKAAGM-

7.2 Accession numbers

All sequences were taken from NCBI gen database (http://www.ncbi.nlm.nih.gov/; as of April 2011) and Tree families database (Treefam; http://www.treefam.org/; as of April 2011).

Organism	Gene Annotation	Accession number	Source
Nicotiana tabacum	NtADF1	AAL91666	NCBI
	NtADF2	AAL91667	NCBI
Arabidopsis thaliana	AtADF1	At3g46010	Treefam
	AtADF2	NP_566882	NCBI
	AtADF3	NP_851227	NCBI
	AtADF4	NP_851228	NCBI
	AtADF5	At2g16700	Treefam
	AtADF6	At2g31200	Treefam
	AtADF7	NP_194289	NCBI
	AtADF8	NP_567182	NCBI
	AtADF9	At4g34970	Treefam
	AtADF10	NP_568769	NCBI
	AtADF11	NP_171680	NCBI
Vitis vinifera	VvADF predicted	XP_002284292	NCBI
	VvADF predicted	XP_002284029	NCBI
	VvADF predicted	XP_002273958	NCBI
	VvADF predicted	XP_002268512	NCBI
Oryza sativa	OsADF predicted	NP_001054456	NCBI
	OsADF predicted	NP_001053519	NCBI
	OsADF predicted	NP_001047657	NCBI
	OsADF predicted	NP_001059648	NCBI
	OsADF predicted	NP_001049525	NCBI
	OsADF predicted	AAG13444	NCBI
	OsADF predicted	NP_001067327	NCBI
	OsADF predicted	NP_001051449	NCBI
	OsADF predicted	NP_001051721	NCBI
	OsADF predicted	NP_001051720	NCBI
Zea mays	ZmADF1	NP_001105463	NCBI
	ZmADF2	NP_001105590	NCBI
	ZmADF3	NP_001105474	NCBI
Saccheromyces cerevisiae	ScCof1	NP_013050	NCBI
Saccheromyces pombe	SpCof1	NP_594741	NCBI

7.3 Primer

7.3.1 Primer for Gateway®-Cloning

Primer	Code	Sequence
attB1-ADF1		5'-GGGG **ACA AGT TTG TAC AAA AAA GCA GGC TTC** ATG GCG AAT GCA GTG TCT GG-3'
attB2-ADF1		5'-GGGG **AC CAC TTT GTA CAA GAA AGC TGG GTC** TCA ATA GGC TCG TGC TTT TAC-3'
attB1-ADF2		5'-GGGG **ACA AGT TTG TAC AAA AAA GCA GGC TTC** ATG GCG AAT GCT GCG TCT GG-3'
attB2-ADF2		5'-GGGG **AC CAC TTT GTA CAA GAA AGC TGG GTC** TCA AAG TGC TCG TGA CTT TAT-3'
attB1-VLN1		5'-GGGG **ACA AGT TTG TAC AAA AAA GCA GGC TTC** GAA GGG GGT GGA AAA ATA GAG GTC-3'
attB2-VLN1		5'-GGGG **AC CAC TTT GTA CAA GAA AGC TGG GTC** CTA GAA GAG ATC AAC TTT CTT TTT GTG-3'
attB1-VLN2		5'-GGGG **ACA AGT TTG TAC AAA AAA GCA GGC TTC** CAG AGA AGA TTA TTA TCT ATG CTG G-3'
attB2-VLN2		5'-GGGG **AC CAC TTT GTA CAA GAA AGC TGG GTC** CTA GAA GAG ATC AAC CTT TC-3'
attB1-WLIM2		5'-GGGG **ACA AGT TTG TAC AAA AAA GCA GGC TTC** ATG TCT TTT ATT GGG ACA C-3'
attB2-WLIM2		5'-GGGG **AC CAC TTT GTA CAA GAA AGC TGG GTC** AGA ATC TGG AAC GGT TGC-3'
attB1-Lifeact-pa-FP		5'-GGGG **ACA AGT TTG TAC AAA AAA GCA GGC TTC** ATG GGA GTA GCA GAT CTA ATC-3'
attB2-Lifeact-mIRIS		5'-GGGG **AC CAC TTT GTA CAA GAA AGC TGG GTC** TTA TCG TCT GGC ATT GTC AG-3'
attB2-Lifeact-psRFP		5'-GGGG **AC CAC TTT GTA CAA GAA AGC TGG GTC** TTA GTG ATG TCC AAG CTT GG-3'

7.3.2 Primer for semi-quantitative expression analysis

Primer	Code	Sequence
sq-ADF1 fw		5'-GAA TGG CAG TGC AAG ATG AAT G-3'
sq-ADF1 rv		5'-CAT CGG CAG GCA GAG AGT TAG-3'
sq-ADF2 fw		5'-AGT GCC GCT ATG CTG TCT TTG-3'
sq-ADF2 rv		5'-GTG TCA GGT GAC CAA GCA ATG-3'
sq-VLN1 fw		5'-GAA GTT CCA GAA CGC AAG GAG-3'
sq-VLN1 rv		5'-CAT TGC CAG TCT CAT CCT GTT-3'
sq-VLN2 fw		5'-GAT CAG CAG ACT CTG GCC CTA C-3'
sq-VLN2 rv		5'-CAT TAG ACT CTG CGG GCT CAA-3'
sq-NFH1 fw		5'-TGG GAA AAC ATC CTT CTT GC-3'
sq-NFH1 rv		5'-GAG CCT CTT CTC TGG CTG AA-3'
sq-NFH2 fw		5'-GAA GGT GCT CGT CTT TCT GG-3'
sq-NFH2 rv		5'-GAA TCC ATG GCA GCA GAT TT-3'
sq-NtActin fw		5'-ACA ACG AGC TTC GTG TTG C-3'
sq-NtActin rv		5'-CAG TGT GAC TCA CAC CAT CAC-3'
sq-NtGAPD fw		5'-CTG GAG AAA GAA GCT ACC TAC GAT GAA A-3'
sq-NtGAPD rv		5'-CAG ACT CCT CAC AGC AGC ACC ACT A-3'

7.4 PCR protocols

7.4.1 Gateway®-Cloning

Timetable for preparative PCRs:

Temperature	Duration	
98°C	240 sec	
98°C	8 sec	
55-58°C	20 sec	35 cycles
72°C	30 sec / kb	
72°C	300 sec	
4°C	∞	

Annealing temperatures were calculated using the web-based Primer3 software (http://frodo.wi.mit.edu/primer3/) ignoring all nucleotides which belonged to the Gateway®-attB-flanks.

PCR preparation (20 µl):

Component	Amount
Template (cDNA, plasmids; 2-500 ng/µl)	1 µl
5x HF Phusion buffer (NEB, Frankfurt, Germany)	4 µl
10 mM each dNTP Mix (NEB, Frankfurt, Germany)	0.4 µl
10 µM primer forward	1 µl
10 µM primer reverse	1 µl
2 U/µl Phusion Polymerase (NEB, Frankfurt, Germany)	0.2 µl
dd H_2O	12.4 µl

7.4.2 Semi-quantitative expression analysis

Annealing temperatures were calculated using the web-based Primer3 software (http://frodo.wi.mit.edu/primer3/). Number of cycles was chosen such that the amplification of templates for all primers was in an exponential range, and the products were clearly visible on 2 % agarose gels. As a representative image of the saturation test the documented gel of both *Nicotiana tabacum* villins was chosen.

Timetable for analytical PCRs:

Temperature	Duration	
94°C	240 sec	
94°C	30 sec	
60°C	30 sec	30 cycles
72°C	45 sec	
72°C	300 sec	
4°C	∞	

PCR preparation (20 µl):

Component	Amount
Template (cDNA; 50 ng/µl)	2 µl
10x ThermoPol buffer (NEB, Frankfurt, Germany)	2 µl
10 mM each dNTP Mix (NEB, Frankfurt, Germany)	0.4 µl
10 µM primer forward	1 µl
10 µM primer reverse	1 µl
5 U/µl Taq Polymerase (NEB, Frankfurt, Germany)	0.2 µl
dd H_2O	13.4 µl

Test for PCR saturation:

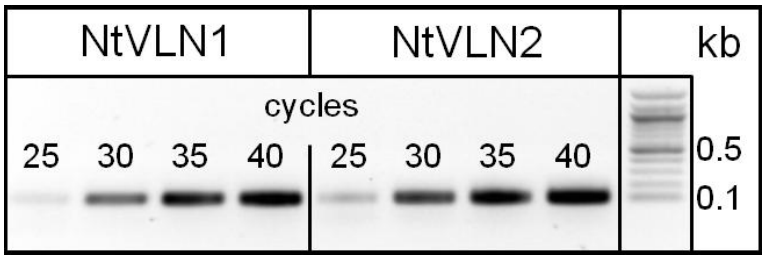

7.5 Gateway® recombination reactions technology

The Gateway® technology (Invitrogen Corporation, Paisley, UK) uses the bacteriophage site-specific lambda recombination system to facilitate transfer of heterologous DNA sequences between vectors (Hartley *et al*., 2000). The components of the lambda recombination sites (*att* sites) are modified to improve the specificity and efficiency of the system (Bushman *et al*., 1985).

Two recombination reactions constitute the basis of this technology:

1. **BP reaction**: Facilitates recombination of an *att*B substrate (*att*B-PCR product) with an *att*P substrate (called “donor vector”) to create an *att*L-containing entry clone. This reaction is catalysed by BP Clonase™ II enzyme mix (Invitrogen).

2. **LR reaction**: Facilitates recombination of an *att*L substrate (called “entry clone”) with an *att*R substrate (called “destination vector”) to create an *att*B-containing expression clone. This reaction is catalysed by LR Clonase™ II enzyme mix (Invitrogen).

The presence of the *ccd*B gene within this system allows negative selection of the donor and destination vectors in *E. coli* following recombination and transformation. The CcdB protein interferes with *E. coli* DNA gyrase (Bernard and Couturier, 1992), thereby inhibiting growth of most *E. coli* strains. When recombination occurs (i.e. between an *att*B-PCR product and a donor vector or between an entry clone and a destination vector), the *ccd*B gene is replaced by the gene of interest. Cells that take up unreacted vectors carrying the *ccd*B gene or by-product molecules retaining the *ccd*B gene will fail to grow. This allows high-efficiency recovery of the desired clones. For more information concerning the Gateway® technology, refer to the manual “Gateway® Technology with Clonase™ II” (Invitrogen; http://www.invitrogen.com). This summary of the Gateway® technology was taken from the doctoral thesis of Dr. Jan Maisch (Botanical Institute I, KIT, Karlsruhe; Maisch, 2007).

In this work chemi-competent *E.coli* (strain DH5α, Invitrogen) were transformed by heat shock (42°C, 90 sec) according to the manufacturer's protocol to amplify the gene of interest carrying vectors after BP (selection by 50 mg/L zeocin) and LR reaction (selection by 75 mg/L spectinomycin) on LB agar plates (1 % [w/v] tryptone, 0.5 % [w/v] NaCl, 0.5 % [w/v] yeast extract, 2 % [w/v] agar).

7.6 Gateway® vectors

7.6.1 Overview

The following codes are used for naming the different elements of the constructs:

K: kanamycin resistance

H: hygromycin resistance

7: t35S terminator

WG: attR2, ccdB, attR1 orientation

GW: attR1, ccdB, attR2 orientation

B: Binary vector

F: GFP

2: p35S promoter

pDONR/Zeo Gateway®-adapted vector designed to generate *att*L-flanked entry clones containing gene of interest; 4291 bp; selection in *E. coli*: zeocin. (Invitrogen Corporation, Paisley, UK)

Used for: pDONOR-NtADF1; pDONR-NtADF2; pDONOR-NtVLN1; pDONOR-NtVLN2; pDONOR-NtWLIM2

pK7WGF2.0 Gateway®-adapted binary vector designed to generate attB-flanked expression clones containing gene of interest; 11876 bp; selection in *E. coli*: spectinomycin; selection in plants: kanamycin; GFP is fused to the N-terminus of the protein of interest. Karimi *et al*., 2002.

Used for: pK7WGF2-NtADF1; pK7WGF2-NtADF2; pK7WGF2-NtVLN1; pK7WGF2-NtVLN2

pK7FWG2.0 Gateway®-adapted binary vector designed to generate attB-flanked expression clones containing gene of interest; 11880 bp; selection in *E. coli*: spectinomycin; selection in plants: kanamycin; GFP is fused to the C-terminus of the protein of interest. Karimi *et al*., 2002.

Used for: pK7FWG2-NtWLIM2

pH7WG2.0 Gateway®-adapted binary vector designed to generate attB-flanked expression clones containing gene of interest; 11880 bp; selection in *E. coli*: spectinomycin; selection in plants: hygromycin; no FP. Karimi *et al*., 2002.

Used for: pH7WG2-Lifeact-psRFP; pH7WG2-Lifeact-mIRIS

pGWB2.0 Gateway®-adapted binary vector designed to generate attB-flanked expression clones containing gene of interest; 17236 bp; selection in *E. coli*: chloramphenicol; selection in plants: hygromycin; no FP. Nakagawa *et al*., 2007; kind gift of Prof. Takashi Ueda (Laboratory of Developmental Cell Biology, University of Tokyo, Japan).

Used for: pGWB2-Lifeact-VENUS

pOpOff2(kan) Dexamethasone inducible Gateway®-adapted binary vector designed to generate hairpin structures for gene silencing in plants; 23017 bp; selection in *E. coli*: spectinomycin; selection in plants: kanamycin; coding for β-glucuronidase gene as expression marker. Wielopolska *et al*., 2005.

Used for: pOpOff2(kan)-NtADF2 RNAi

7.6.2 Vector maps

The following maps represent all vectors of expression clones produced in this work using the Gateway® Cloning system. Further sequence information and a digital version as VectorNTI format can be found on the attached DVD.

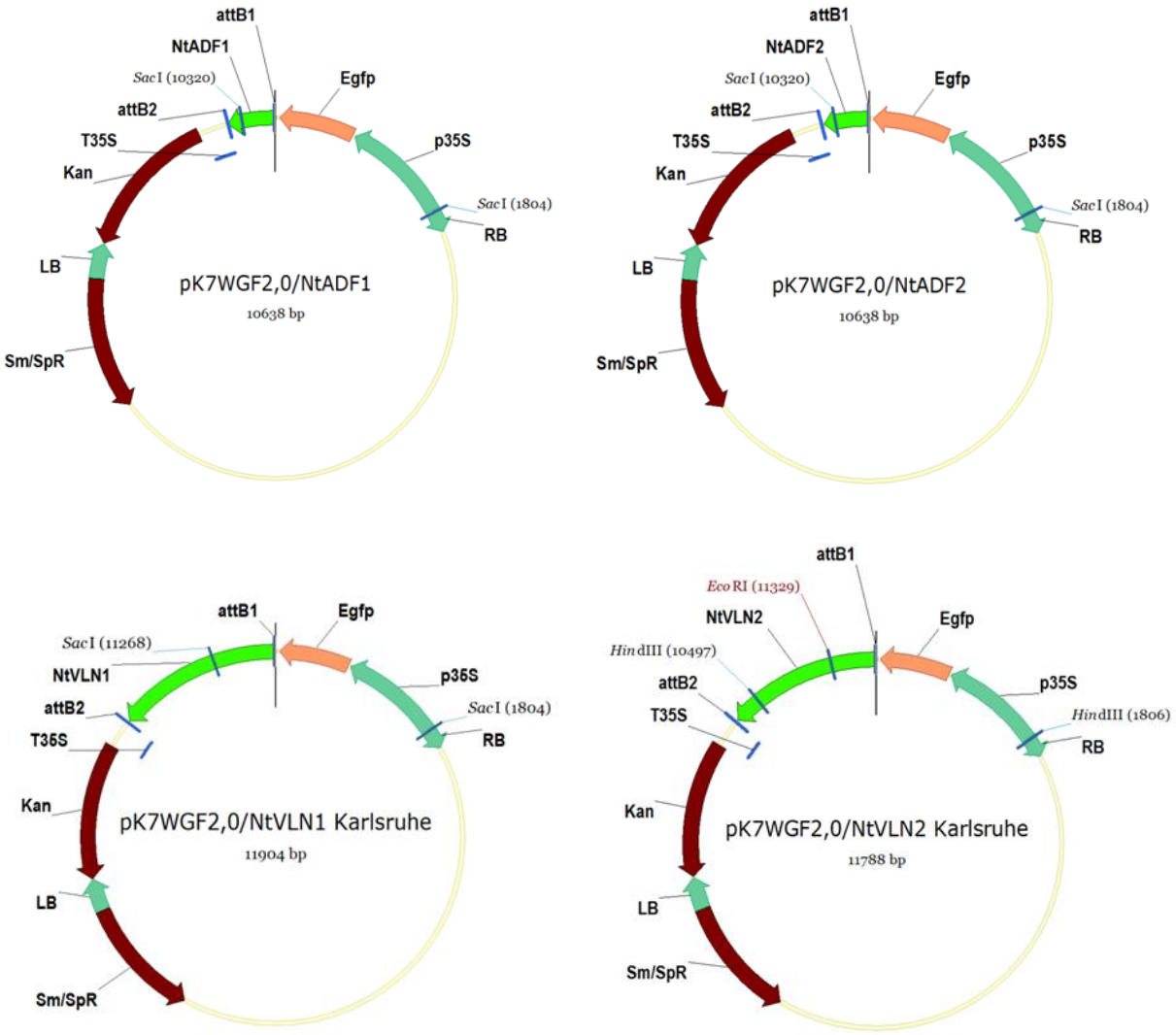

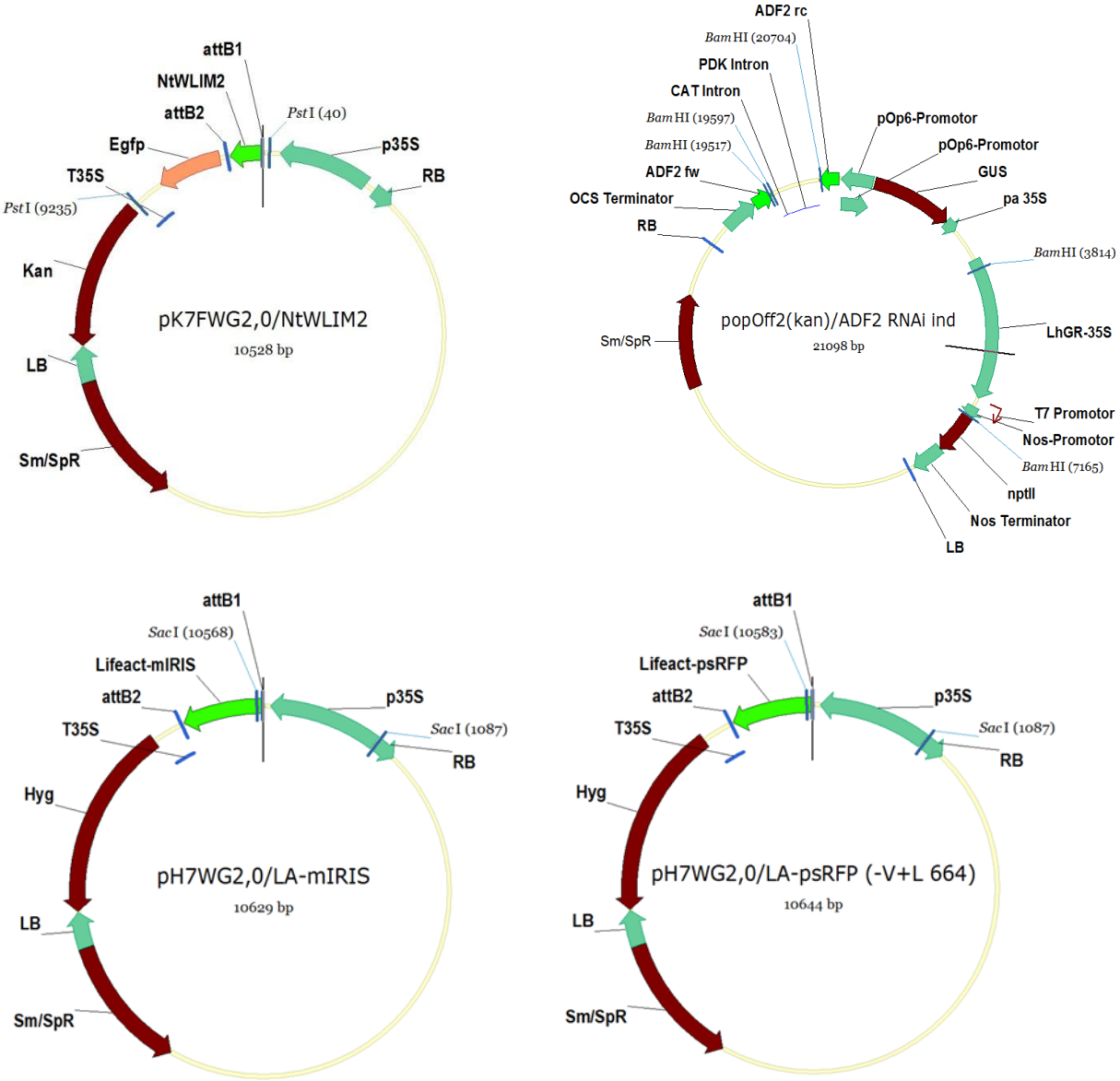

7.7 Preparation of DNA-coated gold particles for biolistic transformation

120 mg of gold particles (1.5–3.0 µm; Sigma-Aldrich) were suspended in 1 mL 50 % (v/v) sterile glycerol by mixing on a platform vortexer (Bender & Hobein, Zurich, Switzerland).

Continuous agitation of the suspended gold particles was needed for uniform DNA precipitation onto gold particles maximizing uniform sampling.

For each sample, 12.5 µL of gold suspension was removed to a 1.5 mL reaction tube.

While mixing vigorously, the following components were added successively: 1 µg of DNA, 12.5 µL of 2.5 M sterile $CaCl_2$, and 5 µL of 0.1 M sterile spermidine (Roth, Karlsruhe, Germany).

Following supplementary mixing for 3 minutes, the DNA-coated gold particles were spun down briefly, and the supernatant was discarded. Subsequently, the gold particles were washed with 125 µL of absolute ethanol and resuspended in 40 µL of absolute ethanol.

DNA-coated gold particles were loaded onto the macrocarrier (BIO-RAD, Hercules, CA, USA) in 10 µL steps. Particle bombardment was performed immediately after total evaporation of the ethanol.

This protocol was taken and modified from the doctoral thesis of Dr. Jan Maisch (Botanical Institute I, KIT, Karlsruhe; Maisch, 2007).

7.8 BY-2 cell line cultivation conditions

BY-2 cell line	sub. volume	antibiotic conc.	source
non-transformed WT	1 mL	---	Nagata *et al*., 1992
GFP-NtADF1 ox	1.5 mL	25 mg/L Kanamycin	this work
GFP-NtADF2 ox	1.5 mL	25 mg/L Kanamycin	this work
GFP-NtVLN1 ox	1.5 mL	25 mg/L Kanamycin	this work
WLIM1-GFP ox	1.5 mL	30 mg/L Hygromycin	Thomas *et al*., 2006
WLIM2-GFP ox	1.5 mL	25 mg/L Kanamycin	this work
mTalin-YFP ox	3.0 mL	25 mg/L Kanamycin	Maisch and Nick, 2007
Lifeact-psRFP ox	1.5 mL	30 mg/L Hygromycin	this work
Lifeact-mIRIS ox	1.5 mL	30 mg/L Hygromycin	this work
Lifeact-VENUS ox	1.5 mL	30 mg/L Hygromycin	this work
NtADF2 RNAi	1.5 mL	50 mg/L Kanamycin	this work

7.9 PALM images

Single section images of a Lifeact-psRFP ox BY-2 cell nucleus total projection (Figure 3.20, p. 50, Bar: 5 µm).

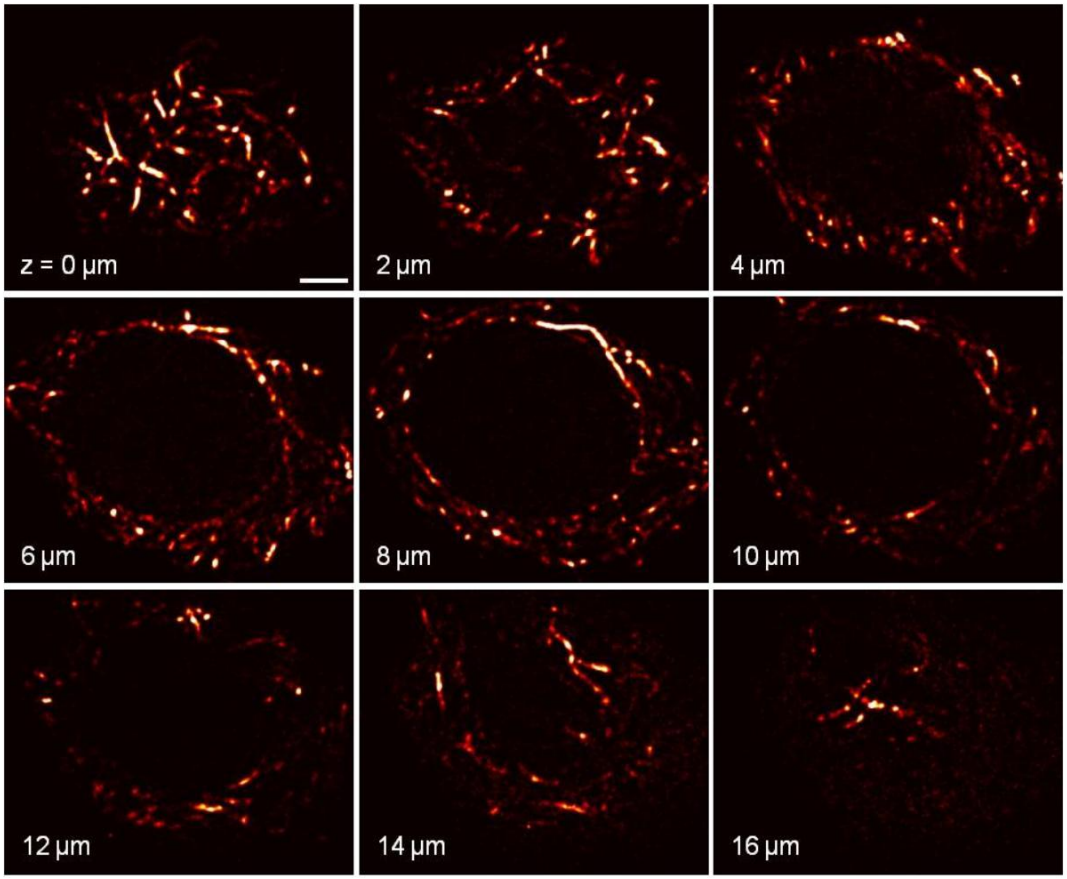

Single section images of a Lifeact-psRFP ox BY-2 cell nucleus total projection (Figure 3.21, p. 51, Bar: 5 µm).

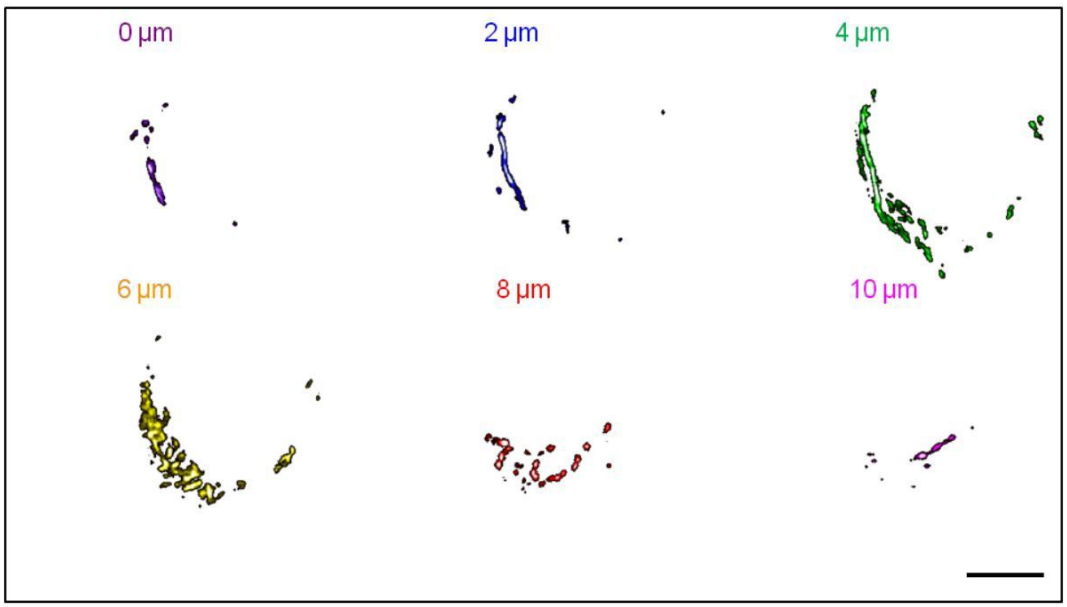

Publikationen

Jovanovic, A., Durst, S. and Nick, P. (2010) Plant cell division is specifically affected by nitrotyrosine. *J. Exp. Bot.* **61**, 901-909.

Hohenberger, P., Eing, C., Straessner, R., Durst, S., Frey, W. and Nick, P. (2011) Plant Actin Controls Membrane Permeability. *Biochem. Biophys. Acta* **1808**, 2304-2312.

Durst, S., Nick, P. and Maisch, J. (2012) *Nicotiana tabacum* Actin-Depolymerizing Factor 2 is Involved in Auxin-Dependent Patterning. *Unpublished manuscript*.

Hiermit erkläre ich, dass ich die vorliegende Dissertation, abgesehen von der Benutzung der angegebenen Hilfsmittel, selbständig verfasst habe.

Alle Stellen, die gemäß Wortlaut oder Inhalt aus anderen Arbeiten entnommen sind, wurden durch Angabe der Quelle als Entlehnungen kenntlich gemacht.

Karlsruhe, im März 2012

Steffen Durst